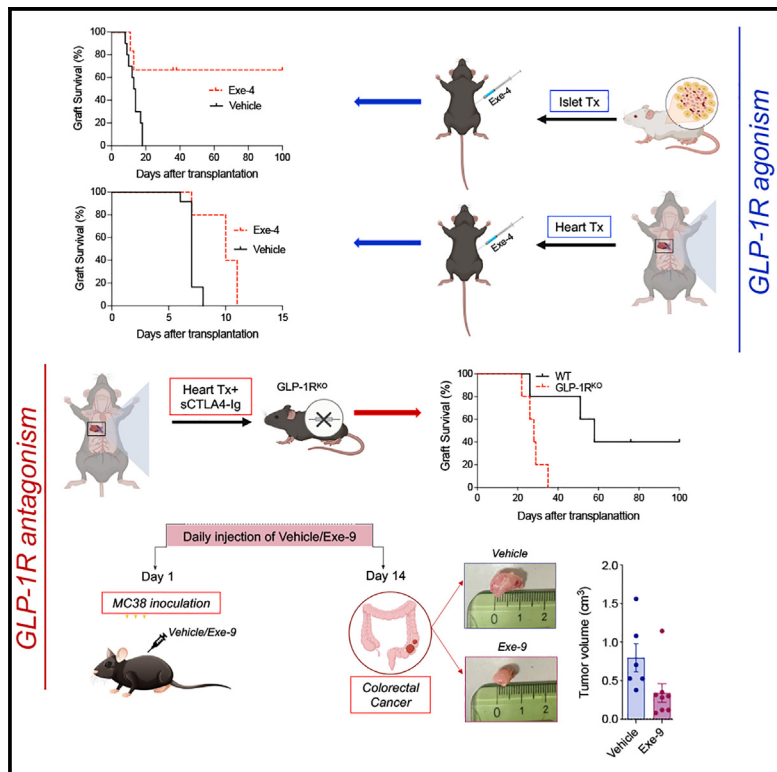


Glucagon-like peptide 1 receptor is a T cell-negative costimulatory molecule

Graphical abstract



Authors

Moufida Ben Nasr, Vera Usuelli,
Sergio Dellepiane, ..., Reza Abdi,
Franco Folli, Paolo Fiorina

Correspondence

franco.folli@unimi.it (F.F.),
paolo.fiorina@
childrens.harvard.edu (P.F.)

In brief

Here, we show that GLP-1R is expressed by T cells, and its signaling prolongs allograft survival and mitigates alloimmunity. Notably, GLP-1R antagonism triggered anti-tumor immunity in a mouse model of colorectal cancer. GLP-1R acts as a T cell-negative costimulatory molecule.

Highlights

- GLP-1R expression is evident in T cells, particularly in those apoptotic anergic
- GLP-1R acts as a T cell-negative costimulatory molecule
- GLP-1R signaling prolongs allograft survival and mitigates alloimmunity
- GLP-1R antagonism triggered anti-tumor immunity in a mouse model of colorectal cancer

Article

Glucagon-like peptide 1 receptor is a T cell-negative costimulatory molecule

Moufida Ben Nasr,^{1,2,3,23} Vera Usuelli,^{1,23} Sergio Dellepiane,^{2,23} Andy Joe Seelam,¹ Teresa Vanessa Fiorentino,⁴ Francesca D'Addio,¹ Emma Fiorina,¹ Cong Xu,⁵ Yanan Xie,⁵ Hari Baskar Balasubramanian,¹ Eduardo Castillo-Leon,² Lara Loreggian,¹ Anna Maestroni,¹ Emma Assi,¹ Cristian Loretelli,¹ Ahmed Abdelsalam,¹ Basset El Essawy,^{3,6} Silvia Uccella,⁷ Ida Pastore,⁸ Maria Elena Lunati,⁸ Gianmarco Sabiu,^{1,3} Adriana Petrazzuolo,¹ Giacomo Ducci,^{9,10} Elena Sacco,^{9,10} Lucia Centofanti,¹⁰ Massimo Venturini,¹¹ Serena Mazzucchelli,¹² Deborah Mattinzoli,¹³ Masami Ikehata,¹³ Giuseppe Castellano,^{13,14} Gary Visner,¹⁵ Liu Kaifeng,¹⁵ Kang Mi Lee,¹⁶ Zhimin Wang,¹⁷ Domenico Corradi,¹⁸ Stefano La Rosa,^{19,20} Silvio Danese,²¹ Jun Yang,⁵ James F. Markmann,¹⁶ Gian Vincenzo Zuccotti,^{1,22} Reza Abdi,³ Franco Folli,^{10,*} and Paolo Fiorina^{1,2,3,8,24,*}

¹International Center for T1D, Pediatric Clinical Research Center Romeo ed Enrica Invernizzi, DIBIC, Università di Milano, Milan, Italy

²Nephrology Division, Boston Children's Hospital, Harvard Medical School, Boston, MA, USA

³Transplantation Research Center, Brigham and Women's Hospital, Harvard Medical School, Boston, MA, USA

⁴Department of Medical and Surgical Sciences, University "Magna Graecia" of Catanzaro, Catanzaro, Italy

⁵Institute of Organ Transplantation, Tongji Hospital, Tongji Medical College, Huazhong University of Science, Wuhan, China

⁶Medicine, Al-Azhar University, Cairo, Egypt

⁷Humanitas University and IRCCS Humanitas Research Hospital, Milan, Italy

⁸Division of Endocrinology, ASST Fatebenefratelli Sacco, Milan, Italy

⁹Department of Biotechnology and Biosciences, University of Milano-Bicocca, Milan, Italy

¹⁰Department of Health Sciences, Universita'degli Studi di Milano, Milan, Italy

¹¹University of Insubria, Varese, Italy

¹²Nanomedicine Laboratory, DIBIC, Università di Milano, Milan, Italy

¹³Nephrology, dialysis and renal transplantation, Fondazione IRCCS Ca' Granda Ospedale Maggiore Policlinico, Milan, Italy

¹⁴Department of Clinical Sciences and Community Health, University of Milan, Milan, Italy

¹⁵Pulmonary Medicine, Boston Children's Hospital/Harvard Medical School, Boston, MA, USA

¹⁶Center for Transplantation Sciences, Department of Surgery, Massachusetts General Hospital and Harvard Medical School, Boston, MA, USA

¹⁷Department of Pediatrics, Tongji Hospital, Tongji Medical College, Huazhong University of Science and Technology, Wuhan, China

¹⁸Department of Biomedical, Biotechnological and Translational Sciences, Unit of Pathology, University of Parma, Parma, Italy

¹⁹Unit of Pathology, Department of Medicine and Technological innovation, University of Insubria, Varese, Italy

²⁰Unit of Pathology, Department of Oncology, ASST Sette Laghi, Varese, Italy

²¹Gastroenterology and Endoscopy, IRCCS Ospedale San Raffaele, Vita-Salute San Raffaele, Milan, Italy

²²Department of Pediatrics, Children's Hospital Buzzi, University of Milan, Milan, Italy

²³These authors contributed equally

²⁴Lead contact

*Correspondence: franco.folli@unimi.it (F.F.), paolo.fiorina@childrens.harvard.edu (P.F.)

<https://doi.org/10.1016/j.cmet.2024.05.001>

SUMMARY

Glucagon-like peptide-1 receptor (GLP-1R) is a key regulator of glucose metabolism known to be expressed by pancreatic β cells. We herein investigated the role of GLP-1R on T lymphocytes during immune response. Our data showed that a subset of T lymphocytes expresses GLP-1R, which is upregulated during alloimmune response, similarly to PD-1. When mice received islet or cardiac allotransplantation, an expansion of GLP-1R^{pos} T cells occurred in the spleen and was found to infiltrate the graft. Additional single-cell RNA sequencing (scRNA-seq) analysis conducted on GLP-1R^{pos} and GLP-1R^{neg} CD3⁺ T cells unveiled the existence of molecular and functional dissimilarities between both subpopulations, as the GLP-1R^{pos} are mainly composed of exhausted CD8 T cells. GLP-1R acts as a T cell-negative costimulatory molecule, and GLP-1R signaling prolongs allograft survival, mitigates alloimmune response, and reduces T lymphocyte graft infiltration. Notably, GLP-1R antagonism triggered anti-tumor immunity when tested in a preclinical mouse model of colorectal cancer.



INTRODUCTION

Glucagon-like peptide-1 (GLP-1) regulates glucose metabolism by signaling through its receptor (GLP-1R), which is expressed by pancreatic β cells, gastric mucosa, the hypothalamic appetite center, and skeletal muscle.^{1–8} GLP-1R agonists reduce the incidence and severity of severe diabetes complications, including cardiovascular events and diabetic kidney disease.⁹ Beside these well-known metabolic effects, an increasing body of literature suggests that GLP-1R may have a role in regulating the immune system.^{10–12} GLP-1R mRNA expression has been detected in various populations of immune cells, including dendritic cells and T lymphocytes; authors have suggested that its signaling may have immunological properties.¹¹ More recently, GLP-1R expression was confirmed in a subset of gut intra-epithelial T lymphocytes.¹³ These cells control the systemic metabolism by modulating hormone secretion from the entero-endocrine epithelial cells. However, there is no conclusive evidence about a possible immunological role of GLP-1R and its signaling. In patients affected simultaneously by diabetes and psoriasis, evidence of an improvement of dermatological symptoms after treatment with the GLP-1R agonist Exendin-4 was reported.¹⁴ Of note, after some patients discontinued the drug as consequence of mild adverse events, psoriasis symptoms substantially worsened but improved again when Exendin-4 was restarted. In non-obese diabetic (NOD) mice, a strain prone to autoimmune diabetes, Exendin-4 treatment delayed diabetes onset as well as islet allograft rejection in a fully mismatched model of islet allotransplantation.^{15,16} More recently, the administration of GLP-1R agonist, Liraglutide, was shown to mitigate nephrotoxic serum nephritis in mice by dampening renal infiltration and the proliferation of effector T cells.¹⁷ In this study, we seek to clarify GLP-1R role in T lymphocytes as we hypothesize that it may act as a negative costimulatory molecule. If proven correct, our study may serve for the basis of the clinical use of GLP-1R antagonists as immune checkpoint inhibitors to stimulate anti-tumor immunity, while agonists may facilitate immune regulation.

RESULTS

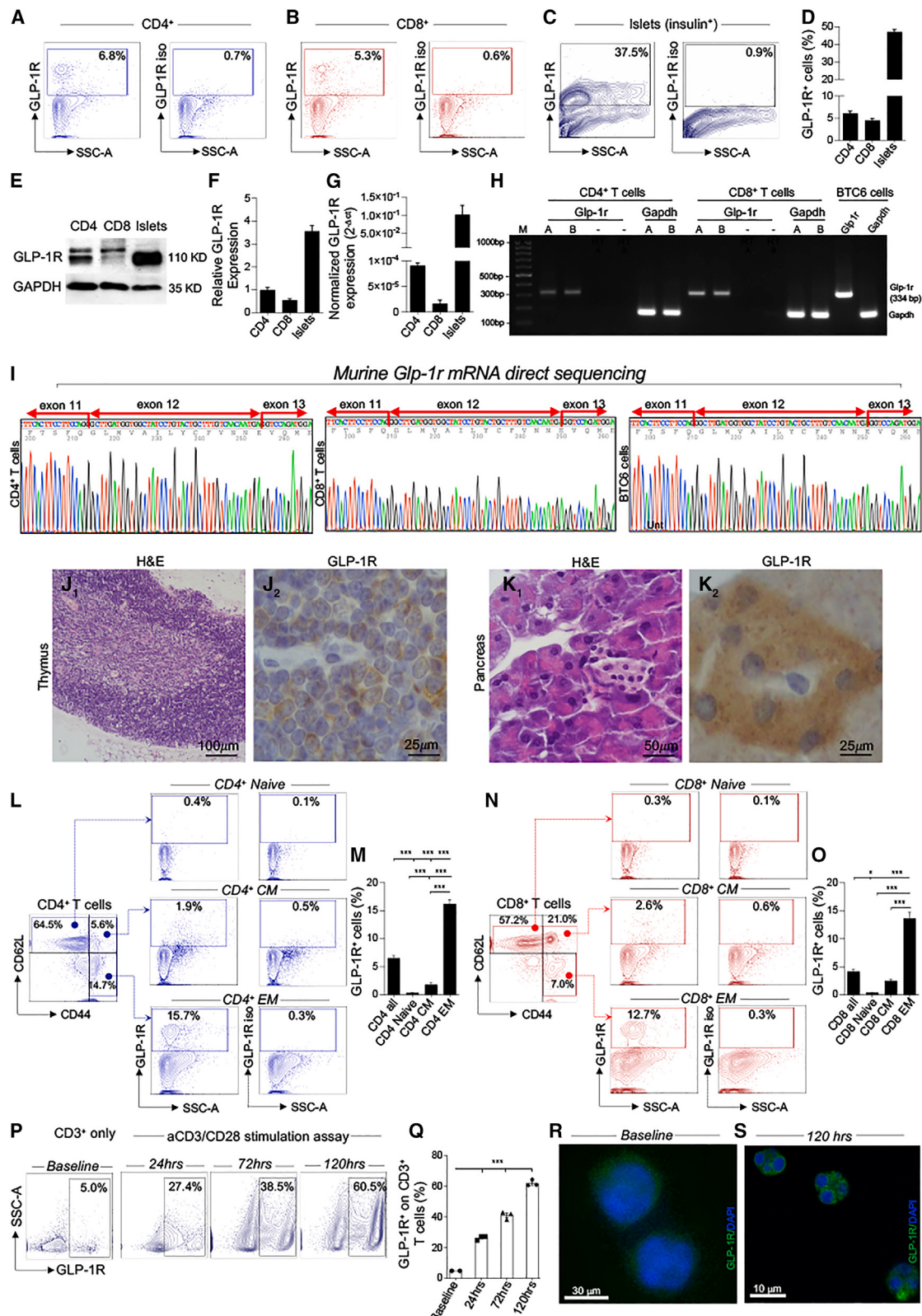
GLP-1R in murine T cells

First, we broadly assessed the expression of GLP-1R on lymphocytes by a variety of techniques. Murine CD4 $^{+}$ and CD8 $^{+}$ cells obtained from C57BL/6 mice expressed GLP-1R at protein and mRNA level, and in all experiments, murine islets were used as control (Figures 1A–1G). Additionally, to confirm the specificity of the GLP-1R expression by T cells, we conducted a due diligence assessment of *Glp-1r* expression at the mRNA level on \approx CD4 $^{+}$, CD8 $^{+}$ T cells, respectively, as compared with a mouse beta cell line (BTC6 cells), used as a positive control (Figures 1H, 1I, S1A, and S1B). We first designed exon junction-spanning primers to amplify a 334 bp-long target amplicon of the murine *Glp-1r* gene from cDNAs obtained from CD4 $^{+}$, CD8 $^{+}$, and BTC6 cells, respectively. The correct amplification of the expected target amplicon size (334 bp) was confirmed/visualized by both melt curve analysis and by agarose gel electrophoresis and subsequent Sanger sequencing, which further confirmed the identity and conformity of *Glp-1r* mRNA in all

tested samples (CD4 $^{+}$, CD8 $^{+}$ T cells, and BTC6 cells) (Figures 1H and 1I). Then the alignment of the PCR endpoint product sequences with nucleotides 950–1,296 of the *Glp-1r* reference cDNA (NM_021332.2) further confirmed the expression of *Glp-1r* in murine CD4 $^{+}$ and CD8 $^{+}$ T cells (Figure S1C). Nearly 5%–6% of CD4 $^{+}$ and CD8 $^{+}$ T lymphocytes expressed GLP-1R on their surface, while control islets are 40%–42% positive (Figures 1A–1D). GLP-1R expression on T lymphocytes was also confirmed by immunohistochemistry staining; indeed, GLP-1R expression was also identified in the thymus and as expected, in pancreatic islets (Figures 1J₁–1K₂). We then investigated whether the expression of GLP-1R varied across the different CD4 $^{+}$ and CD8 $^{+}$ subsets. Although no GLP-1R expression was evident on CD4 $^{+}$ or CD8 $^{+}$ naive T cells, and it was scanty (less than 5%) on memory cells, nearly 10%–13% of CD4 $^{+}$ and CD8 $^{+}$ effector T cells and 14% of regulatory T cells appeared to be GLP-1R $^{\text{pos}}$ (Figures 1L–1O, S2A, and S2B). We then challenged CD3 $^{+}$ T cells isolated from naive C57BL/6 wild-type (WT) mice with anti-CD3/anti-CD28 mAbs, and GLP-1R expression was determined in a time course manner (Figures 1P and 1Q). A substantial increase in GLP-1R expression, confirmed also by immunofluorescence, was evident (Figures 1P–1S). Notably, upon T cell activation, GLP-1R increased in expression matches PD-1 upregulation (Figures S2C–S2H). Finally, we investigated GLP-1R expression on several components of innate immunity and noticed an expression of GLP-1R by mainly natural killer T (NKT) cells, NK cells, CD11c $^{+}$ cells, and CD11b $^{+}$ cells, always with a similar pattern to what was observed for PD-1 expression (Figures S2I–S2K).

GLP-1R $^{\text{pos}}$ T cell profiling

Then in order to probe the existence of a unique GLP-1R interactome specific for T cells, we immunoprecipitated GLP-1R from activated CD3 $^{+}$ T cells followed by mass spectrometry. Using fingerprinting, we identified 20 peptides significantly interacting with GLP-1R, and by spectral counting, we assessed the relative quantification of the 20 identified peptides (Figure 2A; Table S1). Within the 20 peptides, we identified 4 (ZN503 [zinc finger protein 503], PURB [transcriptional regulator protein Pur-beta], MBD2 [methyl-CpG-binding domain protein 2], and bromodomain adjacent to zinc-finger domain protein 2A [BAZ2A]) that were reported to be transcriptional repressor and play a role in gene silencing (Table S1). Interestingly, by bioinformatic analysis (www.uniprot.org, www.genevisible.com, www.gee.org, and www.ebi.ac.uk/gxa/home), we compared the T cell GLP-1R-interactome with those obtained from β cells and other tissues confirming some unique interactors (peptides) for T cells (Figure 2B). After a deeper selection, we delineated 2 unique T cell proteins: CCG8_MOUSE (voltage-dependent calcium channel gamma-8 subunit, a known modulator of AMPA receptors containing TARP- γ 8¹⁸) and BAZ2A_MOUSE (Figure 2C). Next, we demonstrated that, similarly to PD-1, proliferating cells showed a significant increase in GLP-1R protein expression (Figures 2D, 2E, and S2C–S2H). Interestingly, GLP-1R $^{\text{neg}}$ CD3 $^{+}$ T cells revealed an abundant GLP-1R intracellular expression, although to a lower extent than that observed from their counterparts GLP-1R $^{\text{pos}}$ CD3 $^{+}$ T cells (Figure 2F). This may appear to be a reservoir for a rapid conversion of GLP-1R $^{\text{neg}}$ CD3 $^{+}$ T cells into GLP-1R $^{\text{pos}}$ CD3 $^{+}$ T cells (Figures 2G₁ and 2G₂). We further

**Figure 1. GLP-1R in murine T cells**

(A and B) Representative dot plot of GLP-1R expression by murine splenic CD4⁺ and CD8⁺ cells.
(C) Representative dot plots of GLP-1R expression by murine pancreatic β cells.

(legend continued on next page)

characterize GLP-1R^{pos} CD3⁺ T cells, and all data confirmed that GLP-1R^{pos} CD3⁺ T cells have a specific profile resuming those of activated/exhausted T cells as compared with the GLP-1R^{neg} CD3⁺ T cells. Indeed, an increased proliferation, an increased apoptosis, and an enhanced migratory ability in response to SDF-1 were all features observed in GLP-1R^{pos} CD3⁺ T cells as compared with their counterparts GLP-1R^{neg} (Figures 2H–2K). The high migratory capacity of GLP-1R^{pos} CD3⁺ T cells toward SDF-1 (stromal-cell derived factor 1) matched their chemokine receptor profile, which is enriched in CXCR4 and CCR2 expression (Figure S2L). Furthermore, a significantly lower percentage of interferon (IFN)- γ ⁺ cells was obtained within GLP-1R^{pos} CD3⁺ T cells during a stimulation assay as compared with those observed within GLP-1R^{neg} CD3⁺ T cells, while IL-4 and IL-10 expression is higher in the former at steady state (Figures 2L and S2M–S2Q). Oxygen consumption rate (OCR) was similar between GLP-1R^{pos} and GLP-1R^{neg} CD3⁺ T cells under resting conditions (Figures 2M and 2N), while GLP-1R^{pos} CD3⁺ T cells showed a significantly reduced maximal respiration as compared with GLP-1R^{neg} CD3⁺ T cells (Figures 2M and 2N). The spare respiratory capacity (SRC) was significantly reduced in GLP-1R^{pos} CD3⁺ T cells in comparison with their GLP-1R^{neg} counterparts (Figure 2N), while no differences were evident for the glycolytic bioenergetic parameters (Figures 2O and 2P), suggesting that GLP-1R^{neg} are hypermetabolic. All the aforementioned characteristics, including PD-1 expression, were confirmed in CD4⁺/CD8⁺ T cells (Figures 2Q, 2R, S2G, and S2H). GLP-1R^{pos} CD4⁺ and CD8⁺ T cells showed a higher cell death and lower IFN- γ expression as compared with their counterparts GLP-1R^{neg} T cells (Figures 2S and 2T). A transcriptomic analysis of fluorescence-activated cell sorter (FACS) sorted splenic GLP-1R^{pos} CD4⁺/CD8⁺ T cells and compared with their counterparts GLP-1R^{neg} (Figures 2U–2X) identified 25 upregulated genes on GLP-1R^{pos} CD4⁺ T cells mainly associated with anergy, apoptosis (CASP3 [caspase 3], CASP7 [caspase 7], and Bak1 [Bcl2-antagonist/killer 1]), and immunoregulation

(TGFB1 [transforming growth factor-beta 1], TNFSF10 [tumor necrosis factor ligand superfamily member 10], and LGALS3 [galectin-3]) (Figure 2U). Additionally, most of the downregulated genes in GLP-1R^{pos} CD4⁺ T cells belong to mitotic cell-cycle G1/S phase transition, cellular activation, and cytokine production (Figure 2V). The transcriptomic analysis on in GLP-1R^{pos} CD8⁺ T cells revealed the upregulation of genes associated with T cell/Th1 pathway activation, while those downregulated genes were associated with response to oxidative stress and to protein phosphorylation (Figures 2W and 2X). Altogether, our findings suggested that GLP-1R signaling may confer an anergic and exhausted state in activated T lymphocytes and unveil a potential interactor network involved in GLP-1R signaling into T cells.

scRNA-seq of GLP-1R^{pos} T cells

The molecular profiling by single-cell RNA sequencing (scRNA-seq) identified 13 clusters in GLP-1R^{pos} and 7 clusters in GLP-1R^{neg} (Figures 3A and 3B). Annotation with SingleR provided major insights into cell types composing each cluster (Figures S3A and S3B), while manually curated annotation, based on the expression of top marker genes for each cluster revealed the presence of distinct T cell subpopulations, all confirmed by an integrated analysis performed with Seurat standard pipeline (Figures 3C–3G). Our data analysis suggested the presence of a heterogeneous T cell subpopulation within GLP-1R^{pos} CD3⁺ T cells, with the main dominating subset composed of CD8 exhausted T cells, as depicted in the uniform manifold approximation and projection (UMAP) and heatmap (Figures 3D and S3C–S3J). By contrast, the analysis of the GLP-1R^{neg} CD3⁺ T cell subpopulation highlighted the presence of a dominating subset composed of CD8 effector memory T cells, with higher expression of the NK cell gene (Figures S3K–S3P). Additionally, the 11 clusters identified in the integrated dataset were further inspected with manually cured annotation, revealing T cell subpopulations such as CD4, CD8 naive, memory cells, CD4 regulatory T cells, and exhausted T cells (Figures 3F and

(D) Bar graph depicts results of flow cytometric analysis of GLP-1R expression by CD4⁺ and CD8⁺ T lymphocytes, together with pancreatic islets as positive control.

(E and F) Western blot analysis and associated quantification confirmed GLP-1R expression on CD4⁺/CD8⁺ T lymphocytes and on pancreatic islets.

(G) Bar graph representing normalized mRNA expression of *Glp-1r* in CD4⁺/CD8⁺ T lymphocytes and on pancreatic islets.

(H) *Glp-1r* mRNA expression was assessed by RT-qPCR in CD4⁺, CD8⁺ T cells, respectively, and in BTC6 cell line (used as positive control); reactions in which reverse transcriptase was omitted (−RT) were performed in parallel to test for DNA contamination; agarose gel electrophoresis analysis confirmed that the apparent size of the obtained RT-qPCR products was compatible to the expected amplicon length of 334 bp.

(I) Sanger sequencing further confirmed the identity of the amplification products and the expression of *Glp-1r* mRNA in CD4⁺ and CD8⁺ T cells.

(J₁ and J₂) Representative images of hematoxylin and eosin histology staining and immunoreactive GLP-1R^{pos} cells in murine thymus.

(K₁ and K₂) Hematoxylin and eosin histology staining and immunoreactive GLP-1R^{pos} cells in murine pancreas.

(L) Representative dot plots for gating strategy and GLP-1R expression by CD4⁺CD44[−]CD62L⁺ naive T cells, CD4⁺CD44⁺CD62L⁺ memory T cells, and CD4⁺CD44[−]CD62L[−] effector T cells.

(M) Quantification of flow cytometric analysis from (J).

(N) Representative dot plots for gating strategy and GLP-1R expression by CD8⁺CD44[−]CD62L⁺ naive T cells, CD8⁺CD44⁺CD62L⁺ memory T cells, and CD8⁺CD44[−]CD62L[−] effector T cells.

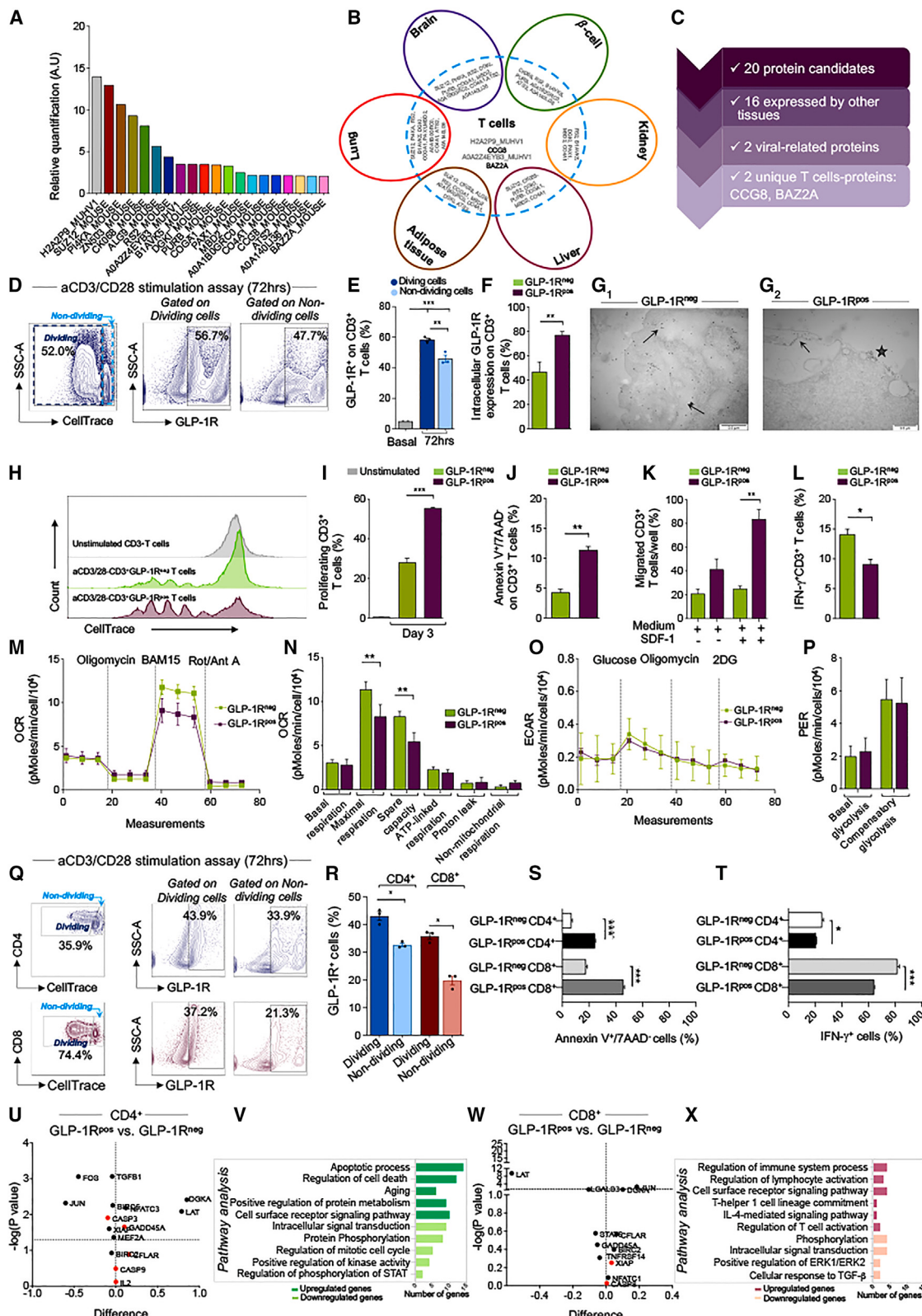
(O) Quantification of flow cytometric analysis from (L).

(P and Q) Representative dot plots for FACS analysis for GLP-1R expression of cell trace violet-labeled activated CD3⁺ T cells after 24, 72, and 120 h, respectively, are shown in (P), and their corresponding bar graphs are shown in (Q).

(R and S) Immunofluorescence staining depicting GLP-1R expression on murine CD3⁺ T cells at baseline as shown in (R) and on murine activated CD3⁺ T cells (S). Data are representative of at least $n = 2$ samples and are expressed as mean \pm standard error of the mean (SEM). * $p < 0.05$; ** $p < 0.01$; *** $p < 0.001$.

See also Figures S1 and S2.

Abbreviations: GLP-1R, glucagon-like peptide 1 receptor; BTC6, beta TC-6 cell line; qRT-PCR, two-step quantitative reverse transcriptase PCR; −RT, minus reverse transcriptase; H&E, hematoxylin and eosin; FACS, fluorescence-activated cell sorter scan; Abs, antibodies; EM, effector memory; and CM, central memory.

**Figure 2. GLP-1R^{pos} T cell profiling**

(A) Proteomic analysis showing the 20 peptides discovered to immunoprecipitate with GLP-1R on activated CD3⁺ T cells.

(B) Schematic Venn diagram depicting the GLP-1R interactome on T cells, versus those known on other tissues.

(legend continued on next page)

3G). Overall, our scRNA-seq analysis showed the existence of molecular and functional dissimilarities and heterogeneity between GLP-1R-expressing cells and their negative counterparts, with the former being mainly composed of CD8-exhausted T cells.

GLP-1R modulates T cell activation

In order to understand the molecular basis of GLP-1R signaling, we performed a phosphoproteomic arrays, with over 1,500 of known proteins tested for expression and activation during a T cell *in vitro* challenge with GLP-1R agonist. GLP-1R signaling in T cells altered several signaling molecules involved in senescence and exhaustion and in T cell receptor (TCR) signaling (Figures 4A and 4B). GLP-1R signaling with Exe-4 significantly reduced the number of IFN- γ producing cells by mitogen-stimulated murine splenocytes (Figure S4A), while the addition of Exe-9 significantly hampered the overseen effects. Exe-4 significantly increased cell death of CD4 $^{+}$ and CD8 $^{+}$ T cells, while the addition of Exe-9 reduced the effect (Figures S4B₁-S4C₂). To extend the importance of the data implicating CCG8 and BAZ2A into GLP-1R signaling on T cells, we tested the effect of their inhibition. Our data indicate that the addition of the BAZ2A inhibitor BAZ2-ICR, but not of CCG8-inhibitor JNJ 55511118, prevented the immunoregulatory effect of Exe-4 on activated CD3 $^{+}$ T cells and reinstated their IFN- γ production (Figure 4C). Exe-4 treatment slightly modulated the proliferation rate of GLP-1R $^{\text{pos}}$ but not of GLP-1R $^{\text{neg}}$ CD3 $^{+}$ T cells (Figure 4D). GLP-1R $^{\text{pos}}$ CD3 $^{+}$ T cells appeared significantly more apoptotic as compared with their counterparts GLP-1R $^{\text{neg}}$ CD3 $^{+}$ T cells, independently of Exe-4 treatment (Figure 4E). Although Exe-4 treatment reduced the migratory potential of GLP-1R $^{\text{neg}}$ CD3 $^{+}$ T cells only, no evident effect was observed on IFN- γ expression, with the GLP-1R $^{\text{pos}}$ CD3 $^{+}$ T cells migrating less and retaining lower IFN- γ expression (Figures 4F and 4G). Notably, the challenge of resting and activated GLP-1R $^{\text{pos}}$ and GLP-1R $^{\text{neg}}$ CD3 $^{+}$

T cells with multiple doses of Exe-4 showed reduced maximal respiration particularly of the former (Figures 4H and 4I). We further assessed the concentration of total GLP-1 in different assays, and we never detected the presence of GLP-1 (Figures S4D). We then wondered whether signaling through GLP-1R may influence Treg induction, function, and stability and upon co-culture with Exe-4. Our data indicate no substantial differences upon addition of Exe-4 to naive CD4 $^{+}$ CD25 $^{-}$ T cells during Treg induction assay (Figures S4E₁ and S4E₂). Additionally, we observed some effect on iTreg stability upon addition of Exe-4 with a significant reduction of Ror- γ T and Tbet (Figures S4F₁-S4G₂). Finally, when iTregs were generated in the presence of Exe-4 at a ratio of 1:4 to effector T cells, a significantly reduced suppression was observed as compared with when untreated iTregs were added at the same ratio (Figures S4H₁-S4H₄).

GLP-1R genetic gain of function

Next, we sought to determine the effect of GLP-1R genetic gain of function; indeed, GLP-1R cDNA was transduced by using a pRetroG-CMV-GLP-1R retroviral vector into CD3 $^{+}$ T cells (GLP-1Rtg CD3 $^{+}$ T cells), and upregulation of GLP-1R expression was confirmed by FACS (Figure S4I₁) and by western blot analysis (Figure S4I₂). Exe-4 treatment has no effect on the proliferation of both untransduced-mock and pmY-GLP-1R transduced CD3 $^{+}$ T cells (Figure 4J), while a significantly increased apoptosis was observed in pmY-GLP-1R transduced CD3 $^{+}$ T cells only (Figure 4K). Moreover, Exe-4 treatment reduced the migratory ability in response to SDF-1 in both untransduced-mock and pmY-GLP-1R transduced CD3 $^{+}$ T cells (Figure 4L) without any effect on IFN- γ expression in both groups (Figure 4M). In pmY-GLP-1R transduced CD3 $^{+}$ T cells, a reduced maximal respiration was observed as compared with untransduced-mock CD3 $^{+}$ T cells (Figures 4N and 4O).

(C) Strategy used to dissect the T cell-relevant interactome.

(D and E) GLP-1R expression by FACS analysis and related quantification of activated and dividing CD3 $^{+}$ T cells as compared with non-dividing CD3 $^{+}$ T cells.

(F and G₁) GLP-1R $^{\text{neg}}$ CD3 $^{+}$ appeared to have a significant intracellular GLP-1R expression by FACS analysis (F) and by electron microscopy in (G₁) where GLP-1R is present in cellular cytoplasm, predominantly in vesicles (arrows), but is absent in cell membrane (magnification: X50000 by electron microscopy).

(G₂) GLP1R is present both in cytoplasmic vesicles (arrows) and in cell membrane (stars) of GLP-1R $^{\text{pos}}$ CD3 $^{+}$ (magnification: X50000).

(H and I) Representative FACS plots of proliferating GLP-1R $^{\text{pos}}$ and GLP-1R $^{\text{neg}}$ CD3 $^{+}$ T cells with related quantification.

(J) GLP-1R $^{\text{pos}}$ CD3 $^{+}$ T cells appeared significantly more apoptotic as compared with their negative counterparts.

(K) The percentage of GLP-1R $^{\text{pos}}$ CD3 $^{+}$ T cells migrating to SDF-1 gradient was significantly higher as compared with their negative counterparts.

(L) Bar graph depicting the quantification of the percentage of IFN- γ on activated GLP-1R $^{\text{pos}}$ CD3 $^{+}$ T cells and on their negative counterparts.

(M and N) Higher OCR, maximal respiration, and spare capacity after mitochondrial membrane uncoupler BAM15 addition were observed in GLP-1R $^{\text{neg}}$ CD3 $^{+}$ T cells as compared with GLP-1R $^{\text{pos}}$ CD3 $^{+}$ T cells.

(O and P) Extracellular acidification rate (ECAR) and proton efflux rate (PER) measurements normalized to cell number, performed on GLP1R $^{\text{pos}}$ and GLP1R $^{\text{neg}}$ CD3 $^{+}$ T cells are shown. All respiratory parameters shown in (M)-(P) are obtained from 3 independent experiments, and data are presented as mean \pm standard error of the mean (SEM). A two-way ANOVA test was used to determine statistical significance.

(Q and R) GLP-1R expression by FACS analysis and related quantification was depicted on activated and dividing CD4 $^{+}$ and CD8 $^{+}$ T cells as compared with non-dividing CD4 $^{+}$ and CD8 $^{+}$ T cells.

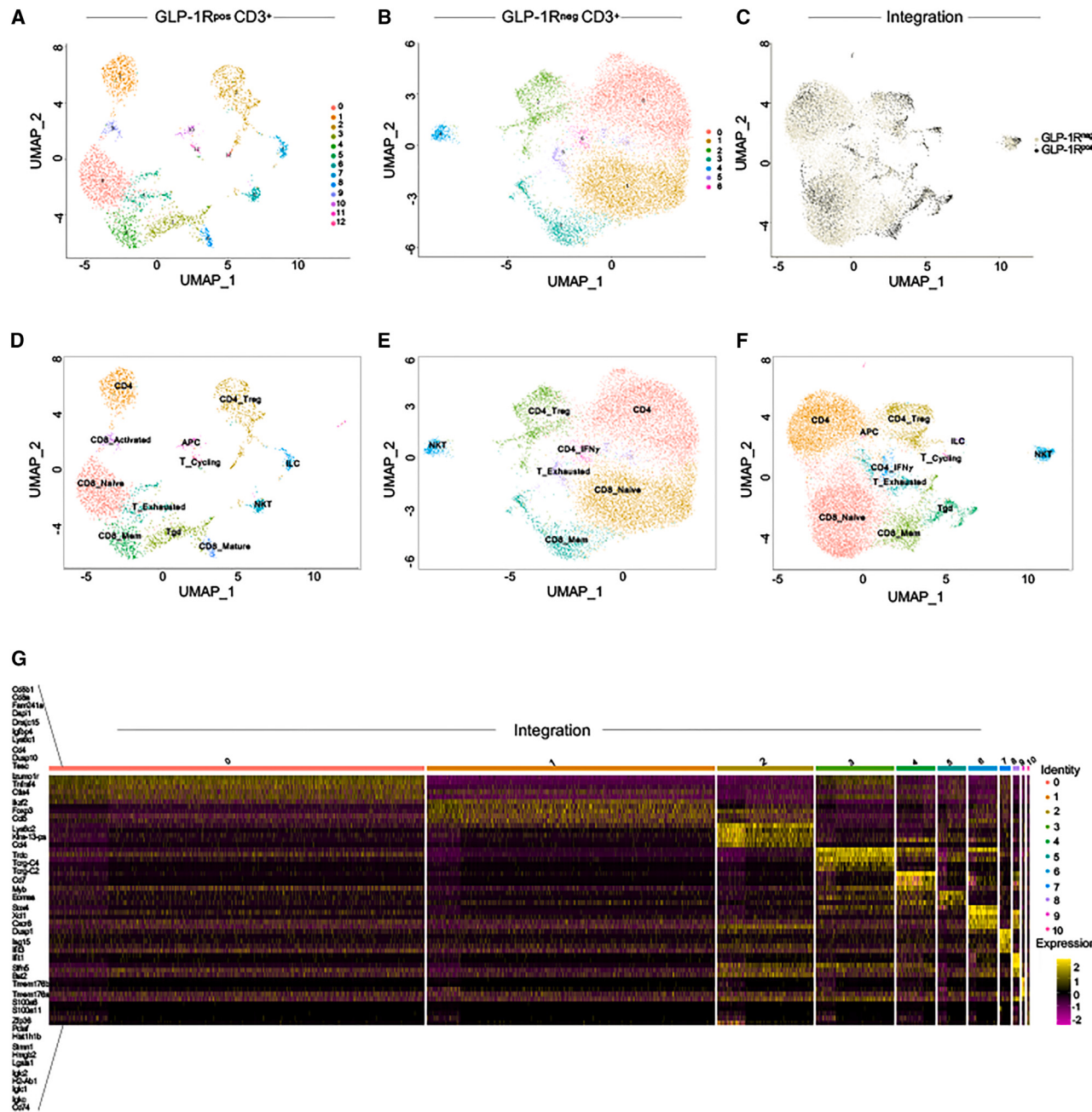
(S) GLP-1R $^{\text{pos}}$ CD4 $^{+}$ and CD8 $^{+}$ T cells were more apoptotic as compared with their negative counterparts.

(T) Bar graph showing the quantification of the percentage of IFN- γ on GLP-1R $^{\text{pos}}$ CD4 $^{+}$ and CD8 $^{+}$ and on their negative counterparts.

(U-X) Volcano plots and their related pathway analysis showing differently expressed genes in GLP-1R $^{\text{pos}}$ CD4 $^{+}$ cells versus GLP-1R $^{\text{neg}}$ CD4 $^{+}$ T cells and in GLP-1R $^{\text{pos}}$ CD8 $^{+}$ cells versus GLP-1R $^{\text{neg}}$ CD8 $^{+}$ T cells. In (V) and (X), the main biological function/pathway analysis of the dataset related to upregulated and downregulated genes on (U) GLP-1R $^{\text{pos}}$ CD4 $^{+}$ and on (W) GLP-1R $^{\text{pos}}$ CD8 $^{+}$ T cells are shown. Data are representative of at least $n = 2$ independent experiments. Data are expressed as mean \pm standard error of the mean (SEM). Data are representative of at least $n = 3$ mice. * $p < 0.05$; ** $p < 0.01$; *** $p < 0.001$.

See also Figure S2 and Table S1.

Abbreviations: GLP-1R, glucagon-like peptide 1 receptor; OCR, oxygen consumption rate; SRC, spare respiratory capacity; CT, cell trace; FACS, fluorescence-activated cell sorter; IFN- γ , interferon gamma; ECAR, extracellular acidification rate; PER, proton efflux rate.

**Figure 3. scRNA-seq of GLP-1R^{pos} T cells**

(A and B) Uniform manifold approximation and projection (UMAP) for, respectively, sorted GLP-1R^{pos} and GLP-1R^{neg} CD3⁺ T cells showing 13 cell clusters in the former (A) and 7 main clusters in the latter (B) by using 30 nPCs and 0.5 resolution and 0.2 resolution, respectively.

(C) UMAP showing the clustering of the integrated dataset.

(D–F) Annotation of different T cell subtypes composing each cluster related to, respectively, GLP-1R^{pos} and GLP-1R^{neg} CD3⁺ T cells, and the integrated dataset is shown.

(G) Heatmap showing the top marker genes for each cluster within the integrated dataset.

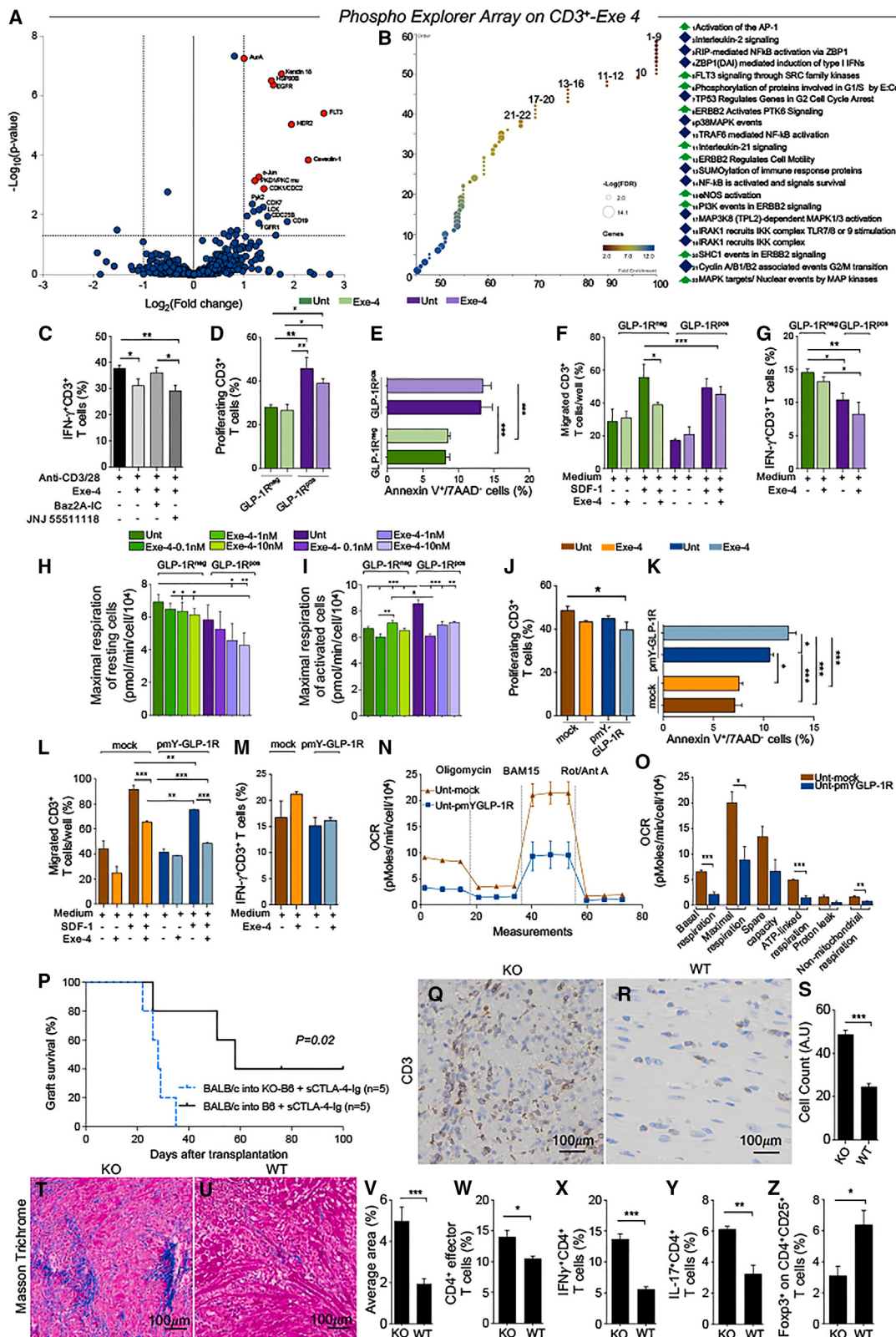
See also [Figure S3](#).

Abbreviations: scRNA-seq, single-cell RNA sequencing; GLP-1R, glucagon-like peptide 1 receptor; and UMAP, uniform manifold approximation and projection.

GLP-1R genetic loss of function

To extend our findings into an *in vivo* setting, we used GLP-1R knockout (KO) mice ([Figure S4J](#)), and the absence of GLP-1R

was confirmed within several immune organs ([Figures S4K1–S4O₂](#) and [S4P₁–S4P₃](#)). A reduced CD3⁺ T cell apoptotic rate with an increased percentage of IFN- γ ⁺CD3⁺ T cells was seen



(legend on next page)

when GLP-1R is genetically knocked down (Figures S4Q–S4S and S4T₁). Moreover, the percentage of CD3⁺ T cells from GLP-1R KO mice migrating to SDF-1 gradient was significantly lower as compared with their counterparts from WT mice (Figure S4T₂). We then tested the effect of lacking a viable GLP-1R signaling in an *in vivo* murine model of allograft tolerance in the tolerogenic low-dose CTLA4-Ig model. Although WT recipients showed an extended survival of the allograft (MST = 58 days), an acceleration of heart allograft rejection was observed in the GLP-1R KO mice (MST = 28 days) (Figure 4P). Pathology of allograft showed a severe and accentuated infiltration of CD3⁺ and CD8⁺ T cells (Figures 4Q–4S, S4U₁–S4V₂, and S4W), with an increase in the degree of fibrosis in the GLP-1R KO group (Figures 4T–4V). A substantial increase in CD4 effector T cells as well as significant increases in the percentages of IFN- γ ⁺ CD4⁺ T cells and IL-17⁺ CD4⁺ T cells (Figures 4W–4Y) and slightly in CD8 effector T cells (Figure S4X) were evident in the GLP-1R KO mice. Importantly, significant increase in the percentage of IL-17⁺ CD8⁺ T cells, but not of IFN- γ ⁺ CD8⁺ T cells, was observed in GLP-1R KO recipients as compared with WT recipients (Figures S4Y and S4Z), with a marked decrease in CD4⁺ Tregs in the GLP-1R KO group (Figure 4Z). Our results indicate that GLP-1R signaling may modulate the alloimmune response.

GLP-1R and islet allograft

In an *in vivo* murine models of islet allotransplantation, GLP-1R expression was confirmed on splenic CD4⁺ and CD8⁺ T cells at baseline without infiltration (Figures 5A–5D and S5A–S5D). At day 14, all mice displayed acute allograft rejection associated

with an increase in GLP-1R^{pos} cells among both splenic and islet allograft infiltrating CD4⁺ and CD8⁺ T cells (Figures 5A–5D and S5A–S5D). The presence of graft-infiltrating GLP-1R^{pos} T lymphocytes at day 14 was further confirmed by confocal microscopy and immunohistochemistry analysis (Figures 5D₁–5F). Interestingly, the administration of low dose of the GLP-1R agonist (Exe-4) resulted in a prolongation of islet survival up to 100 days in 20% of the recipients ([MST] = 41 days), while 60% of those that received high doses of Exe-4 preceded by a pre-treatment showed a prolongation of islet survival up to 100 days ([MST] = 67 days) (Figure 5G). The co-administration of Exe-4 and rapamycin was associated with 100% of graft survival at the end of follow-up (day 100) (Figure 5G). The beneficial effects of Exe-4 were partly abolished by the co-administration of its antagonist Exe-9 (Figure S5E). A decreased graft infiltration was evident in Exe-4-treated mice, while the co-administration of Exe-9 restored the graft infiltration (Figures S5F₁–S5J). Notably, SDF-1 immunostaining revealed a mild SDF-1 expression within islet allograft infiltrate, matching CXCR4 expression by GLP-1R^{pos} cells (Figures S5K₁–S5L₂). Taken together, our results confirmed that GLP-1R is upregulated on T cells during islet allograft rejection and GLP-1R signaling has immunoregulatory effect.

GLP-1R and heart allograft

Because of the wide range of effects that GLP-1R has on islets,⁷ which may confound the immunological effect, we next sought to confirm the islet-independent immunoregulation of GLP-1R-signaling by using a major histocompatibility complex (MHC)-fully mismatched model of heart transplantation. At day 7, all

Figure 4. GLP-1R modulates T cell activation

(A and B) Differential profiling analysis of phosphoproteomic array performed on murine CD3⁺ T cells challenged with Exe-4 (1 nM) as compared with their counterparts untreated; volcano plot depicting main differences in phosphoproteomics between the 2 groups of cells (A); the bubble chart of the reactome analysis of the main 60 phosphoproteomics dysregulated during Exe-4 treatment (B). Data represent $n = 3$ samples per conditions.

(C) BAZ2A inhibitor BAZ2-ICR, but not of CCG8-inhibitor JNJ 55511118, prevented the immunoregulatory effect of Exe-4 on activated CD3⁺ T cells and reinstated their IFN- γ production.

(D) Exe-4-treatment slightly modulated the proliferation rate of GLP-1R^{pos} T cells.

(E) GLP-1R^{pos} CD3⁺ T cells appeared significantly more apoptotic as compared with their negative counterparts.

(F) Exe-4-treatment reduced the migratory potential of GLP-1R^{neg} CD3⁺ T cells only.

(G) GLP-1R^{pos} CD3⁺ T cells retained lower IFN- γ expression as compared with their negative counterparts.

(H and I) Exe-4 treatment reduced the maximal respiration of resting and activated GLP-1R^{pos} CD3⁺ T cells.

(J) Exe-4 treatment has no effect on the proliferation of both untransduced-mock and pmY-GLP-1R transduced CD3⁺ T cells.

(K) Exe-4 treatment increased significantly apoptosis in pmY-GLP-1R transduced CD3⁺ T cells only.

(L) Exe-4 treatment reduced the migratory ability in response to SDF-1 in both untransduced-mock and pmY-GLP-1R transduced CD3⁺ T cells.

(M) No effect on IFN- γ expression was observed in both untransduced-mock and pmY-GLP-1R transduced CD3⁺ T cells in response to Exe-4 treatment.

(N and O) In pmY-GLP-1R transduced CD3⁺ T cells, a reduced maximal respiration was observed as compared with untransduced-mock CD3⁺ T cells. Data are representative of at least $n = 3$ /group and are expressed as mean \pm standard error of the mean (SEM). Statistical significance was assessed by two-way ANOVA.

* $p < 0.05$; ** $p < 0.01$; *** $p < 0.001$.

(P) Heart allograft survival curves from GLP-1R^{-/-} mice or from WT recipients' mice of heart allograft from fully mismatched BALB/c mice and treated with low-dose CTLA4-Ig.

(Q–S) Micrographs of CD3 staining in heart allograft sections from either WT or GLP-1R KO recipients; in (S) bar graph shows the relative quantification of heart infiltrating CD3⁺ cells in both groups.

(T–V) Representative Masson-trichrome histology staining of heart allografts, respectively, from GLP-1R KO or from WT recipients' mice; the average area of fibrosis in heart allografts from both groups of recipients' mice is shown in (V).

(W) Bar graph depicting the quantification of CD4⁺ effector-memory splenocytes in GLP-1R KO or WT recipients' mice.

(X) Bar graph depicting the quantification of IFN- γ ⁺ CD4⁺ T cells in GLP-1R KO or WT recipients' mice.

(Y) Bar graph depicting the quantification of IL-17⁺ CD4⁺ T cells in GLP-1R KO or WT recipients' mice.

(Z) Bar graph depicting the quantification of CD4⁺ regulatory splenocytes in both groups of mice that underwent heart allograft transplantation. Data are representative of at least $n = 3$ mice and are expressed as mean \pm standard error of the mean (SEM). * $p < 0.05$; ** $p < 0.01$; *** $p < 0.001$.

See also Figure S4.

Abbreviations: GLP-1R, glucagon-like peptide 1 receptor; Exe-4, exendin-4; Exe-9, exendin-9-39; FACS, fluorescence-activated cell sorter scan; BAZ2A, bromodomain adjacent to zinc-finger domain 2A; CCG8, voltage-dependent calcium channel gamma-8 subunit; WT, wild type; IFN- γ , interferon gamma; CTLA4, cytotoxic T lymphocyte antigen 4; BAM15 (N5,N6-bis(2-Fluorophenyl)[1,2,5]oxadiazolo[3,4-b]pyrazine-5,6-diamine); and FoxP3, forkhead box P3.

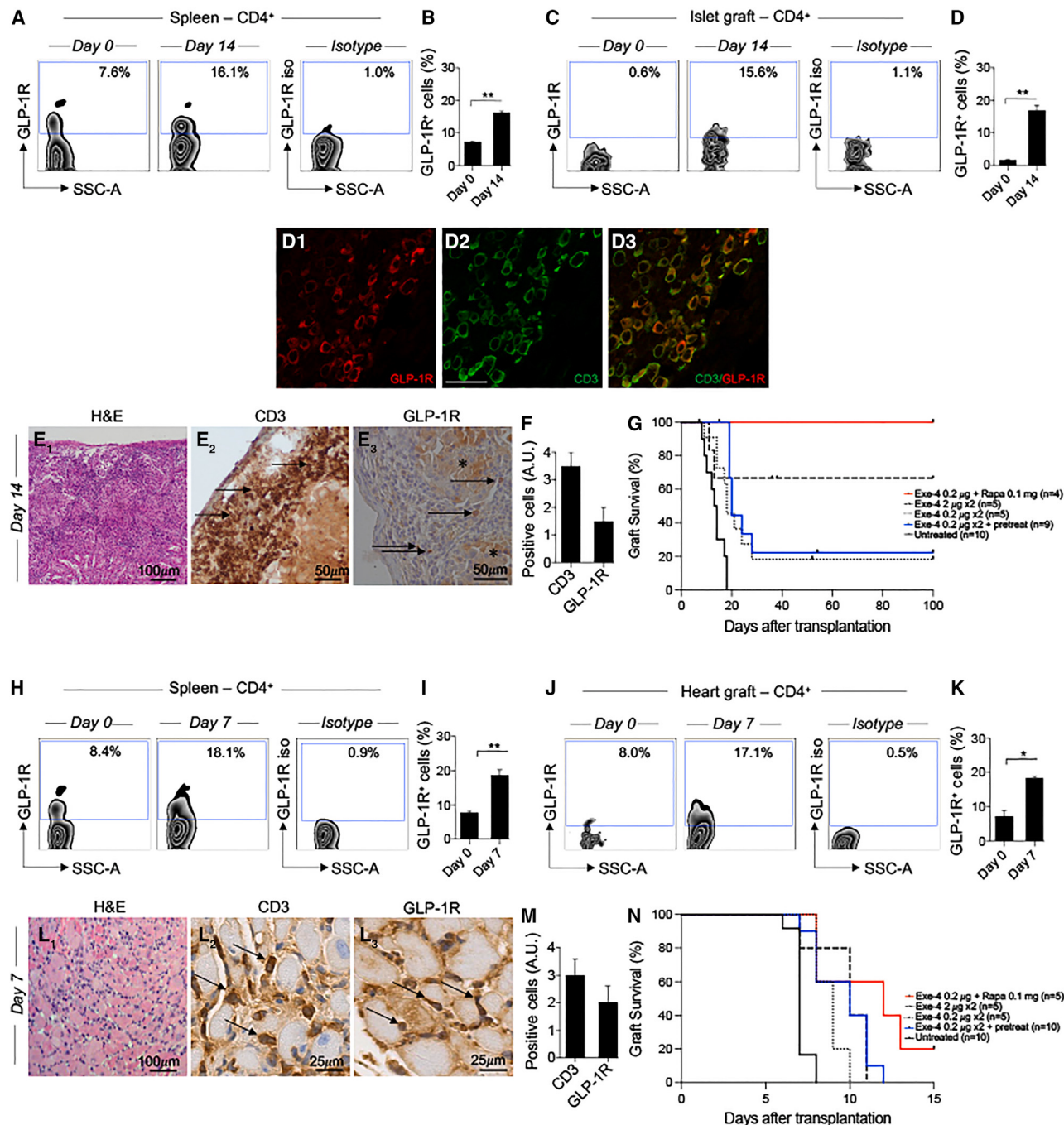


Figure 5. GLP-1R and allograft

- (A) Representative zebra plot of GLP-1R expression by splenic murine CD4⁺ T lymphocytes in basal condition and after islet allotransplantation.
- (B) Bar graph representing quantification of GLP-1R expression by spleen CD4⁺ lymphocytes in basal condition and after islet allotransplantation.
- (C) Representative zebra plot of GLP-1R expression by murine kidney CD4⁺ T lymphocytes in basal condition and after islet allotransplantation under kidney capsule.
- (D) Bar graph representing quantification of GLP-1R expression by CD4⁺ lymphocytes in normal kidneys and after islet allotransplantation.
- (D₁–D₃) Confocal microscopy analysis of islet infiltrating lymphocytes within islet allograft at day 14, depicting the colocalization of GLP-1R on CD3⁺ T cells, magnification: 63×, scale bars, 20 μm.
- (E₁) Hematoxylin and eosin staining depicts the immune infiltrate within the islet allograft at day 14.
- (E₂) Islet allograft immunohistochemistry for CD3⁺ cells (arrows).
- (E₃) Islet allograft immunohistochemistry for GLP-1R^{pos} cells (arrows).

(legend continued on next page)

mice displayed acute allograft rejection associated with an increase in GLP-1R^{pos} cells among both splenic (Figures 5H, 5I, S5M, and S5N) and heart allograft infiltrating CD4⁺ and CD8⁺ T cells (Figures 5J, 5K, S5O, and S5P). The presence of graft-infiltrating GLP-1R^{pos} T lymphocytes at day 7 was confirmed by immunohistochemistry analysis, while cardiomyocytes and other parenchymal cells appeared negative for GLP-1R staining (Figures 5L₁–5M). Moreover, while untreated recipients rejected cardiac allograft within a range of 7 days ([MST] = 7 days) (Figure 5N), Exe-4-treated recipients receiving either a low or a high dose of Exe-4 proceeded or not with pre-treatment showed a significant delay in allograft rejection (respectively [MST] = 9 and 10 days) (Figure 5N). Notably, transplanted mice receiving a combination therapy with Exe-4 and rapamycin showed indefinite long-term cardiac transplant survival in almost 20% of recipients ([MST] = 39 days) (Figure 5N). The beneficial effects of Exe-4 were partly abolished by the co-administration of Exe-9 (Figure S5Q). A decrease of graft infiltration was shown in Exe-4-treated mice and abolished by Exe-9 co-administration (Figures S5R1–S5V). We also confirmed that total/active GLP-1 and Exe-4 peripheral levels were not affected by allotransplantation, while GLP-1, but not Exe-4 levels, increased in Exe-4-treated mice (Figures S5W–S5Y). In a tentative to test the effect of GLP-1R on a more selective way, we performed a series of adoptive transfer studies of WT and GLP-1R KO T cells in a model of heterotopic intra-abdominal heart transplantation, where recipients C57BL/6 Rag1^{-/-} mice received a heart transplant from BALB/c. On the day of transplant, all recipients received an adoptive transfer of either splenic WT CD3⁺ T cells or of splenic GLP-1R KO CD3⁺ T cells in the latter accelerating allograft rejection in the Rag1^{-/-} group (Figure S5Z₁). Furthermore, genetic loss of function of GLP-1R did not affect alloantibody formation neither the levels of circulating follicular helper T cells (cTfh) in both groups (Figures S5Z₂ and S5Z₃). Heart transplantation data confirmed what is obtained in the islet model and further suggested the relevance of GLP-1R signaling for T cell compartment.

GLP-1R antagonism triggers antitumor immunity

To investigate the hypothesis that GLP-1R may play a role as an immune checkpoint, we studied the tumor response to a systemic administration of a GLP-1R antagonist, Exendin-9-39 (Exe-9), in an experimental murine model of colorectal cancer.

In this model, we injected MC38 colorectal cancer cells into the distal posterior rectum as described previously,¹⁹ a group of mice ($n = 8$) were assigned to receive 2 µg of Exe-9 once a day for 14 days; another group of mice ($n = 6$) were left untreated (Figures 6A and 6B). Indeed, mice treated with Exe-9 showed a significantly reduced tumor size (Figure 6C) and mesenteric lymph nodes volume (Figure 6D), while no differences were observed comparing spleen weight and colon length in both groups (Figures 6E and 6F). Pathological examination of the tumors in both groups revealed a significant intratumoral infiltration of CD3⁺ T cells within Exe-9-treated group (Figures 6G–6I). Additional mechanistic studies on the tumors from both groups further confirmed the increased infiltration of CD3⁺ T cells in the Exe-9-treated group (Figure 6J) and of particularly activated effector memory CD8⁺ T cells (Figures 6K–6M). However, no major differences were observed comparing CD3⁺ and CD8⁺ effector memory T cells within the spleen and mesenteric lymph nodes of both groups (Figures 6N–6Q). Altogether, our data showed an evident proof of concept that GLP-1R antagonist may trigger T cell-mediated anti-tumor activity.

GLP-1R in human T cells

Our data confirmed the expression of GLP-1R on human CD4⁺ and CD8⁺ T cells (Figures 7A–7D). Human peripheral blood mononuclear cells (PBMCs) extracted from healthy individuals revealed at FACS analysis an average GLP-1R expression on CD4⁺ and CD8⁺ T cells of about 6.1% ± 1.2% and 28.3% ± 4.1%, respectively (Figures 7A–7D), while human islets express GLP-1R at an average of 46.3% ± 0.2% (Figures 7C and 7D). GLP-1R expression on T cells was further confirmed at protein level and at mRNA transcript (Figures 7E–7G). Consistently with murine data, GLP-1R expression was found by immunohistochemistry in human thymus and pancreas (Figures 7H₁–7I₂). *In situ* hybridization confirmed the expression of GLP-1R mRNA in human thymus and spleen (Figures S6A and S6B). Notably, GLP-1R expression was evident in human regulatory CD4⁺ T cells (Figures S6C and S6D), in effector memory CD4⁺ and CD8⁺ T cells (Figures 7J–7M), although central memory CD4 and CD8 T cells appeared to express GLP-1R at a lower extent (Figures 7J–7M). Importantly, CD4⁺/CD8⁺ terminally differentiated effector memory T cells appeared highly positive for GLP-1R (Figures 7J–7M). Paralleling our findings in murine studies, we sought to determine whether GLP-1R plays a role during

(F) Bar graph displaying the quantification of CD3⁺ and GLP-1R^{pos} cells in islet allograft.

(G) Islet allograft survival curves from mice treated with different doses of exenatide (dashed line) or saline (continuous line).

(H) Representative zebra plot of GLP-1R expression by splenic murine CD4⁺ T lymphocytes obtained from mice in basal condition or after heart allograft transplantation.

(I) Bar graph representing quantification of (H).

(J) Representative zebra plot of GLP-1R expression by heart allograft infiltrating CD4⁺ T lymphocytes obtained from mice in basal condition or after heart allograft transplantation.

(K) Bar graph representing the quantification of (J).

(L) (L₁) Hematoxylin and eosin histology staining depicts the immune infiltrate within the heart allograft at day 7.

(L₂) Heart allograft immunohistochemistry for CD3⁺ cells (arrows).

(L₃) Heart allograft immunohistochemistry for GLP-1R^{pos} cells (arrows).

(M) Bar graph displaying the quantification of CD3⁺ and GLP-1R^{pos} cells in heart allograft.

(N) Heart allograft survival curves from mice treated with different doses of exenatide (dashed line) or saline (continuous line). Data are representative of at least $n = 3$ mice and are expressed as mean ± standard error of the mean (SEM). * $p < 0.05$; ** $p < 0.01$; *** $p < 0.001$.

See also Figure S5.

Abbreviations: GLP-1R, glucagon-like peptide 1 receptor; FACS, fluorescence-activated cell sorter scan; H&E, hematoxylin and eosin.

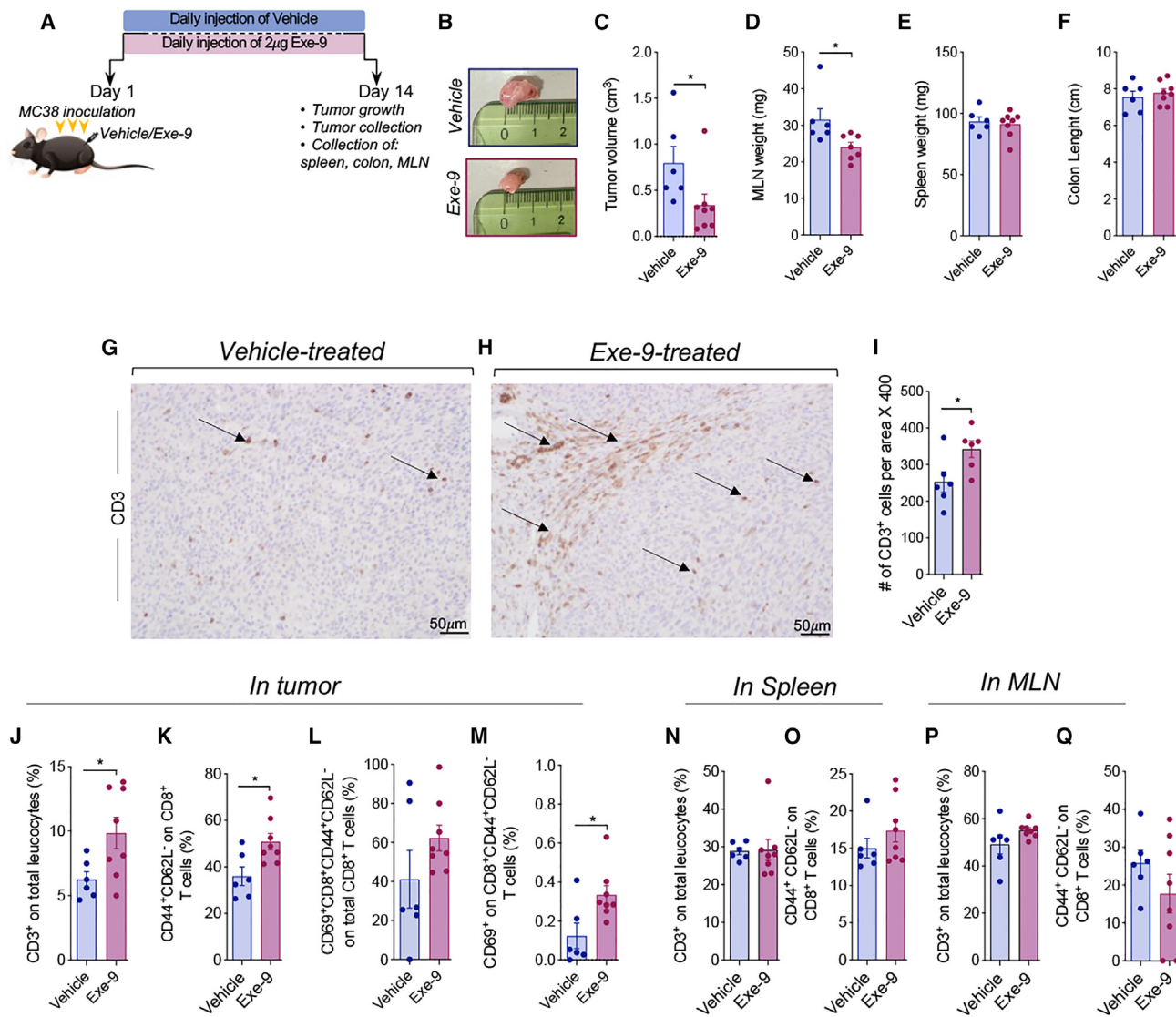


Figure 6. GLP-1R antagonism triggers an antitumor immunity

(A) Schematic overview of the study protocol.

(B) Representative pictures of tumors extracted from, respectively, MC38 tumor-bearing mice treated with vehicle (PBS) or treated with Exe-9 at day 14.

(C–F) Quantitative bar graph depicting tumor volume, mesenteric lymph nodes (MLN) weight, spleen weight, and colon weight of vehicle-treated or Exe-9-treated mice.

(G–I) Representative immunohistochemical images showing intratumoral CD3 staining from vehicle-treated or Exe-9-treated mice and their related quantification are shown in (I).

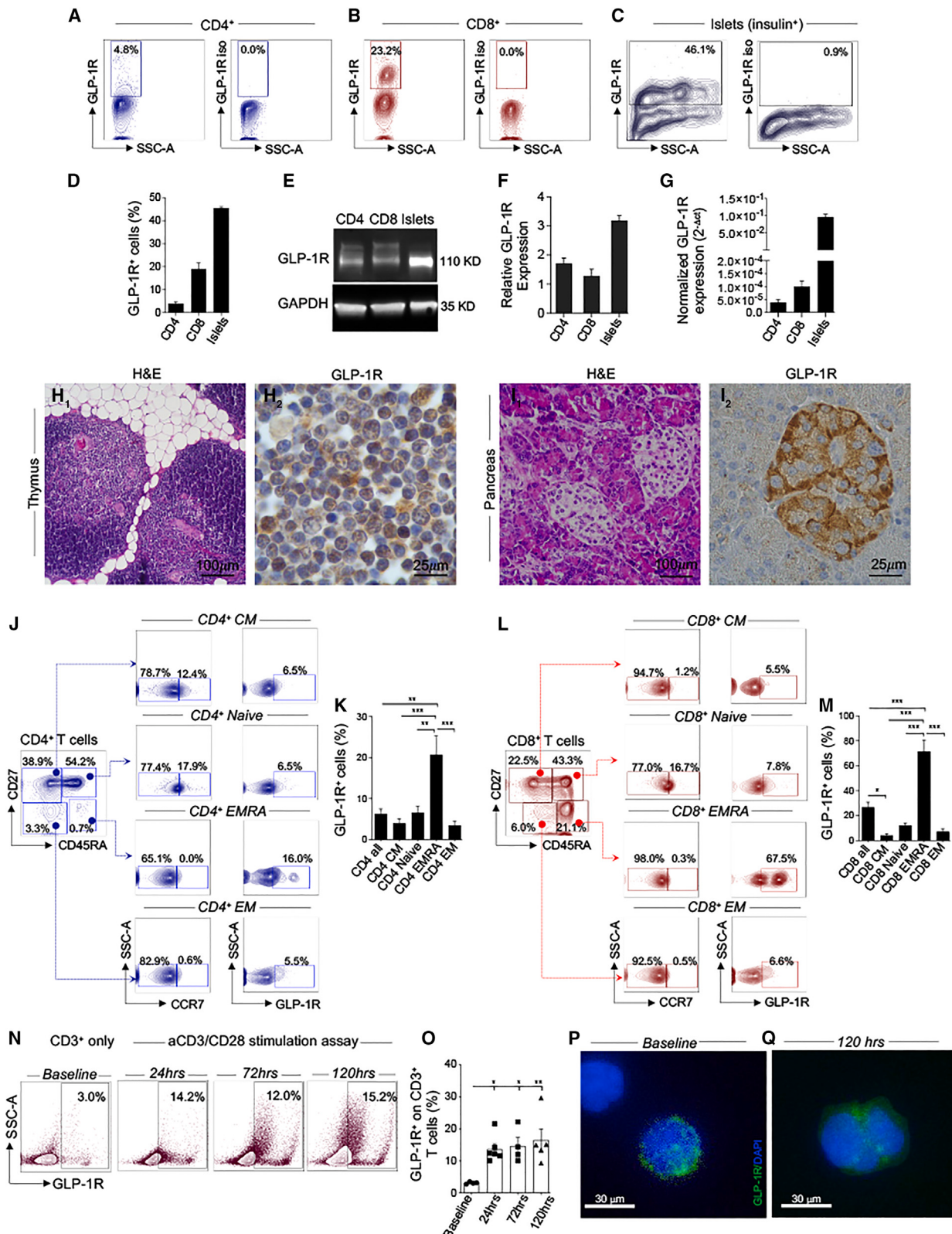
(J–M) Quantitative bar graph depicting FACS quantification of tumor-infiltrating CD3⁺ T cells, CD8⁺ effector memory T cells, and activated CD8⁺ T cells within total CD8⁺ T cells (L) or within CD8⁺ effector memory T cells (M), extracted from vehicle-treated or Exe-9-treated mice.

(N–Q) Quantitative bar graph depicting FACS quantification of total splenic CD3⁺ T cells and CD8⁺ effector memory T cells or CD3⁺ T cells and total CD8⁺ effector memory T cells extracted from MLNs of vehicle-treated or Exe-9-treated mice. Data are representative of, respectively, $n = 6$ and $n = 8$ samples from vehicle-treated and Exe-9-treated mice and are expressed as mean \pm standard error of the mean (SEM). * $p < 0.05$; ** $p < 0.01$; *** $p < 0.001$.

Abbreviations: GLP-1R, glucagon-like peptide 1 receptor; Abs, antibodies; FACS, fluorescence-activated cell sorter scan; and MLNs, mesenteric lymph nodes.

TCR-mediated stimulation. GLP-1R protein expression increased after 24 h following TCR stimulation and peaked at 120 h (Figures 7N and 7O). Immunofluorescence confirmed our observation showing substantial increase in GLP-1R protein expression on CD3⁺ T cells (Figures 7P and 7Q). Proliferating CD3⁺ T cells, analyzed with cell trace dilution upon TCR stimulation, appeared highly expressing GLP-1R as compared with their

counterparts non-dividing/proliferating CD3⁺ T cells (Figures S6E and S6F). The same observation was confirmed on dividing CD4⁺ T cells and CD8⁺ T cells where a significant increase in GLP-1R expression was evident as well (Figures S6G and S6H). Taken together, these findings underlined the expression of GLP-1R in human T cells and a substantial upregulation upon proximal TCR stimulation. Next, we posit to explore the

**Figure 7. GLP-1R in human T cells**

(A and B) Representative dot plot of GLP-1R expression by human circulating CD4⁺ and CD8⁺ cells.
(C) Representative dot plots of GLP-1R expression by human pancreatic islets (positive control).

(legend continued on next page)

relevance and the presence of GLP-1R in a series of graft-rejecting biopsies obtained from individuals recipients of kidney, heart, or lung allografts (Figure S7; Tables S2 and S3). We first evaluated the expression of GLP-1R in human renal biopsies obtained from patients experiencing allograft rejection. Significant GLP-1R^{pos} CD3⁺ T cell intragraft infiltration was observed, while no evidence of GLP-1R^{pos} CD3⁺ T cells was found neither in control biopsies nor in cases of antibody-mediated kidney rejection (Figures S7A₁–B₃ and S7I–S7L₃). We then confirmed the relevance of GLP-1R^{pos} CD3⁺ T cells in heart and lung allograft rejection. Particularly, GLP-1R^{pos} CD3⁺ T cells were observed in biopsies obtained from cardiac-transplanted patients, with and without features of cardiac allograft rejection and vasculopathy (Figures S7C₁–S7D₃). Additionally, we reported the presence of intragraft GLP-1R^{pos} CD3⁺ T cells in lung biopsies obtained from cases with chronic lung allograft rejection (Figures S7E₁–S7F₃). Taken together, our clinical finding further reinforced and confirmed the relevance of GLP-1R in clinical allograft rejection.

DISCUSSION

Our study demonstrated that GLP-1R receptor is expressed by a variety of T cell subsets, and it has a role in controlling T cell activation, IFN- γ production, cell metabolism, and death, thus acting as a negative costimulatory molecule. Recent evidence suggested that GLP-1R may have a role in immune response²⁰; indeed the use of several GLP-1R agonists (exenatide and liraglutide) offered substantial benefits in a wide range of inflammatory diseases.^{14,16,21,22} We detected a discrete population of GLP-1R^{pos} cells, mainly located within CD4⁺ and CD8⁺ effector memory T cells, which increased substantially after alloimmune response. Interestingly, we also show that the use of GLP-1R agonist modulates the T cell alloimmune response and preserve allograft survival. The presence of GLP-1R on T cells is associated with a shift toward an anergic profile, as confirmed by the substantial expression of exhaustion and anergy-related genes, which may support the hypothesis that GLP-1R plays a role of negative costimulatory molecule during immune response. GLP-1R modulation is a successful therapeutic strategy for patients affected by type 2 diabetes.^{23–25} Either the direct receptor

agonists or the inhibitors of GLP-1 inactivating enzyme (DPP4) are effective, safe, and associated with a variety of beneficial effects not always connected to glycemic control.^{26–29} In parallel, the wide distribution of GLP-1R outside of the endocrine and digestive tissues has been associated in clinical trials with a variety of intriguing findings, again not associated with glycemic control. Exenatide therapy was able to improve Parkinson disease symptoms,³⁰ was able to resolve non-alcoholic steatohepatitis (NASH) in a higher percentage of patients as compared with placebo,³¹ and was able to reduce myocardial infarct size after revascularization,³² and in diabetic patients, it may have prevented chronic kidney disease independently from the glycemic control.³³ The first clinical proof of the role of GLP-1R in the immune system was a serendipity finding: a small series of patients, affected by both psoriasis and diabetes, experienced a substantial improvement of dermatitis with Exenatide therapy.^{14,34} Subsequently, symptoms worsened when Exenatide was discontinued, due to nausea, and improved again when it was restarted. After this report, different authors investigated the anti-inflammatory proprieties of GLP-1R: several studies focused on macrophages³⁵ and some on T lymphocytes.^{11,13,16,36–38} The importance of GLP-1R in limiting gut intraepithelial-lymphocyte-related inflammation has been reportedly described by suppressing their effector function and dampening TCR proximal signaling in a PKA-dependent manner.³⁹ *In vivo*, Exenatide was able to delay diabetes onset and to prolong islet transplantation in NOD mice.^{15,16} Our data showed that GLP-1R expression is limited to CD4 and CD8 effector-memory and regulatory T cells and is not detectable in central-memory and naive subsets. Furthermore, our study showed that a population of terminally differentiated effector memory CD4⁺ and CD8⁺ T cells (i.e., EMRA T cells) expresses GLP-1R at the highest levels; indeed, terminally differentiated effector memory T cells are described in the literature as having high tendency to apoptosis and cytotoxic activity, and their active role in allotransplant rejection has been established.^{40,41} On the contrary, most of the quiescent T cells do not express GLP-1R. Interestingly, the existence of a large GLP-1R reservoir within T cells, which can be mobilized at time during T cell activation and during *in vitro* assays, may render some of the assays themselves less reproducible. Although, several cellular compartments of innate immunity

(D) Bar graph depicts results of flow cytometric analysis of GLP-1R expression by CD4⁺/CD8⁺ T lymphocytes and pancreatic islets.

(E and F) Western blot analysis and associated quantification confirm GLP-1R expression on CD4⁺/CD8⁺ T lymphocytes and pancreatic islets.

(G) Bar graph representing normalized mRNA expression of GLP-1R in CD4⁺/CD8⁺ T lymphocytes and pancreatic islets.

(H and I) (H₁–I₂) Representative images of hematoxylin and eosin histology staining and immunoreactive GLP-1R^{pos} cells in human thymus and pancreas, respectively.

(J) Representative dot plots for gating strategy and GLP-1R expression by CD4⁺CD45RA⁺CD27⁺CCR7⁺ naive T cells, CD4⁺CD45RA⁻CD27⁺CCR7⁺ central memory T cells, CD4⁺CD45RA⁻CD27⁻CCR7⁺ effector memory T cells, and CD4⁺CD45RA⁺CD27⁻CCR7⁺ terminally differentiated effector memory T cells.

(K) Quantification of flow cytometric analysis from (J).

(L) Representative dot plots for gating strategy and GLP-1R expression by CD8⁺CD45RA⁺CD27⁺CCR7⁺ naive T cells, CD8⁺CD45RA⁻CD27⁺CCR7⁺ central memory T cells, CD8⁺CD45RA⁻CD27⁻CCR7⁺ effector memory T cells, and CD8⁺CD45RA⁺CD27⁻CCR7⁺ terminally differentiated effector memory T cells.

(M) Quantification of flow cytometric analysis from (L).

(N and O) Representative dot plots for FACS analysis of activated cell trace violet-labeled CD3⁺ T cells after, respectively, 24, 72, and 120 h (N) and their corresponding bar graphs (O).

(P) Immunofluorescence staining depicting GLP-1R expression on CD3⁺ T cells at baseline.

(Q) Immunofluorescence staining depicting GLP-1R expression on activated CD3⁺ T cells. Data are representative of at least $n = 3$ samples and are expressed as mean \pm standard error of the mean (SEM). * $p < 0.05$; ** $p < 0.01$; *** $p < 0.001$.

See also Figures S6 and S7 and Tables S2 and S3.

Abbreviations: GLP-1R, glucagon-like peptide 1 receptor; Abs, antibodies; FACS, fluorescence-activated cell sorter scan; EM, effector memory; CM, central memory; EMRA, terminally differentiated effector memory expressing CD45RA.

express GLP-1R at a moderate level.^{42–44} GLP-1R^{pos} CD4 and CD8 cells infiltrate the graft at high percentage and are expanded in the spleen of transplanted mice, while the treatment with GLP-1R agonist was able to prevent heart and islet graft infiltration and to prolong graft survival. Pharmacological and genetic modulation of GLP-1R all confirm that the signaling through the receptor is immunoregulatory, while the absence of GLP-1R accelerate the rejection in chronic heart transplant model of CTLA4-Ig-induced tolerance. Interestingly, GLP-1R expression and function mimick those shown by PD-1; indeed, GLP-1R antagonism applied into a relevant murine cancer model *in vivo* was able to trigger an anti-tumor immune response. Gain-of-function experiments confirmed the aforementioned GLP-1R-mediated effects; indeed, GLP-1R showed a unique interactome in T cells involving many rRNA gene repressors including Baz2a, which appeared mandatory for the delivery of the negative costimulatory effect. A scRNA-seq study clarified the deep difference and specificity of GLP-1R^{pos} T cells as compared with their negative counterparts. In conclusion, in this paper, we demonstrated that the expression of GLP-1R delineates a subset of activated T lymphocytes. GLP-1R^{pos} T lymphocytes are expanded during the alloimmune response, and GLP-1R signaling strives a T cell-negative costimulatory signal mimicking those shown by PD-1^{45–49} but through an rRNA gene repressor interactome, which recognizes Baz2a as main player.

Limitations of the study

Our study demonstrated that GLP-1R is a key regulator of lymphocyte activation during immune response, and it may act as a T cell-negative costimulatory molecule. However, we should consider that because of the wide expression of GLP-1R, some of the observed effects may not be entirely related to the targeting of T cells but of other immune cells. We then demonstrated that the antagonism of GLP-1R triggers an anti-tumor immunity, whereas only one model of murine cancer was tested, and we cannot assure that the mechanism is replicable in other murine cancer models. Moreover, it is interesting to observe that because the expression of GLP-1R parallel the expression of PD-1, the interaction between GLP-1R and other costimulatory molecules (i.e., CTLA-4, ICOS, and CD160) may explain some of the effects seen in our system, and thus, the results might be redundantly over-reported. We injected 2 µg of Exendin (9–39) two times a day for 14 days in a colorectal murine cancer model; however, it is possible that this amount may increase glycemic levels in mice and reduce insulin levels, thus inducing glucose toxicity, which may interfere with tumor growth. Finally, some of the *in vitro* experimental data may be suffering by the presence of a large GLP-1R intracytoplasmic reservoir, rendering the intracytoplasmic GLP-1R dynamic hard to be understood, creating a potential confounder of the study.

STAR★METHODS

Detailed methods are provided in the online version of this paper and include the following:

- KEY RESOURCES TABLE
- RESOURCE AVAILABILITY
 - Lead contact
 - Materials availability

● EXPERIMENTAL MODEL AND SUBJECT DETAILS

- Human studies
- Murine studies
- METHOD DETAILS
 - Human PBMCs isolation
 - Human flow cytometric analysis
 - Immunohistochemistry staining
 - Immunohistochemistry staining on kidney, lung, and heart biopsies
 - Murine islet allotransplantation and interventional studies
 - Murine cardiac allotransplantation and interventional studies
 - Colorectal tumor model
 - Adoptive transfer of CD3⁺ T cells from GLP-1R KO mice or from naïve C57BL/6 mice
 - Donor Specific Alloantibody Measurement
 - Treg induction assay
 - Heart tissue digestion and leukocyte isolation
 - Histology and immunohistochemistry
 - SDF-1 staining on islet allograft
 - Immunofluorescence and confocal imaging of GLP-1R^{+/CD3⁺} T cells on islet allograft
 - ELISA GLP-1 total and active and Exe-4
 - Flow cytometry
 - ELISpot assay
 - Western blot
 - qRT-PCR
 - Transcriptomic array of GLP-1R^{pos} and GLP-1R^{neg} CD4⁺/CD8⁺ T cells
 - Phosphoproteomic screen of CD3⁺ T cells
 - Immunoprecipitation of GLP-1R on CD3⁺ T cells
 - Immunofluorescence of GLP-1R on CD3⁺ T cells
 - Immunoelectron microscopy
 - Mass Spectrometry
 - GLP-1R transfection of T cells
 - Transwell migration assays
 - Bioenergetic analysis
 - scRNA seq of GLP-1R^{pos} and GLP-1R^{neg} CD3⁺ T cells
 - mRNA GLP-1R due diligence assessment on T cells

● QUANTIFICATION AND STATISTICAL ANALYSIS

SUPPLEMENTAL INFORMATION

Supplemental information can be found online at <https://doi.org/10.1016/j.cmet.2024.05.001>.

ACKNOWLEDGMENTS

We thank Dr. Thorens for providing us with the anti-GLP-1R antibody used for pathology studies. We thank “Fondazione Romeo and Enrica Invernizzi” for their extraordinary support. F.D. was supported by the Italian Ministry of Health grant RF-2021-12372897 and by the Italian Ministry of University and Research grant 2022JY9CP. R.A. is supported by the NIH grant K24 AI116925. P.F., C.L., and M.B.N. are supported by the Italian Ministry of University Research grants 20229ZA2YF, 2022NH9MXB, and 20225HWJMB, respectively.

AUTHOR CONTRIBUTIONS

M.B.N., S. Dellepiane, and F.F. designed and performed experiments, analyzed data, and wrote and edited the paper. V.U., T.V.F., F.D., A.J.S., E.F., C.X., Y.X., H.B.B., E.C.-L., L.L., A.M., E.A., C.L., A.A., B.E.E., G.S., A.P., G.D., E.S., I.P., M.E.L., L.C., M.V., L.K., K.M.L., G.V., R.A., J.F.M., J.Y., S. Danese, Z.W., and G.V.Z. performed experiments, analyzed data, and coordinated research. S.U., S.M., S.L.R., D.C., D.M., M.I., and G.C. helped with pathology. P.F. conceived the study, designed research, wrote, and edited the paper. All authors reviewed and edited the paper.

DECLARATION OF INTERESTS

The authors declare no competing interests.

Received: July 27, 2023

Revised: December 6, 2023

Accepted: May 2, 2024

Published: June 4, 2024

REFERENCES

1. Ast, J., Arvaniti, A., Fine, N.H.F., Nasteska, D., Ashford, F.B., Stamatakis, Z., Koszegi, Z., Bacon, A., Jones, B.J., Lucey, M.A., et al. (2020). Super-resolution microscopy compatible fluorescent probes reveal endogenous glucagon-like peptide-1 receptor distribution and dynamics. *Nat. Commun.* 11, 467. <https://doi.org/10.1038/s41467-020-14309-w>.
2. Burmeister, M.A., Brown, J.D., Ayala, J.E., Stoffers, D.A., Sandoval, D.A., Seeley, R.J., and Ayala, J.E. (2017). The glucagon-like peptide-1 receptor in the ventromedial hypothalamus reduces short-term food intake in male mice by regulating nutrient sensor activity. *Am. J. Physiol. Endocrinol. Metab.* 313, E651–E662. <https://doi.org/10.1152/ajpendo.00113.2017>.
3. Broide, E., Bloch, O., Ben-Yehudah, G., Cantrell, D., Shirin, H., and Rapoport, M.J. (2014). Reduced GLP-1R expression in gastric glands of patients with type 2 diabetes mellitus. *J. Clin. Endocrinol. Metab.* 99, E1691–E1695. <https://doi.org/10.1210/jc.2014-1114>.
4. Fiorentino, T.V., Casiraghi, F., Davalli, A.M., Finzi, G., La Rosa, S., Higgins, P.B., Abrahamian, G.A., Marando, A., Sessa, F., Perego, C., et al. (2019). Exenatide regulates pancreatic islet integrity and insulin sensitivity in the nonhuman primate baboon Papio hamadryas. *JCI Insight* 4, e93091. <https://doi.org/10.1172/jci.insight.93091>.
5. Fiorentino, T.V., Owston, M., Abrahamian, G., La Rosa, S., Marando, A., Perego, C., Di Cairano, E.S., Finzi, G., Capella, C., Sessa, F., et al. (2015). Chronic continuous exenatide infusion does not cause pancreatic inflammation and ductal hyperplasia in non-human primates. *Am. J. Pathol.* 185, 139–150. <https://doi.org/10.1016/j.ajpath.2014.09.009>.
6. Drucker, D.J., Habener, J.F., and Holst, J.J. (2017). Discovery, characterization, and clinical development of the glucagon-like peptides. *J. Clin. Invest.* 127, 4217–4227. <https://doi.org/10.1172/JCI97233>.
7. Thorens, B. (1992). Expression cloning of the pancreatic beta cell receptor for the gluco-incretin hormone glucagon-like peptide 1. *Proc. Natl. Acad. Sci. USA* 89, 8641–8645. <https://doi.org/10.1073/pnas.89.18.8641>.
8. Andreozzi, F., Raciti, G.A., Nigro, C., Mannino, G.C., Procopio, T., Davalli, A.M., Beguinot, F., Sesti, G., Miele, C., and Folli, F. (2016). The GLP-1 receptor agonists exenatide and liraglutide activate glucose transport by an AMPK-dependent mechanism. *J. Transl. Med.* 14, 229. <https://doi.org/10.1186/s12967-016-0985-7>.
9. Muskiet, M.H.A., Tonnieijk, L., Smits, M.M., van Baar, M.J.B., Kramer, M.H.H., Hoorn, E.J., Joles, J.A., and van Raalte, D.H. (2017). GLP-1 and the kidney: from physiology to pharmacology and outcomes in diabetes. *Nat. Rev. Nephrol.* 13, 605–628. <https://doi.org/10.1038/nrneph.2017.123>.
10. Drucker, D.J., and Rosen, C.F. (2011). Glucagon-like peptide-1 (GLP-1) receptor agonists, obesity and psoriasis: diabetes meets dermatology. *Diabetologia* 54, 2741–2744. <https://doi.org/10.1007/s00125-011-2297-z>.
11. Hadjiyanni, I., Siminovitch, K.A., Danska, J.S., and Drucker, D.J. (2010). Glucagon-like peptide-1 receptor signalling selectively regulates murine lymphocyte proliferation and maintenance of peripheral regulatory T cells. *Diabetologia* 53, 730–740. <https://doi.org/10.1007/s00125-009-1643-x>.
12. Drucker, D.J. (2018). Mechanisms of Action and Therapeutic Application of Glucagon-like Peptide-1. *Cell Metab.* 27, 740–756. <https://doi.org/10.1016/j.cmet.2018.03.001>.
13. He, S., Kahles, F., Rattik, S., Nairz, M., McAlpine, C.S., Anzai, A., Selgrade, D., Fenn, A.M., Chan, C.T., Mindur, J.E., et al. (2019). Gut intraepithelial T cells calibrate metabolism and accelerate cardiovascular disease. *Nature* 566, 115–119. <https://doi.org/10.1038/s41586-018-0849-9>.
14. Buysschaert, M., Tennstedt, D., and Preumont, V. (2012). Improvement of psoriasis during exenatide treatment in a patient with diabetes. *Diabetes Metab.* 38, 86–88. <https://doi.org/10.1016/j.diabet.2011.11.004>.
15. Hadjiyanni, I., Baggio, L.L., Poussier, P., and Drucker, D.J. (2008). Exendin-4 modulates diabetes onset in nonobese diabetic mice. *Endocrinology* 149, 1338–1349. <https://doi.org/10.1210/en.2007-1137>.
16. Xue, S., Wasserfall, C.H., Parker, M., Brusko, T.M., McGrail, S., McGrail, K., Moore, M., Campbell-Thompson, M., Schatz, D.A., Atkinson, M.A., and Haller, M.J. (2008). Exendin-4 therapy in NOD mice with new-onset diabetes increases regulatory T cell frequency. *Ann. N. Y. Acad. Sci.* 1150, 152–156. <https://doi.org/10.1196/annals.1447.049>.
17. Moschovaki Filippidou, F., Kirsch, A.H., Thelen, M., Kétszeri, M., Artinger, K., Aringer, I., Schabköhl, C., Mooslechner, A.A., Frauscher, B., Pollheimer, M., et al. (2020). Glucagon-Like Peptide-1 Receptor Agonism Improves Nephrotoxic Serum Nephritis by Inhibiting T-Cell Proliferation. *Am. J. Pathol.* 190, 400–411. <https://doi.org/10.1016/j.ajpath.2019.10.008>.
18. Maher, M.P., Wu, N., Ravula, S., Ameriks, M.K., Savall, B.M., Liu, C., Lord, B., Wyatt, R.M., Matta, J.A., Dugovic, C., et al. (2016). Discovery and Characterization of AMPA Receptor Modulators Selective for TARPs-gamma8. *J. Pharmacol. Exp. Ther.* 357, 394–414. <https://doi.org/10.1124/jpet.115.231712>.
19. Tacconi, C., Ungaro, F., Correale, C., Arena, V., Massimino, L., Detmar, M., Spinelli, A., Carvello, M., Mazzone, M., Oliveira, A.I., et al. (2019). Activation of the VEGFC/VEGFR3 Pathway Induces Tumor Immune Escape in Colorectal Cancer. *Cancer Res.* 79, 4196–4210. <https://doi.org/10.1158/0008-5472.CAN-18-3657>.
20. Bendotti, G., Montefusco, L., Lunati, M.E., Usuelli, V., Pastore, I., Lazzaroni, E., Assi, E., Seelam, A.J., El Essawy, B., Jang, J., et al. (2022). The anti-inflammatory and immunological properties of GLP-1 Receptor Agonists. *Pharmacol. Res.* 182, 106320. <https://doi.org/10.1016/j.phrs.2022.106320>.
21. Wang, V., Kuo, T.T., Huang, E.Y.K., Ma, K.H., Chou, Y.C., Fu, Z.Y., Lai, L.W., Jung, J., Choi, H.I., Choi, D.S., et al. (2021). Sustained Release GLP-1 Agonist PT320 Delays Disease Progression in a Mouse Model of Parkinson's Disease. *ACS Pharmacol. Transl. Sci.* 4, 858–869. <https://doi.org/10.1021/acspcs.1c00013>.
22. Rakipovski, G., Rolin, B., Nøhr, J., Klewe, I., Frederiksen, K.S., Augustin, R., Hecksher-Sørensen, J., Ingvorsen, C., Polex-Wolf, J., and Knudsen, L.B. (2018). The GLP-1 Analogs Liraglutide and Semaglutide Reduce Atherosclerosis in ApoE(-/-) and LDLr(-/-) Mice by a Mechanism That Includes Inflammatory Pathways. *JACC Basic Transl. Sci.* 3, 844–857. <https://doi.org/10.1016/j.jacbs.2018.09.004>.
23. Kolic, J., and MacDonald, P.E. (2015). cAMP-independent effects of GLP-1 on beta cells. *J. Clin. Invest.* 125, 4327–4330. <https://doi.org/10.1172/JCI85004>.
24. Drucker, D.J. (2018). The Ascending GLP-1 Road From Clinical Safety to Reduction of Cardiovascular Complications. *Diabetes* 67, 1710–1719. <https://doi.org/10.2337/db18-0008>.
25. Fayfman, M., Galindo, R.J., Rubin, D.J., Mize, D.L., Anzola, I., Urrutia, M.A., Ramos, C., Pasquel, F.J., Haw, J.S., Vellanki, P., et al. (2019). A Randomized Controlled Trial on the Safety and Efficacy of Exenatide Therapy for the Inpatient Management of General Medicine and Surgery Patients With Type 2 Diabetes. *Diabetes Care* 42, 450–456. <https://doi.org/10.2337/dc18-1760>.
26. Hocher, B., and Tsuprykov, O. (2017). Diabetic nephropathy: Renoprotective effects of GLP1R agonists and SGLT2 inhibitors. *Nat. Rev. Nephrol.* 13, 728–730. <https://doi.org/10.1038/nrneph.2017.140>.
27. Moellmann, J., Klinkhammer, B.M., Onstein, J., Stöhr, R., Jankowski, V., Jankowski, J., Lebherz, C., Tacke, F., Marx, N., Boor, P., and Lehrke, M. (2018). Glucagon-Like Peptide 1 and Its Cleavage Products Are Renoprotective in Murine Diabetic Nephropathy. *Diabetes* 67, 2410–2419. <https://doi.org/10.2337/db17-1212>.
28. Aung, M.M., Slade, K., Freeman, L.A.R., Kos, K., Whatmore, J.L., Shore, A.C., and Gooding, K.M. (2019). Locally delivered GLP-1 analogues

- liraglutide and exenatide enhance microvascular perfusion in individuals with and without type 2 diabetes. *Diabetologia* 62, 1701–1711. <https://doi.org/10.1007/s00125-019-4918-x>.
29. Chaudhuri, A., Ghanim, H., Vora, M., Sia, C.L., Korzeniewski, K., Dhindsa, S., Makdissi, A., and Dandona, P. (2012). Exenatide exerts a potent antiinflammatory effect. *J. Clin. Endocrinol. Metab.* 97, 198–207. <https://doi.org/10.1210/jc.2011-1508>.
30. Athauda, D., MacLagan, K., Skene, S.S., Bajwa-Joseph, M., Letchford, D., Chowdhury, K., Hibbert, S., Budnik, N., Zampedri, L., Dickson, J., et al. (2017). Exenatide once weekly versus placebo in Parkinson's disease: a randomised, double-blind, placebo-controlled trial. *Lancet* 390, 1664–1675. [https://doi.org/10.1016/S0140-6736\(17\)31585-4](https://doi.org/10.1016/S0140-6736(17)31585-4).
31. Newsome, P.N., Buchholtz, K., Cusi, K., Linder, M., Okanoue, T., Ratiu, V., Sanyal, A.J., Sejling, A.S., and Harrison, S.A.; NN9931-4296 Investigators (2021). A Placebo-Controlled Trial of Subcutaneous Semaglutide in Nonalcoholic Steatohepatitis. *N. Engl. J. Med.* 384, 1113–1124. <https://doi.org/10.1056/NEJMoa2028395>.
32. Woo, J.S., Kim, W., Ha, S.J., Kim, J.B., Kim, S.J., Kim, W.S., Seon, H.J., and Kim, K.S. (2013). Cardioprotective effects of exenatide in patients with ST-segment-elevation myocardial infarction undergoing primary percutaneous coronary intervention: results of exenatide myocardial protection in revascularization study. *Arterioscler. Thromb. Vasc. Biol.* 33, 2252–2260. <https://doi.org/10.1161/ATVBAHA.113.301586>.
33. Li, J., Albajrami, O., Zhuo, M., Hawley, C.E., and Paik, J.M. (2020). Decision Algorithm for Prescribing SGLT2 Inhibitors and GLP-1 Receptor Agonists for Diabetic Kidney Disease. *Clin. J. Am. Soc. Nephrol.* 15, 1678–1688. <https://doi.org/10.2215/CJN.02690320>.
34. Faurschou, A., Pedersen, J., Gyldenløve, M., Poulsen, S.S., Holst, J.J., Thyssen, J.P., Zachariae, C., Vilbsbøll, T., Skov, L., and Knop, F.K. (2013). Increased expression of glucagon-like peptide-1 receptors in psoriasis plaques. *Exp. Dermatol.* 22, 150–152. <https://doi.org/10.1111/exd.12081>.
35. Tate, M., Robinson, E., Green, B.D., McDermott, B.J., and Grieve, D.J. (2016). Exendin-4 attenuates adverse cardiac remodelling in streptozocin-induced diabetes via specific actions on infiltrating macrophages. *Basic Res. Cardiol.* 111, 1. <https://doi.org/10.1007/s00395-015-0518-1>.
36. Tsai, S., Winer, S., and Winer, D.A. (2019). Gut T Cells Feast on GLP-1 to Modulate Cardiometabolic Disease. *Cell Metab.* 29, 787–789. <https://doi.org/10.1016/j.cmet.2019.03.002>.
37. Hogan, A.E., Tobin, A.M., Ahern, T., Corrigan, M.A., Gaqatswe, G., Jackson, R., O'Reilly, V., Lynch, L., Doherty, D.G., Moynagh, P.N., et al. (2011). Glucagon-like peptide-1 (GLP-1) and the regulation of human invariant natural killer T cells: lessons from obesity, diabetes and psoriasis. *Diabetologia* 54, 2745–2754. <https://doi.org/10.1007/s00125-011-2232-3>.
38. Buyschaert, M., Baeck, M., Preumont, V., Marot, L., Hendrickx, E., Van Belle, A., and Dumoutier, L. (2014). Improvement of psoriasis during glucagon-like peptide-1 analogue therapy in type 2 diabetes is associated with decreasing dermal gammadelta T-cell number: a prospective case-series study. *Br. J. Dermatol.* 171, 155–161. <https://doi.org/10.1111/bjd.12886>.
39. Wong, C.K., Yusta, B., Koehler, J.A., Baggio, L.L., McLean, B.A., Matthews, D., Seeley, R.J., and Drucker, D.J. (2022). Divergent roles for the gut intraepithelial lymphocyte GLP-1R in control of metabolism, microbiota, and T cell-induced inflammation. *Cell Metab.* 34, 1514–1531.e7. <https://doi.org/10.1016/j.cmet.2022.08.003>.
40. Geginat, J., Lanzavecchia, A., and Sallusto, F. (2003). Proliferation and differentiation potential of human CD8+ memory T-cell subsets in response to antigen or homeostatic cytokines. *Blood* 101, 4260–4266. <https://doi.org/10.1182/blood-2002-11-3577>.
41. Doan Ngoc, T.M., Tilly, G., Danger, R., Bonizé, O., Masset, C., Guérif, P., Bruneau, S., Giemain, A., Harb, J., Cadoux, M., et al. (2022). Effector Memory-Expressing CD45RA (TEMRA) CD8(+) T Cells from Kidney Transplant Recipients Exhibit Enhanced Purinergic P2X4 Receptor-Dependent Proinflammatory and Migratory Responses. *J. Am. Soc. Nephrol.* 33, 2211–2231. <https://doi.org/10.1681/ASN.2022030286>.
42. Huang, X., Venet, F., Wang, Y.L., Lepape, A., Yuan, Z., Chen, Y., Swan, R., Kherouf, H., Monneret, G., Chung, C.S., and Ayala, A. (2009). PD-1 expression by macrophages plays a pathologic role in altering microbial clearance and the innate inflammatory response to sepsis. *Proc. Natl. Acad. Sci. USA* 106, 6303–6308. <https://doi.org/10.1073/pnas.0809422106>.
43. Yu, Y., Tsang, J.C.H., Wang, C., Clare, S., Wang, J., Chen, X., Brandt, C., Kane, L., Campos, L.S., Lu, L., et al. (2016). Single-cell RNA-seq identifies a PD-1(hi) ILC progenitor and defines its development pathway. *Nature* 539, 102–106. <https://doi.org/10.1038/nature20105>.
44. Patsoukis, N., Wang, Q., Strauss, L., and Boussiotis, V.A. (2020). Revisiting the PD-1 pathway. *Sci. Adv.* 6. <https://doi.org/10.1126/sciadv.abd2712>.
45. Sandner, S.E., Clarkson, M.R., Salama, A.D., Sanchez-Fueyo, A., Domenig, C., Habicht, A., Najafian, N., Yagita, H., Azuma, M., Turka, L.A., and Sayegh, M.H. (2005). Role of the programmed death-1 pathway in regulation of alloimmune responses in vivo. *J. Immunol.* 174, 3408–3415. <https://doi.org/10.4049/jimmunol.174.6.3408>.
46. Fife, B.T., Pauken, K.E., Eagar, T.N., Obu, T., Wu, J., Tang, Q., Azuma, M., Krummel, M.F., and Bluestone, J.A. (2009). Interactions between PD-1 and PD-L1 promote tolerance by blocking the TCR-induced stop signal. *Nat. Immunol.* 10, 1185–1192. <https://doi.org/10.1038/ni.1790>.
47. Ito, T., Ueno, T., Clarkson, M.R., Yuan, X., Jurewicz, M.M., Yagita, H., Azuma, M., Sharpe, A.H., Auchincloss, H., Jr., Sayegh, M.H., and Najafian, N. (2005). Analysis of the role of negative T cell costimulatory pathways in CD4 and CD8 T cell-mediated alloimmune responses in vivo. *J. Immunol.* 174, 6648–6656. <https://doi.org/10.4049/jimmunol.174.11.6648>.
48. Lipson, E.J., Bagnasco, S.M., Moore, J., Jr., Jang, S., Patel, M.J., Zachary, A.A., Pardoll, D.M., Taube, J.M., and Drake, C.G. (2016). Tumor Regression and Allograft Rejection after Administration of Anti-PD-1. *N. Engl. J. Med.* 374, 896–898. <https://doi.org/10.1056/NEJMMc1509268>.
49. Lee, B.T., Horwitz, B.H., Chopra, S., Ahearn, A., and Han, H.H. (2019). Checkpoint Inhibitor-Induced Rejection of a Liver Allograft: A Combination of Acute T Cell-Mediated and Antibody-Mediated Rejection. *Liver Transpl.* 25, 1845–1848. <https://doi.org/10.1002/lt.25622>.
50. De la Fuente, L.R., Law, A.M.K., Gallego-Ortega, D., and Valdes-Mora, F. (2021). Tumor dissociation of highly viable cell suspensions for single-cell omic analyses in mouse models of breast cancer. *STAR Protocols* 2 (100841). (Accessed December 17).
51. Tacconi, C., Correale, C., Gandelli, A., Spinelli, A., Dejana, E., D'Alessio, S., and Danese, S. (2015). Vascular endothelial growth factor C disrupts the endothelial lymphatic barrier to promote colorectal cancer invasion. *Gastroenterology* 148, 1438–1451.e8. <https://doi.org/10.1053/j.gastro.2015.03.005>.
52. Li, L.S., Wang, Z.M., Xu, C., Che, F.H., Hu, X.F., Cao, R., Xie, Y., Qiu, Y., and Shi, H.B. (2022). Liraglutide Attenuates Hepatic Ischemia-Reperfusion Injury by Modulating Macrophage Polarization. *Front Immunol* 13, 869050. <https://doi.org/10.3389/fimmu.2022.869050>.
53. Usuelli, V., Ben Nasr, M., D'Addio, F., Liu, K., Vergani, A., El Essawy, B., Yang, J., Assi, E., Uehara, M., Rossi, C., et al. (2021). miR-21 antagonism reprograms macrophage metabolism and abrogates chronic allograft vasculopathy. *Am. J. Transplant.* 21, 3280–3295. <https://doi.org/10.1111/ajt.16581>.
54. Vergani, A., Tezza, S., D'Addio, F., Fotino, C., Liu, K., Niewczas, M., Bassi, R., Molano, R.D., Kleffel, S., Petrelli, A., et al. (2013). Long-term heart transplant survival by targeting the ionotropic purinergic receptor P2X7. *Circulation* 127, 463–475. <https://doi.org/10.1161/CIRCULATIONAHA.112.123653>.
55. D'Addio, F., Vergani, A., Potena, L., Maestroni, A., Usuelli, V., Ben Nasr, M., Bassi, R., Tezza, S., Dellepiane, S., El Essawy, B., et al. (2018). P2X7R mutation disrupts the NLRP3-mediated Th program and predicts

- poor cardiac allograft outcomes. *J. Clin. Invest.* 128, 3490–3503. <https://doi.org/10.1172/JCI94524>.
56. Ben Nasr, M., Vergani, A., Avruch, J., Liu, L., Kefaloyianni, E., D'Addio, F., Tezza, S., Corradi, D., Bassi, R., Valderrama-Vasquez, A., et al. (2015). Co-transplantation of autologous MSCs delays islet allograft rejection and generates a local immunoprivileged site. *Acta Diabetol.* 52, 917–927. <https://doi.org/10.1007/s00592-015-0735-y>.
57. Tezza, S., Ben Nasr, M., D'Addio, F., Vergani, A., Usuelli, V., Falzoni, S., Bassi, R., Dellepiane, S., Fotino, C., Rossi, C., et al. (2018). Islet-Derived eATP Fuels Autoreactive CD8(+) T Cells and Facilitates the Onset of Type 1 Diabetes. *Diabetes* 67, 2038–2053. <https://doi.org/10.2337/db17-1227>.
58. Vergani, A., Gatti, F., Lee, K.M., D'Addio, F., Tezza, S., Chin, M., Bassi, R., Tian, Z., Wu, E., Maffi, P., et al. (2015). TIM4 Regulates the Anti-Islet Th2 Alloimmune Response. *Cell Transplant.* 24, 1599–1614. <https://doi.org/10.3727/096368914X678571>.
59. Fotino, C., Molano, R.D., Ben Nasr, M., Umland, O., Fraker, C.A., Ulissi, U., Balasubramanian, H.B., Lunati, M.E., Usuelli, V., Seelam, A.J., et al. (2023). Reversal of Experimental Autoimmune Diabetes With an sCD39/Anti-CD3 Treatment. *Diabetes* 72, 1641–1651. <https://doi.org/10.2337/db23-0178>.
60. Petrelli, A., Carvello, M., Vergani, A., Lee, K.M., Tezza, S., Du, M., Kleffel, S., Chengwen, L., Mfarrej, B.G., Hwu, P., et al. (2011). IL-21 is an antitolerogenic cytokine of the late-phase alloimmune response. *Diabetes* 60, 3223–3234. <https://doi.org/10.2337/db11-0880>.
61. D'Addio, F., La Rosa, S., Maestroni, A., Jung, P., Orsenigo, E., Ben Nasr, M., Tezza, S., Bassi, R., Finzi, G., Marando, A., et al. (2015). Circulating IGF-I and IGFBP3 Levels Control Human Colonic Stem Cell Function and Are Disrupted in Diabetic Enteropathy. *Cell Stem Cell* 17, 486–498. <https://doi.org/10.1016/j.stem.2015.07.010>.
62. Chesnokova, L.S., and Yurochko, A.D. (2021). Using a Phosphoproteomic Screen to Profile Early Changes During HCMV Infection of Human Monocytes. *Methods Mol. Biol.* 2244, 233–246. https://doi.org/10.1007/978-1-0716-1111-1_12.
63. Batycka, M., Inglis, N.F., Cook, K., Adam, A., Fraser-Pitt, D., Smith, D.G.E., Main, L., Lubben, A., and Kessler, B.M. (2006). Ultra-fast tandem mass spectrometry scanning combined with monolithic column liquid chromatography increases throughput in proteomic analysis. *Rapid Commun. Mass Spectrom.* 20, 2074–2080. <https://doi.org/10.1002/rcm.2563>.
64. German, N.J., Yoon, H., Yusuf, R.Z., Murphy, J.P., Finley, L.W.S., Laurent, G., Haas, W., Satterstrom, F.K., Guarnerio, J., Zaganjor, E., et al. (2016). PHD3 Loss in Cancer Enables Metabolic Reliance on Fatty Acid Oxidation via Deactivation of ACC2. *Mol. Cell* 63, 1006–1020. <https://doi.org/10.1016/j.molcel.2016.08.014>.
65. Ben Nasr, M., Robbins, D., Parone, P., Usuelli, V., Tacke, R., Seelam, A.J., Driver, E., Le, T., Sabouri-Ghomi, M., Guerrettaz, L., et al. (2022). Pharmacologically Enhanced Regulatory Hematopoietic Stem Cells Revert Experimental Autoimmune Diabetes and Mitigate Other Autoimmune Disorders. *J. Immunol.* 208, 1554–1565. <https://doi.org/10.4049/jimmunol.2100949>.
66. Pasquale, V., Ducci, G., Campioni, G., Ventrici, A., Assalini, C., Busti, S., Vanoni, M., Vago, R., and Sacco, E. (2020). Profiling and Targeting of Energy and Redox Metabolism in Grade 2 Bladder Cancer Cells with Different Invasiveness Properties. *Cells* 9, 2669. <https://doi.org/10.3390/cells9122669>.
67. Aran, D., Looney, A.P., Liu, L., Wu, E., Fong, V., Hsu, A., Chak, S., Naikawadi, R.P., Wolters, P.J., Abate, A.R., et al. (2019). Reference-based analysis of lung single-cell sequencing reveals a transitional profibrotic macrophage. *Nat. Immunol.* 20, 163–172. <https://doi.org/10.1038/s41590-018-0276-y>.

STAR★METHODS

KEY RESOURCES TABLE

REAGENT or RESOURCE	SOURCE	IDENTIFIER
Antibodies		
PE Anti-IgG Antibody	Southern Biotech	Cat#1030-09 RRID: AB_2794298
Hamster Anti-CD3e Antibody	BD Biosciences	Cat#553058 RRID: AB_394591
Rat Anti-IL-4 Antibody	Invitrogen	Cat# 16-7041-81 RRID: AB_469208
Mouse Anti-IFN gamma Antibody	Invitrogen	Cat# AHC4032 RRID: AB_2536278
Rat Anti-IFN gamma Antibody	Invitrogen	Cat#16-7311-81 RRID: AB_469242
Brilliant Violet 421 Anti-T-bet Antibody	BD Biosciences	Cat#563318 RRID: AB_2687543
PE Anti-ROR γ t Antibody	BD Biosciences	Cat#562607 RRID: AB_11153137
Rabbit Anti-GLP-1R Antibody	Alomone Lab	Cat#AGR-021 RRID: AB_10917158
FITC Anti-GLP-1R Antibody	Alomone Lab	Cat#AGR-021-F RRID: AB_2756626
Mouse Anti-CXCL12 Antibody	Invitrogen	Cat#MA5-23759 RRID: AB_2608711
APC Anti-CD62L Antibody	BD Biosciences	Cat#553152 RRID: AB_398533
PE Anti-CD44 Antibody	BD Biosciences	Cat#553134 RRID: AB_394649
PerCP Anti-CD4 Antibody	BioLegend	Cat#100538 RRID: AB_893325
PerCP Anti-CD8a Antibody	BioLegend	Cat#100734 RRID: AB_2075238
APC Anti-Insulin Antibody	R&D systems	Cat# IC1417A RRID: N/A
BUV737 Anti-CD4 Antibody	BD Biosciences	Cat#612761 RRID: N/A
BUV395 Anti-CD8a Antibody	BD Biosciences	Cat#563786 RRID: AB_2732919
Brilliant Blue 700 Anti-CD4 Antibody	BD Biosciences	Cat#742099 RRID: AB_2871375
Pacific Blue Anti-NK-1.1 Antibody	BioLegend	Cat#108722 RRID: AB_2132712
Brilliant Violet 605 Anti-CD127 Antibody	BD Biosciences	Cat# 569295 RRID: N/A
PE Anti-CD44 Antibody	BD Biosciences	Cat#553134 RRID: AB_394649
FITC Anti-CD279 (PD-1) Antibody	BioLegend	Cat#135214 RRID: AB_10680238
Brilliant Violet 786 Anti-CD45 Antibody	BD Biosciences	Cat#564225 RRID: AB_2716861
Brilliant Blue 700 Anti-CD3e Antibody	BD Biosciences	Cat#566494 RRID: AB_2744393

(Continued on next page)

Continued

REAGENT or RESOURCE	SOURCE	IDENTIFIER
Brilliant Blue 700 Anti-CD3 Antibody	BD Biosciences	Cat#745836 RRID: AB_2871412
Brilliant Blue 700 Anti-CD45 Antibody	BD Biosciences	Cat#566440 RRID: AB_2744406
Brilliant Violet 786 CD11c Antibody	BD Biosciences	Cat#563735 RRID: AB_2738394
eFluor 450 CD11b Antibody	Invitrogen	Cat#48-0112-82 RRID: AB_1582236
PE-CF594 Anti-CD45 Antibody	BD Biosciences	Cat# 562313 RRID: AB_11151901
Brilliant Violet 786 Anti-CD335 (NKp46) Antibody	BD Biosciences	Cat#569694 RRID: N/A
Brilliant Violet 650 Anti-CD49a Antibody	BD Biosciences	Cat#740519 RRID: AB_2740235
Brilliant Blue 700 Anti-CD117 Antibody	BD Biosciences	Cat#566415 RRID: N/A
PE Anti-IL33R (ST2) Antibody	BD Biosciences	Cat#566312 RRID: AB_2744490
Brilliant Violet 711 Anti-IL23R Antibody	BD Biosciences	Cat#744372 RRID: AB_2742186
PE Anti-CD184 (CXCR4) Antibody	BD Biosciences	Cat#551966 RRID: AB_394305
Brilliant Violet 605 Anti- CX3CR1 Antibody	BD Biosciences	Cat#567822 RRID: N/A
Brilliant Violet 421 Anti-CD192 (CCR2) Antibody	BD Biosciences	Cat#747963 RRID: AB_2872424
Brilliant Violet 650 Anti-CD195 (CCR5) Antibody	BD Biosciences	Cat#743698 RRID: AB_2741680
BV786 Anti-CD197 (CCR7) Antibody	BD Biosciences	Cat#564355 RRID: AB_2738765
Brilliant Blue 700 Anti-CD183 (CXCR3) Antibody	BD Biosciences	Cat#742274 RRID: AB_2871450
Brilliant Blue 711 Anti-CD186 (CXCR6) Antibody	BioLegend	Cat#151111 RRID: AB_2721558
BUV395 Anti-CD27 Antibody	BD Biosciences	Cat# 563815 RRID: AB_2744349
Brilliant Violet 510 Anti-CD45RA Antibody	BD Biosciences	Cat#563031 RRID: AB_2722499
Brilliant Violet 711 Anti-CD197 (CCR7) Antibody	BD Biosciences	Cat#563712 RRID: AB_2738386
Brilliant Blue 700 Anti-CD4 Antibody	BD Biosciences	Cat# 566392 RRID: AB_2744421
Brilliant Violet 605 Anti-CD8 Antibody	BD Biosciences	Cat#564116 RRID: AB_2869551
Brilliant Violet 421 Anti-CD25 Antibody	BD Biosciences	Cat#564033 RRID: AB_2738555
PE Anti-FoxP3 Antibody	BD Biosciences	Cat#560046 RRID: AB_1645508
FITC Anti-Rabbit IgG Antibody	BioLegend	Cat#406403 RRID: AB_893531
Mouse Anti-CD3 Antibody	Dako	Cat# M725401-2 RRID: N/A
Rabbit Anti-GAPDH (D16H11) Antibody	Cell Signaling Technology	Cat#5174S RRID: N/A

(Continued on next page)

Continued

REAGENT or RESOURCE	SOURCE	IDENTIFIER
Mouse Anti-CTLA-4 (CD152) Antibody	Bio X Cell	Cat#BE0164 RRID: AB_10949609
PE Anti-GLP-1R Antibody	Abcam	Cat#ab274122 RRID: N/A
Goat Anti-IgG, HRP-linked Antibody	Cell Signaling Technology	Cat#7074 RRID: N/A
Rabbit anti-GAPDH (D16H11) XP Antibody	Cell Signaling Technology	Cat#5174 RRID: N/A
Hamster Anti-CD28 Antibody	BD Biosciences	Cat#553295 RRID: AB_394764
DyLight 488 Anti-IgM Antibody	Invitrogen	Cat#SA5-10010 RRID: AB_2556590
DyLight 650 Anti-IgG (H+L) Antibody	Invitrogen	Cat#SA5-10041 RRID: AB_2556621
Mouse Anti-IFN gamma Antibody	Invitrogen	Cat# AHC4032 RRID: AB_2536278
Bacterial and virus strains		
Retro-CMV Blank Retrovirus	Applied Biological Materials	Cat# RVP001
Biological samples		
Healthy human blood	Boston Children's Hospital IRB & Luigi Sacco Hospital	N/A
Patient renal tissue	Fondazione IRCCS Ca' Granda Ospedale Maggiore Policlinico Hospital	N/A
Patient cardiac tissue	De Gasperis Cardio Center and Transplant Center, Niguarda Hospital,	N/A
Patient lung tissue	Pulmonary Division, Boston Children's Hospital	N/A
Chemicals, peptides, and recombinant proteins		
Recombinant Mouse IL-2 Protein	Bio-technne	Cat#402-ML
Recombinant Mouse TGF-beta 1 Protein	Bio-technne	Cat#7666-MB
Exendin-4	Merck	Cat#E7144
Exendin Fragment 9-39	Merck	Cat#E7269
Phorbol 12-myristate 13-acetate	Merck	Cat#P8139
Ionomycin calcium salt	Merck	Cat#I0634
BD GolgiStop Protein Transport Inhibitor	BD Biosciences	Cat#554724
Collagenase Type IV	Merck	Cat#C4-BIOC
Collagenase from Clostridium histolyticum	Merck	Cat#C9891 CAS: 9001-12-1
CD8a (Ly-2) MicroBeads	Miltenyi Biotec	Cat#130-117-044
Dynabeads Protein G	Invitrogen	Cat#10003D
Recombinant Mouse CXCL12/SDF-1 alpha Protein	Bio-Techne	Cat#460-SD-010/CF
Seahorse XF RPMI medium	Agilent	Cat#103576-100
DTSSP (3,3'-dithiobis (sulfosuccinimidyl propionate))	Thermo Fisher	Cat# 21578
PowerUp SYBR Green Master Mix	Thermo Fisher	Cat#A25742
SuperPicture Polymer Detection Kit	Thermo Fisher	Cat#10364213
BD Cytofix/Cytoperm Plus Fixation/Permeabilization Solution Kit	BD Biosciences	Cat#555028 RRID: AB_2869013
ELISPOT AEC Substrate Set	BD Biosciences	Cat#551951 RRID: AB_2868954

(Continued on next page)

Continued

REAGENT or RESOURCE	SOURCE	IDENTIFIER
ELISPOT HRP Streptavidin	BD Biosciences	Cat#557630
Fixable Viability Stain 510	BD Biosciences	Cat#564406 RRID: AB_2869572
CellTrace Violet Cell Proliferation Kit	Invitrogen	Cat#C34557
Mouse IFN-γ ELISPOT Pair	BD Biosciences	Cat#551881
Ficoll Paque Plus	Merck	Cat#GE17-1440-03
Percoll	Merck	Cat#P1644
Hoechst 33342	Bio-Techne	Cat#5117 CAS: 875756-97-1
CD8a+ T Cell Isolation Kit	Miltenyi Biotec	Cat#130-104-075
RPMI 1640	Euroclone	Cat#ECB9006LX10
BAZ2A-ICR	Merck	Cat#SML1276
JNJ55511118	Bio-Techne	Cat#6278 CAS: 2036081-86-2
CFSE	BD Biosciences	Cat#565082 RRID: AB_2869649
CD4+CD25+ Regulatory T Cell Isolation Kit	Miltenyi Biotec	Cat#130-091-041
CD4 (L3T4) MicroBeads	Miltenyi Biotec	Cat#130-117-043
Hyaluronidase from bovine testes	Merck	Cat#H3506 CAS: 37326-33-3
DNase I	Roche	Cat#10104159001
Dispase II	Roche	Cat#4942078001
TEG	De la Fuente et al. ⁵⁰	DOI: https://doi.org/10.1016/j.xpro.2021.100841
Pan T Cell Isolation Kit II	Miltenyi Biotec	Cat#130-095-130
SuperPicture Polymer Detection Kit, HRP, broad spectrum	Fisher Scientific	Cat#878963
L-Glutamine	Gibco	Cat#878963
Penicillin-Streptomycin	Gibco	Cat#15140122
Fetal Bovine Serum	CliniSciences	Cat#FBS-22B
Polybrene	Santa Cruz Biotechnology	Cat#sc-134220 CAS: 28728-55-4
Pierce BCA Protein Assay Kits	Thermo Fisher	Cat#23227
Critical commercial assays		
RNeasy Plus Kits	Qiagen	Cat#74136
QuantiNova Reverse Transcription Kit	Qiagen	Cat#205411
Phospho Explorer Antibody Array	Full Moon Biosystems	Cat#PEX100
EMbed 812 Embedding Kit	Electron Microscopy Sciences	Cat#14120
Seahorse XF T Cell Metabolic Profiling Kit	Agilent	Cat#103772-100
Seahorse XF Glycolytic Rate Assay Kit	Agilent	Cat#103344-100
SuperScript III First-Strand Synthesis System	Invitrogen	Cat#18080051
Glucagon-Like Peptide-1 (Active) ELISA Kit	Merck	Cat#EGLP-35K
Exendin-4 ELISA kit	Duotech	Cat#ABIN627775
GLP-1 Total ELISA Kit	Merck	Cat#EZGLP1T-36K
Lineage Cell Depletion Kit	Miltenyi Biotec	Cat#130-090-858
Direct-zol RNA Miniprep Kits	Zymo Research	Cat#R2052
Zymoclean Gel DNA Recovery Kit	Zymo Research	Cat#D4008
PE / RPhycoerythrin Conjugation Kit - Lightning-Link	Abcam	Cat#ab102918
Mouse IFNg ELISPOT Set	BD Biosciences	Cat#551083 RRID: AB_2868922

(Continued on next page)

Continued

REAGENT or RESOURCE	SOURCE	IDENTIFIER
Deposited data		
Raw data of scRNA sequencing	This paper	Dataverse "GLP1R is a T cell negative costimulatory molecule - Cell Metabolism - 2024" https://doi.org/10.13130/RD_UNIMI/D7QMDE
Raw and unprocessed data (including proteomics) used for plotting the figures in this manuscript	This paper	Data S1
Experimental models: Cell lines		
MC 38 CRC cells	ATCC	(Tacconi et al. ⁵¹ ; Tacconi et al. ¹⁹)
Beta-TC-6	ATCC	ATCC D4008
HEK293	ATCC	ATCC CRL-1573
Experimental models: Organisms/strains		
GLP-1R KO	Li et al. ⁵²	DOI: https://doi.org/10.3389/fimmu.2022.869050
C57BL/6J	Jackson Laboratory	Strain#:000664
BALB/cJ	Jackson Laboratory	Strain#:000651
Oligonucleotides		
Forward Primer for Murine GLP-1R: 5'-TGCTATCGCGTCAACTTCT-3'	Eurofins	N/A
Reverse Primer for Murine GLP-1R: 5'- ATTCAAGTGCTCCAGCCTCC-3'	Eurofins	N/A
Forward Primer for Murine GAPDH: 5'- CCAGGGCTGCCATTGCACTGGCAAAGTGG-3'	Eurofins	N/A
Reverse Primer for Murine GAPDH: 5'- CCTGGAAGATGGTGATGGVTTCCCGTTGA-3'	Eurofins	N/A
GLP-1R Taqman assays	Thermo Fisher	Mm00445292_m1
GLP-1R Taqman assays	Thermo Fisher	Hs00157705_m1
GAPDH Taqman assays	Thermo Fisher	Hs027589991_g1
GAPDH Taqman assays	Thermo Fisher	Mm99999915_g1
Recombinant DNA		
pMYS-IRES-GFP Retroviral Expression Vector	Cell BioLabs	Cat#RTV-021
pRetroG-CMV-GLP-1R	This paper	Cat#216140740194
Software and algorithms		
FlowJo v.10.6.2	https://www.flowjo.com	RRID:SCR_008520
ImageJ	https://imagej.nih.gov/ij/	RRID:SCR_003070
Seurat package v.4.3.0	https://satijalab.org/seurat/	RRID:SCR_016341
AxioVision Imaging System software v.4.8	https://carl-zeiss-vision-axiovision-viewer.software.informer.com	RRID:SCR_002677
Primer3plus	https://www.primer3plus.com	RRID: SCR_003081
GraphPad Prism v.10	https://www.graphpad.com	RRID:SCR_002798
Biorender	http://biorender.com	RRID:SCR_018361

RESOURCE AVAILABILITY**Lead contact**

Additional information and requests for resources and reagents should be addressed to the lead contact, Paolo Fiorina (pao.lo.fiorina@childrens.harvard.edu).

Materials availability

- All of the data supporting this study are included in the article.

- The phosphoproteomics, transcriptomic, and scRNA sequencing data have been deposited in the Dataverse “GLP1R is a T cell negative costimulatory molecule - Cell Metabolism -2024” Digital Repository:
 - https://doi.org/10.13130/RD_UNIMI/P1OESM Phosphoproteomics
 - https://doi.org/10.13130/RD_UNIMI/DYN4RW Transcriptomics
 - https://doi.org/10.13130/RD_UNIMI/D7QMDE scRNASeq
- All raw data used to generate the figures throughout the manuscript can be found within the [Data S1](#) document.
- This paper does not report original code.
- All additional datasets included in the manuscript will be provided upon request from the [lead contact](#).

EXPERIMENTAL MODEL AND SUBJECT DETAILS

Human studies

For characterization of GLP-1R on human T lymphocytes, human peripheral blood mononuclear cells (PBMCs) were isolated from healthy donors' blood. Study protocol was approved by Boston Children's Hospital IRB. For immunohistochemistry staining on kidney, lung and heart biopsies, human renal biopsies obtained from patients experiencing allograft rejection were obtained from Nephrology, dialysis and renal transplantation, Fondazione IRCCS Ca' Granda Ospedale Maggiore Policlinico Hospital, all patients' characteristics as well as their immunosuppressive regimen are described in [Table S2](#). As regarding cardiac samples used in this study, samples were obtained from the right side of the interventricular septum of cardiac transplant recipients at De Gasperis Cardio Center and Transplant Center, Niguarda Hospital, Milan, Italy. Samples were then formalin-fixed, paraffin-embedded, sectioned, and histologically graded by a cardiac pathologist according to the International Society for Heart and Lung Transplantation criteria as previously reported.⁵³ The Additional characteristics of patients and the immunosuppressive regimen are depicted in [Table S3](#). As far regarding the lung samples used in this study obtained from Pulmonary Division, Boston Children's Hospital, the cases were blinded samples, with chronic lung allograft rejection, where evidences of obliterative bronchitis and the presence of lymphocytic bronchitis, epithelial cell injury and necrosis, have been confirmed. All patients provided informed consent prior to participation in the study, and all related procedures were performed with the approval of the internal review and ethics boards of the indicated hospitals.

Murine studies

C57BL/6 and BALB/c mice were obtained from the Jackson Laboratory (Bar Harbor, Maine). Experiment with GLP-1R KO mice, were performed in Wuhan at the J. Yang Lab and all procedures involving these animals were performed and monitored in accordance with the guidelines of Tongji Animal Use Regulations and approved by the Institutional Animal Care and Use Committee of Tongji Medical College. All mice were cared for and used in accordance with Harvard Medical School institutional guidelines and housed 2 weeks in Boston Children Hospital pathogen-free animal house in isolated cages with 12-hr light/dark cycle and *ad libitum* access to food and water before undergoing experiments. Spleen, heart and renal cells were obtained by collagenase tissue digestion as previously described.⁵⁴ Lymphocytes were extracted from murine spleen by apposite CD4 or CD8 mAb-coated microbeads (Miltenyi).

METHOD DETAILS

Human PBMCs isolation

Blood samples were obtained from healthy controls in accordance with Institutional Review Board committee approval.

Peripheral blood mononuclear cell fractions were isolated by Lymphoprep density gradient medium (Stem Cell Technology, Vancouver, BC–Canada) and processed for further analysis for FACS staining. In other assays, lymphocytes were extracted by apposite CD4 or CD8 mAb-coated microbeads (Miltenyi Biotec, Bergisch Gladbach – Germany) as previously described.⁵⁵

Human flow cytometric analysis

To assess GLP-1R expression on human T cell subsets, peripheral blood mononuclear cell fractions isolated from healthy subjects were stained. The following antibodies were used for flow cytometric analysis in human studies: FITC-conjugated anti-human GLP-1R, BUV395-conjugated anti-human CD27, BV510-conjugated anti-human CD45RA, BV711-conjugated anti-human CCR7, BB700-conjugated anti-human CD4, BV605-conjugated anti-human-CD8, BV421-conjugated anti-human CD25, and PE-conjugated anti-human FoxP3. Antibodies were purchased from BD Biosciences, Alomone (Israel). FITC-conjugated donkey anti-rabbit IgG was used as related isotype controls. A BD Celesta flow cytometer (BD Biosciences) was used to analyze cells with the light scatter properties of stem cells or lymphocytes. Background staining was determined using nonreactive isotype-matched control mAbs with gates positioned to exclude 99% of non-reactive cells. FlowJo software version 10.6.2 (BD Bioscience) was used for analysis.

Immunohistochemistry staining

Immunohistochemistry was performed with 4-μm-thick formalin-fixed, paraffin-embedded tissue sections. Photomicrographs (400X) were obtained using an Olympus BX41 microscope (Olympus, Center Valley, PA). The following primary antibodies were used: anti-GLP-1R, anti-CD3 (respectively from Alomone [Israel], Abcam [Cambridge, MA, and BD Biosciences [San Jose, CA]).

Immunohistochemistry staining on kidney, lung, and heart biopsies

The renal biopsies from transplant patients were paraffin-embedded following hospital standard protocol: paraformaldehyde (PFA) 4% for 30', dH₂O for 5', ethanol (ETOH) 95% (10'x 3times), ETOH 100% (10'x 3times), Xylene (10'x 3times). Three different renal biopsies from transplant patients of 3 µm thick were evaluated for Haematoxylin Eosin (H&E Biopctica, Milan, Italy), CD3 (mouse anti-human Dako 1:20), and GLP-1R (rabbit Alomone Labs, Israel, 1:100) with the following final diagnosis f: i) Renal biopsies without major histological abnormalities, ii) Renal biopsies showing antibody-mediated rejection, iii) Renal biopsies showing T cell-mediated rejection. The hematoxylin & eosin was performed using a standard protocol and histochemistry was performed using super picture HRP polymer conjugated broad spectrum (Invitrogen, CA, United States). Images were acquired by AxioVision software 4.8 (Carl Zeiss). The IMAGE J program was used for the CD3 and GLP-1R quantification (n=18 region of interest).

Murine islet allotransplantation and interventional studies

Pancreatic islets from BALB/c mice were isolated by collagenase digestion and density gradient separation as previously described.^{56,57} Subsequently, four to five hundred islets were inoculated under the renal capsule of each C57BL/6 recipient rendered diabetic with streptozotocin (STZ) (200 mg/kg, administered i.p. Sigma-Aldrich). Islet transplantation success was confirmed by glycaemia normalization. Rejection of islet allografts was defined as blood glucose levels >250 mg/dl for at least 2 consecutive days.⁵⁸ Treatment modalities were the following: transplanted mice were intraperitoneally injected according to the following protocols: 1) Exendin-4 (Exe-4) (Amylin Pharmaceuticals, San Diego, CA–USA) 0.2µg twice/day for two weeks after transplant; 2) Exe-4 0.2µg twice/day from the day before until two weeks after transplant; 3) Exendin-4 2µg twice/day from the day before until two weeks after transplant; 4) Exendin-4 2µg twice/day + Exendin-9-39 (Exe-9) (Sigma-Aldrich) 2µg twice/day from the day before until two weeks after transplant; 5) Exendin-4 2µg twice/day from the day before until two weeks after transplant + Rapamycin 0.1mg/die for two weeks; 6) saline 0.5ml twice/day for two weeks. The follow-up of the transplanted mice was for 100 days.

Murine cardiac allotransplantation and interventional studies

Cardiac allografts from BALB/c mice were transplanted intra-abdominally in C57BL/6 mice using microsurgical techniques as described.⁵⁵ Rejection was determined as complete cessation of cardiac contractility and was confirmed by direct visualization. Transplanted mice were intraperitoneally injected according to the following protocols: 1) Exendin-4 (Exe-4) (Amylin Pharmaceuticals, San Diego, CA –USA) 0.2µg twice/day for two weeks after transplant; 2) Exe-4 0.2µg twice/day from the day before until two weeks after transplant; 3) Exe-4 2µg twice/day from the day before until two weeks after transplant; 4) Exe-4 2µg twice/day + Exen-din-9-39 (Exe-9) (Sigma-Aldrich) 2µg twice/day from the day before until two weeks after transplant; 5) Exe-4 2µg twice/day from the day before until two weeks after transplant + Rapamycin 0.1mg/die for two weeks; 6) saline 0.5ml twice/day for two weeks.

Colorectal tumor model

Female C57BL/6 mice were anesthetized with 100 mg/kg of ketamine and 50 mg/kg of xylazine. Next, by using a 29-gauge syringe, 2x10⁵ MC38 cells were injected submucosally into the distal posterior rectum in a final volume of 50 mL, as described previously.^{19,51} MC38-injected mice were randomly assigned into 2 groups: (i) Exe-9-treated group (n=8), where all mice received an intraperitoneal injection of 2 µg of Exendin-9-39 (Exe-9) starting by Day1 for a total of 14 days; (ii) untreated-group (n=6), where all mice received an IP injection of PBS starting by day 1 and for a total of 14 days. Tumour growth was visually monitored daily. After animals' sacrifice, tumours were measured by a digital calliper measuring tumour length, width, and height and were weighted using a digital scale. Procedures involving mice were conformed to institutional guidelines in agreement with national and international law and were approved by the ethics committee by the Ministry of Health.

Adoptive transfer of CD3⁺ T cells from GLP-1R KO mice or from naïve C57BL/6 mice

2-4x10⁶ CD3⁺ T cells obtained from naïve C57BL/6 mice and 2-4x10⁶ CD3⁺ T cells obtained from GLP-1R KO mice, were injected into BALB/c cardiac-transplanted C57BL/6 Rag1^{-/-} mice, and survival was assessed as previously described.⁵⁴

Donor Specific Alloantibody Measurement

At day 7 post heart allotransplantation, we collected sera from all the recipients and determined the levels of donor-specific alloantibodies (DSA) using splenocytes from C57BL/6 donors as probes. In brief, splenic tissues were ground and filtered through a 70-µm cell strainer. The resulting splenocytes were then resuspended in PBS, seeded at 5x10⁵ per well into 96-well plates, incubated with an equal volume of fetal bovine serum (FBS) for 10 minutes to block nonspecific binding, washed with PBS containing 2% FBS, and then incubated with serum (1:8, 1:16 and 1:32 dilution) for 20 min at 4°C in the dark. Next, cells were washed twice and incubated for 20 minutes with PE-conjugated anti-mouse IgG (Southern Biotech, Birmingham, AL, USA; Cat# 1030-09). The level of donor-specific IgG was then determined by FACS analysis and is presented as the mean fluorescence intensity (MFI).

Treg induction assay

Naïve CD4⁺ CD25⁻ T cells were selected and activated for 5 days with 1 µg/ml of plate-bound soluble anti-CD3 and anti-CD28 antibodies (BD Biosciences). Cells were cultured for 5-days in the presence of IL-2 (10ng/ml; R&D Systems) and TGFβ (2ng/mL; R&D Systems), anti-IL-4 (0.5µg/ml; PeproTech) and anti-IFNγ (2µg/mL; PeproTech) and were treated with Exe-4 (1nM) or left untreated. Then, cells were washed, pulsed for 4-hrs with phorbol myristate acetate (PMA; 50ng/mL; Sigma-Aldrich), ionomycin

(500ng/mL; Sigma-Aldrich) and Golgi-stop (1.0 μ L/mL; BD Biosciences) and then analyzed by FACSCelesta (BD Biosciences) for the expression of Foxp3, Tbet and Ror γ T as previously reported.⁵⁹

Heart tissue digestion and leukocyte isolation

Hearts were removed and washed with saline solution (PBS). For preparing single cell suspensions, heart tissue was minced with surgical scissors and incubated in 1 mg/ml collagenase type IV (Sigma-Aldrich, St. Louis, MO) in DMEM medium (Lonza, Walkersville, MD, USA) for 20 minutes at 37°C with gentle agitation. Cells were filtered through 70 μ m filters and centrifuged (5 minutes at 4°C, 300 g). Cell pellets were resuspended in 33% Percoll solution (Sigma-Aldrich) and separated by gradient centrifugation by layering the cell suspension on top of a 66% Percoll solution before centrifugation for 20 minutes at 4°C. Cells at the interphase of the two solutions were carefully collected, washed in PBS and re-suspended in appropriate buffer for further experiments.

Histology and immunohistochemistry

Immunohistochemistry was performed on formalin-fixed, paraffin-embedded tissue (23). Photomicrographs were taken using an Olympus BX41 microscope (Center Valley, PA - USA). Dr. Bernard Thorens kindly provided us with the anti-GLP-1R antibody for pathology studies. An expert pathologist evaluated selected micrographs.

SDF-1 staining on islet allograft

Harvested islet allografts were fixed in PFA and paraffin-embedded. Tissues were cut into 5 μ m sections, and respectively de-paraffinized, rehydrated and antigen-retrieved. Then, sections were incubated with the following antibody: mouse anti-CXCL12 monoclonal antibody (1:300, ThermoFisher Scientific, MA5-23759). Images were acquired an Olympus BX41 microscope (Center Valley, PA) and analyzed by an expert pathologist.

Immunofluorescence and confocal imaging of GLP-1R $^+$ /CD3 $^+$ T cells on islet allograft

Primary antibodies against CD3 (mouse CD3 antibody (MAB4841), R&D Systems, dilution 1:100) and GLP-1R (mouse GLP-1R (Mab 3F52), Developmental Studies Hybridoma Bank, Iowa City, IA, USA, dilution 1:50) were tested in a 3 mm-thick histological section to identify the receptor positivity in T lymphocytes. Immunoreactive signals were detected using fluorescently labeled secondary antibodies (goat anti-rat 488 (SA5-10010), Invitrogen dilution 1:70 and Donkey anti-rabbit 650 (SA5-10041), Sigma Aldrich, St. Louis, MO, USA, dilution 1:70, respectively). This section was viewed by confocal microscopy (Stellaris 5; Leica, Wetzlar, Germany) through a \times 63 oil objective. Images were acquired in a multi-track mode, using consecutive and independent optical pathways and observed by the Las X software (Leica, Wetzlar, Germany).

ELISA GLP-1 total active and Exe-4

Total GLP-1, active GLP-1 and Exendin-4 levels were assessed in the individual serum of all groups of treated and untreated mice using commercially available ELISA kits, according to the manufacturer's instructions (BlueGene E03E0022). Briefly, the Exen4 ELISA kit applies the quantitative sandwich enzyme immunoassay technique. The microtiter plate is already pre-coated with a monoclonal antibody specific for Exen4. Standards and samples are then added to the microtiter plate wells and Exen4 if present, will bind to the antibody pre-coated wells. In order to quantitatively determine the amount of Exen4 present in the sample, a standardized preparation of horseradish peroxidase (HRP)-conjugated polyclonal antibody, specific for Exen4 are added to each well. The microtiter plate undergoes incubation (1 hour at 37°C), and then the wells are thoroughly washed to remove all unbound components. Next, substrate solutions are added to each well. The enzyme (HRP) and substrate are allowed to react over a short incubation period (15-20 minutes at 37°C). The enzyme-substrate reaction is terminated by addition of a sulphuric acid solution and the color change is measured spectrophotometrically at a wavelength of 450nm.

Flow cytometry

FACS analysis was performed with a FACSCelesta (BD Bioscience) on murine splenocytes or on single cells suspension prepared upon collagenase-digestion of grafted organs. We used the following antibodies: APC conjugated Rat anti-mouse CD62L, PE conjugated Rat anti-mouse CD44, PerCp conjugated Rat anti-mouse CD4 or PerCp conjugated Rat anti-mouse CD8, (Biolegend, San Diego, CA, USA), and APC conjugated anti-mouse/human insulin (R&D, Minneapolis, MN - USA). GLP-1R was detected by indirect staining; the primary antibody was purchased from Alomone Lab (Jerusalem, Israel) and variably associated with FITC or APC-conjugated anti-isotype Ab (BD and Biolegend respectively). For intracellular staining, splenocytes were isolated from BL6 mice were incubated with and w/o anti CD3/CD28 used both at 0.5 μ g/ml, Exe-4 (0.1nM, 1nM and 10nM) or with Exe-4+Exe-9-39 (0.1nM, 1nM and 10nM). After 24hours incubation, cells were collected, washed and plated in RPMI 10% FBS, then stimulated with 50 ng/ml PMA (Sigma Aldrich), 500 ng/ml ionomycin (Sigma Aldrich) and Golgi Stop as recommended by the manufacturer (BD Biosciences, San Diego, CA, USA) for 4h in a humidified incubator 37°C, 5% CO₂. After incubation, cells were collected, washed and stained for surface markers, i.e CD4 BUV737, CD8 BUV395, (BD Biosciences, San Diego, CA, USA) and GLP-1R FITC (Alomone Lab, Jerusalem, Israel). They were further fixed, permeabilized using the BD Cytofix/Cytoperm Kit (BD Biosciences, San Diego, CA, USA), and stained with a mAb against IFN- γ (eBioscience). Finally, CD4 $^+$ GLP-1R $^+$ IFN- γ $^+$ and CD8 $^+$ GLP-1R $^+$ IFN- γ $^+$ T cells were assessed by flow cytometry analysis. For the expression of GLP-1R on innate immune cells, the following antibodies were used: CD4 BB700, NK1.1 BV421, CD127 BV605, CD44 PE, GLP-1R FITC/PD1 FITC, Viability Dye BV510 (NKT subset); CD45 BV786, CD3 BB700, NK1.1

BV421, GLP-1R FITC/PD1 FITC, Viability Dye BV510 (NK subset); CD45 BB700, CD11c BV786, CD11b BV421, GLP-1R FITC/PD1 FITC, Viability Dye BV510; CD45 PE-CF594, CD127 BV605, NK1.1 BV421, CD335 BV786, CD49a BV650, CD117 BB700, IL33R PE, IL23R BV711, GLP-1R FITC/PD1 FITC, Viability Dye BV510 (LCs subset). For the determination of the chemokine receptors profile of GLP-1R⁺ CD3⁺ T cells, the following antibodies were used: GLP-1R FITC, CXCR4 PE, CX3CR1 BV605, CCR2 BV421, CCR5 BV650, CCR7 BV786, CXCR3 BB700, CXCR6 BV711, Viability Dye BV510.

ELISpot assay

An ELISPOT assay was used to measure the number of IFN- γ -producing cells according to the manufacturer's protocol (BD Biosciences) as previously performed by our group.⁶⁰ To test the role of GLP-1R-driven immunity on the anti-CD3/28 non-autoimmune specific response, 1x10⁶ splenocytes isolated from C57BL/6 mice were cultured in a microwell plate (BD Biosciences) coated with IFN- γ capture antibody (Ab) in the presence of the following soluble anti-CD3 and anti-CD28 at 0.5ug/ml for 24 hours. Exe-4 and/or Exe-4+Exe-9-39 at concentrations of 0.1, 1 or 10 nM were added to the culture. After 24 hours, bound secondary Ab was visualized using HRP-streptavidin and the AEC substrate kit (BD Biosciences). Spots were counted using an Immunospot analyzer (Cellular Technology Ltd., Cleveland, OH) and expressed as the number of cytokine-producing spots per 1x10⁶ cells. After 24 hours, ELISpot plates were developed and acquired on an ELISpot reader, as previously described.

Western blot

Western Blot was performed with protein lysates from human and murine islets or CD4 and CD8 cells purified with magnetic beads (Miltenyi) from murine spleen or human Protein concentration in cell lysates was measured using a Bradford assay (Bio-rad, Hercules, CA). After an SDS polyacrylamide gel electrophoresis, proteins were transferred to a nitrocellulose membrane and incubated with primary GLP-1R (Alomone) or GAPDH (Cell Signaling Technology, Danvers, MA-USA) detecting Ab. The secondary incubation was performed with HRP-conjugated anti-isotype Ab (Cell Signaling). Quantification of band size was performed using ImageJ software and was normalized for GAPDH expression.

qRT-PCR

Total RNA was extracted from human or murine immune cells. RNA was purified by using RNeasy kit (Qiagen, Valencia, CA), then reverse-transcribed into cDNA using Superscript III (Invitrogen, Carlsbad, CA). Transcripts were amplified using a 7300 Real-Time PCR System and analyzed by the ΔCT method; GAPDH was used as the internal reference.⁶¹ Both GLP-1R and GAPDH primers were obtained from Applied Biosystems (Foster City, CA).

Transcriptomic array of GLP-1R^{pos} and GLP-1R^{neg} CD4⁺/CD8⁺ T cells

Transcriptomic array was performed on samples the following samples of GLP-1R^{pos} CD4⁺, GLP-1R^{neg} CD4⁺ T cells, GLP-1R^{pos} CD8⁺ and GLP-1R^{neg} CD8⁺ T cells isolated from splenocytes of C57BL/6 mice. 1 μ g of RNA was reverse transcribed using a QuantiNova Reverse Transcription Kit (Qiagen, Hilden, Germany) following the manufacturer instructions. The obtained cDNA of each sample was then analyzed by quantitative real time PCR analysis using a SYBR green-based Quantinova LNA murine custom panel (Qiagen) according to the manufacturer's instruction. Relative quantification of each gene in the panel was calculated by delta-Ct method using averaged levels of *ACTB*, *B2M*, *GAPDH*, *HSP90AB1* genes for data normalization. Volcano plot shows statistical significance log (P value) versus difference (fold change).

Phosphoproteomic screen of CD3⁺ T cells

Isolated CD3⁺ T cells from splenocytes were treated with Exendin-4 (Exe-4) for 24 hrs or left untreated. Total soluble proteins from both cell extracts, approximately 7x10⁶ cells per conditions were used, all steps were performed using the Phospho Explorer Anti-body Array kit (Full Moon Biosystems, PEX100) as recommended by the manufacturer.⁶² Next, soluble extracted proteins were biotinylated and were next incubated with a mixture of Cy3-streptavidin-detection buffer and the array slides were incubated on a rotating shaker for 30 min at RT. After, several washing steps, the array slides were allowed to dry by centrifugation. Dry array slides were analyzed by a slide-based microarray scanner as recommended by the manufacturer.

Immunoprecipitation of GLP-1R on CD3⁺ T cells

Protein lysates were extracted from murine CD3⁺ T cells (30 mg per sample), previously selected from splenocytes of C57BL/6 mice and stimulated for 24 hours with anti-CD3/anti-CD28 (1 μ g/each). We first added GLP-1R antibody to the Dynabeads and incubated for 10 min at room temperature. Then, we crosslinked the antibody to the Dynabeads Protein G (Invitrogen) magnetic beads before immunoprecipitation in order to avoid co-elution of the antibody. Immunoprecipitation was then carried out overnight at 4 °C by adding protein lysate to Ab-Dynabeads complex. Material was eluted from the Ab-Dynabeads complex using Elution Buffer (50mM glycine pH 2.8) for 2 min at room temperature, to dissociate the complex, and was separated by SDS/PAGE and respectively visualized using silver staining/Coomassie staining. Gel bands that were unique to lanes containing GLP-1R as well as the corresponding areas in the control lane were excised and subjected to in-gel digestion with trypsin and to analysis by MS/MS as previously described.⁶³

Immunofluorescence of GLP-1R on CD3⁺ T cells

Immunofluorescence analysis of isolated CD3⁺ T cells and anti-CD3/anti-CD28-treated CD3⁺ T cells, was performed using the following antibody rabbit anti-GLP-1R FITC (AGR021F, Alomone) at a 1:200 dilution. Analysis of immunofluorescence and collection of images were conducted using a confocal system (TCS SP5 laser scanning confocal, Leica) as previously described.

Immunoelectron microscopy

For electron microscopy immunocytochemistry, the pellets of lymphocytes were fixed for 2 hrs at 4 °C in a mixture of 2% paraformaldehyde and 1.25% glutaraldehyde in 0.05 M (pH 7.3) cacodylate buffer, post-fixed in 1% osmium tetroxide and embedded in EMBed-812 embedding kit (Electron Microscopy Sciences Hatfield, PA, UK). Thin sections were incubated with GLP-1R primary antibody (Alomone labs) diluted 1:10, then with colloidal gold conjugated anti-rabbit antibody diluted 1:50 (EY laboratories, San Mateo CA USA), and, after counterstaining with uranyl acetate and lead citrate, were examined with a TEM Jeol 1010 (Jeol, Tokyo, Japan), of Centro Grandi Attrezzature of Varese Insubria University.

Mass Spectrometry

CD3⁺ T cells selected from C57BL/6 mice and consecutively stimulated for 24 hours with anti-CD3/anti-CD28 (1 µg/each) were immunoprecipitated with anti-GLP-1R antibody (AGR021, Ijomone). Then, bound material was washed and separated by SDS-PAGE as recommended by the manufacturer and the Silver-stained band was analyzed by LC-MS2 as previously described.⁶⁴

GLP-1R transfection of T cells

The mGLP-1R cDNA construct (Origene) was inserted into the pMY-IRES-GFP plasmid (Cell BioLabs, Inc., San Diego, CA). The Platinum-E Retroviral Packaging cell line was transfected with the pMY-IRES-GFP plasmid expressing GLP-1R using polybrene (Santa Cruz Biotechnology), and supernatant was collected. T cells were activated for 48 hours in the presence of soluble anti-CD3/CD28 at 0.5 µg/ml each in the presence of IL-2 (400 ng/ml) (R&D Systems), and viral supernatant was added. The upregulation of GLP-1R was assessed by FACS and western blot analysis.

Transwell migration assays

Transwell migration assays were performed on GLP-1R^{pos} and GLP-1R^{neg} CD3⁺ cells or respectively untransduced-mock CD3⁺ T cells or pmY-GLP-1R transduced CD3⁺ T cells, freshly isolated or activated with anti-CD3/CD28 (0.5 µg /ml each) in the presence or not of Exe-4 (1 nM). Chemotaxis assessments via transwell migration assay were performed using polycarbonate membranes with 5 µm pores (Corning) in accordance with the manufacturer's instructions and as previously published.⁶⁵ Cells were washed, re-suspended in migration media (RPMI), and added to the upper chamber of the plate, while migration media containing 0 or 50 ng/mL SDF-1 (R&D Systems) was added to the bottom chamber. Treated cells were incubated over night at 37°C to migrate through the polycarbonate membrane into the bottom chamber. Input cell counts were obtained by flow cytometry with a BD FACSCelesta (BD, Biosciences) as well as cell counts of migrated cells in the lower chambers. Migration percentage was calculated as the number of cells in the lower chamber (migrated) compared to total input cell count for three separate wells. Mean migration percentages and standard deviations (SD) were calculated across the different donor cell lots. Analysis of lower chambers without SDF-1 (negative gradients) was used to control for any nonspecific increase in chemotaxis.

Bioenergetic analysis

Cellular Bioenergetics were analyzed using the Seahorse Extracellular Flux Analyzer Xfe96 (Agilent Technologies, Santa Clara, CA, United States), which simultaneously measures Oxygen Consumption Rate (OCR, pmolO₂/min), ExtraCellular Acidification Rate (ECAR, mph/min) and Proton Efflux Rate (PER, pmolH⁺/min). For Seahorse experiments 150.000 cells either freshly isolated GLP-1R^{pos} or GLP-1R^{neg} CD3⁺ T cells or activated with soluble anti-CD3/CD28 at 0.5 µg/ml each in the presence or not of Exe-4 (1 nM); in another setting untransduced mock CD3⁺ T cells or pmY-GLP-1R CD3⁺ T cells already activated with soluble anti-CD3/CD28 at 0.5 µg/ml each in the presence or not of Exe-4 (1 nM). Cells were resuspended in 50 µL assay medium (Agilent #103576-100 RPMI Medium pH7.4, supplemented with 10mM glucose, 2mM glutamine and 1mM Na-pyruvate) were seeded in each CellTak-precoated well of an Agilent Xfe96 Pro well plate. The cell plate was centrifuged 2 times at 40 × g (zero braking) for 1 minute. After centrifugation, 150 µL warm assay medium was gently added to each well. After 45 minutes incubation at 37 °C in a no-CO₂ incubator, Seahorse assays were performed according to:

Seahorse XF T Cell Metabolic Profiling Kit (Agilent #103772-100) protocol which includes three measurements under basal condition and after the injection of the ATP synthase inhibitor oligomycin A (1.5 µM), the electron transport chain (ETC) accelerator ionophore BAM15 (2.5 µM) and the ETC inhibitors mixture rotenone (0.5 µM) + antimycin A (0.5 µM);

- Seahorse XF Glycolytic Rate assay Kit (Agilent protocol #103344-100) which includes three measurements under basal condition and after the injection of the mixture rotenone (0.5 µM) + antimycin A (0.5 µM) and the glycolysis inhibitor 2-deoxyglucose (2-DG).
- Seahorse parameters were normalized to cell number in each well. To this purpose, at the end of the Seahorse analysis, cell nuclei were stained with Hoechst 33342 (1 µg/mL) for about 15 min, imaged and counted with Operetta CLS™ software Harmony, as previously described.⁶⁶

Bioenergetic parameters were calculated using the following formulas:

$$\text{Basal Respiration} = \text{mitoOCR} = \text{OCR}_{\text{basal}} - \text{OCR}_{\text{rot/ant}};$$

$$\text{Maximal Respiration} = \text{OCR}_{\text{BAM15}} - \text{OCR}_{\text{rot/ant}};$$

$$\text{Spare respiratory capacity} = \text{OCR}_{\text{BAM15}} - \text{OCR}_{\text{basal}};$$

$$\text{ATP linked Respiration} = \text{OCR}_{\text{basal}} - \text{OCR}_{\text{oligo}};$$

$$\text{Proton Leak} = \text{OCR}_{\text{oligo}} - \text{OCR}_{\text{rot/ant}};$$

$$\text{Non-mitochondrial respiration} = \text{OCR}_{\text{rot/ant}}$$

$$\text{Basal glycolysis} = \text{PER basal} - \text{mitoPER}$$

$$\text{mitoPER} = \text{mitoOCR} * \text{CCF}; \text{ CCF} = 0.61;$$

$$\text{Compensatory glycolysis} = \text{PER}_{\text{rot/ant}}$$

scRNA seq of GLP-1R^{pos} and GLP-1R^{neg} CD3⁺ T cells

Live GLP-1R^{pos} and GLP-1R^{neg} CD3⁺ T cells isolated from splenocytes of C57BL/6 mice were FACS sorted through a BD FACSAria Fusion and were then washed and recovered in PBS containing 0.04% BSA. Recovered cells were counted and a viability > 90% was verified and the 2 cell suspensions (GLP-1R^{pos} and GLP-1R^{neg} CD3⁺ T cells) were then concentrated at a concentration of 1000 cells/μl and were subsequently used for library preparation. scRNA seq libraries were prepared using “Chromium scRNA 3'NEXTGEM 3.1” (10x GENOMIX) at the Center for Omics Sciences (COSR), IRCCS San Raffaele Scientific Institute, Italy, following manufacturer's instructions. Prepared libraries were then sequenced through an Illumina NovaSeq6000 on a S1 flow cell at 100 cycles.

Bioinformatic analysis

UMItool v.1.0.0 was used to map the raw reads to the mouse genome (vs mm10) and to obtain the gene expression level for each cell, annotated with Genecode, release M22. The counts were then imported in the R environment v.4.0.3 and analyzed with the Seurat package v.4.3.0 (<https://satijalab.org/seurat/>). The two samples were first analyzed individually, following the standard Seurat pipeline. Cells with a total number of detected genes < 200 or > 5000 were filtered out, as well as cells with a relative count of mitochondrial genes > 0.1. Counts were then normalized with the Seurat global-scaling normalization method “LogNormalize” with a 10,000 scale factor. The FindVariableFeatures function was used to identify a subset of features that exhibit high cell-to-cell variation that were then used as input for the RunPCA function to perform the principal component analysis (PCA). Both the datasets were then scaled with the ScaleData function, regressing out the number of feature and the percentage of mitochondrial genes to obtain equal weight in downstream analysis. CellCycleScoring was employed to assess cell cycle scores on scaled data and the distribution of the variable genes resulted to be unaffected by the cell cycle phases. Clustering was carried out through the FindCluster function, using the original Louvain algorithm and considering 1-30 principal components. Resolutions equal to 0.5 and 0.2 for sample GLP-1R^{pos} and sample GLP-1R^{neg}, respectively, were considered. The integrated analysis was performed with the standard Seurat pipeline. The two single samples were combined selecting the integration anchors through the SelectIntegrationFeatures and FindIntegrationAnchors functions. The final integration step was then performed with the IntegrateData function. Data were scaled as described above and the new integrated matrix was employed for clustering and visualization with a 0.3 resolution.

Identification of differentially expressed genes

The function FindAllMarkers was used to perform a Wilcoxon test and to determine the genes differentially expressed in each cluster compared to the rest of the cells (logfc.threshold = 0.25, min.pct = 0.25). This allowed to detect the top marker genes for each cluster.

Annotation

Cells were first classified using the SingleR package, with the ImmGen database Aran et al.⁶⁷ Then, a more detailed manually cured annotation was performed, considering the top marker genes for each cluster.

mRNA GLP-1R due diligence assessment on T cells

In order to confirm the expression of GLP-1R on T cells, total RNA was extracted from CD4⁺ and CD8⁺ T cells isolated by positive selection with microbeads (CD8a⁺ T Cell Isolation Kit, mouse and LT34 for CD4 isolation; MiltenyiBiotech.com) and from Beta-TC-6 cell line (BTC6), a murine beta cell line initially derived from insulinoma and used here as a positive control for GLP-1R expression. RNA was extracted by using the Direct-zol RNA Kit (Zymo Research Irvin, CA, USA) following manufacturer's instructions and then quality checked and quantified by spectrophotometry. A total of 10 ng RNA from the aforementioned cells was retrotranscribed into cDNA with the Superscript III kit (Life Technologies) and *Glp-1r* expression was quantified by qPCR using PowerUp SYBR Green Master Mix 2X (Life Technologies) on a QuantStudio S6 Real-Time PCR System (Thermo Fisher Scientific). Specificity of the amplifications was assessed by melt curve analysis. Primers for murine *Glp-1r* amplification (Fw: 5'-TGCTATCGGCGTCAACTTTCT-3'; Rv: 5'-ATTCAAGTGCTCCAGCCTCC-3') were designed in-house by an online tool (<https://www.primer3plus.com>), to yield a 334 bp-long amplicon from *Glp-1r* mRNA. Murine *Gapdh* mRNA was amplified in parallel using specific primers (Fw: 5'-CCAGGGCTGC CATTGCAAGTGGCAAAGTGG-3'; Rv: 5'-CCTGGAAGATGGTGATGGVTTCCCGTTGA-3') to be used as positive internal control. Reactions in which reverse transcriptase was omitted (-RT) were run in parallel to test for potential DNA contamination. PCR products were separated on a 0.8% agarose gel in TAE buffer. Bands corresponding to the putative *Glp-1r* amplicon (334 bp) were excised from the gel and DNA was extracted using the Gel DNA Recovery Kit (Zymo research, Irvin, CA, USA). Both strands of recovered DNA were then sequenced by the Sanger method with the same forward and reverse primers used for gene amplification. The obtained amplicon sequences were aligned with that of nucleotides 950-1296 of murine *Glp-1r* mRNA NCBI Reference sequence NM_021332.2 by the Clustal Omega Multiple Sequence Alignment tool (<https://www.ebi.ac.uk/Tools/msa/clustalo>).

QUANTIFICATION AND STATISTICAL ANALYSIS

Data are expressed as mean ± SEM. Kaplan-Meier analysis was used for analysis of survival. When two groups were compared, a two-sided unpaired Student *t* test (for parametric data) or a Mann-Whitney test (for nonparametric data) was used. A P value < 0.05 (by two-tailed testing) was considered an indicator of statistical significance and were reported within the corresponding panels of the figure legends. Graphs were generated using GraphPad Prism 10 software (GraphPad Software, San Diego, CA).

Supplemental information

**Glucagon-like peptide 1 receptor
is a T cell-negative costimulatory molecule**

Moufida Ben Nasr, Vera Usuelli, Sergio Dellepiane, Andy Joe Seelam, Teresa Vanessa Fiorentino, Francesca D'Addio, Emma Fiorina, Cong Xu, Yanan Xie, Hari Baskar Balasubramanian, Eduardo Castillo-Leon, Lara Loreggian, Anna Maestroni, Emma Assi, Cristian Loretelli, Ahmed Abdelsalam, Bassett El Essawy, Silvia Uccella, Ida Pastore, Maria Elena Lunati, Gianmarco Sabiu, Adriana Petrazzuolo, Giacomo Ducci, Elena Sacco, Lucia Centofanti, Massimo Venturini, Serena Mazzucchelli, Deborah Mattinzoli, Masami Ikehata, Giuseppe Castellano, Gary Visner, Liu Kaifeng, Kang Mi Lee, Zhimin Wang, Domenico Corradi, Stefano La Rosa, Silvio Danese, Jun Yang, James F. Markmann, Gian Vincenzo Zuccotti, Reza Abdi, Franco Folli, and Paolo Fiorina

Supplemental Information:

Inventory of Supplemental information

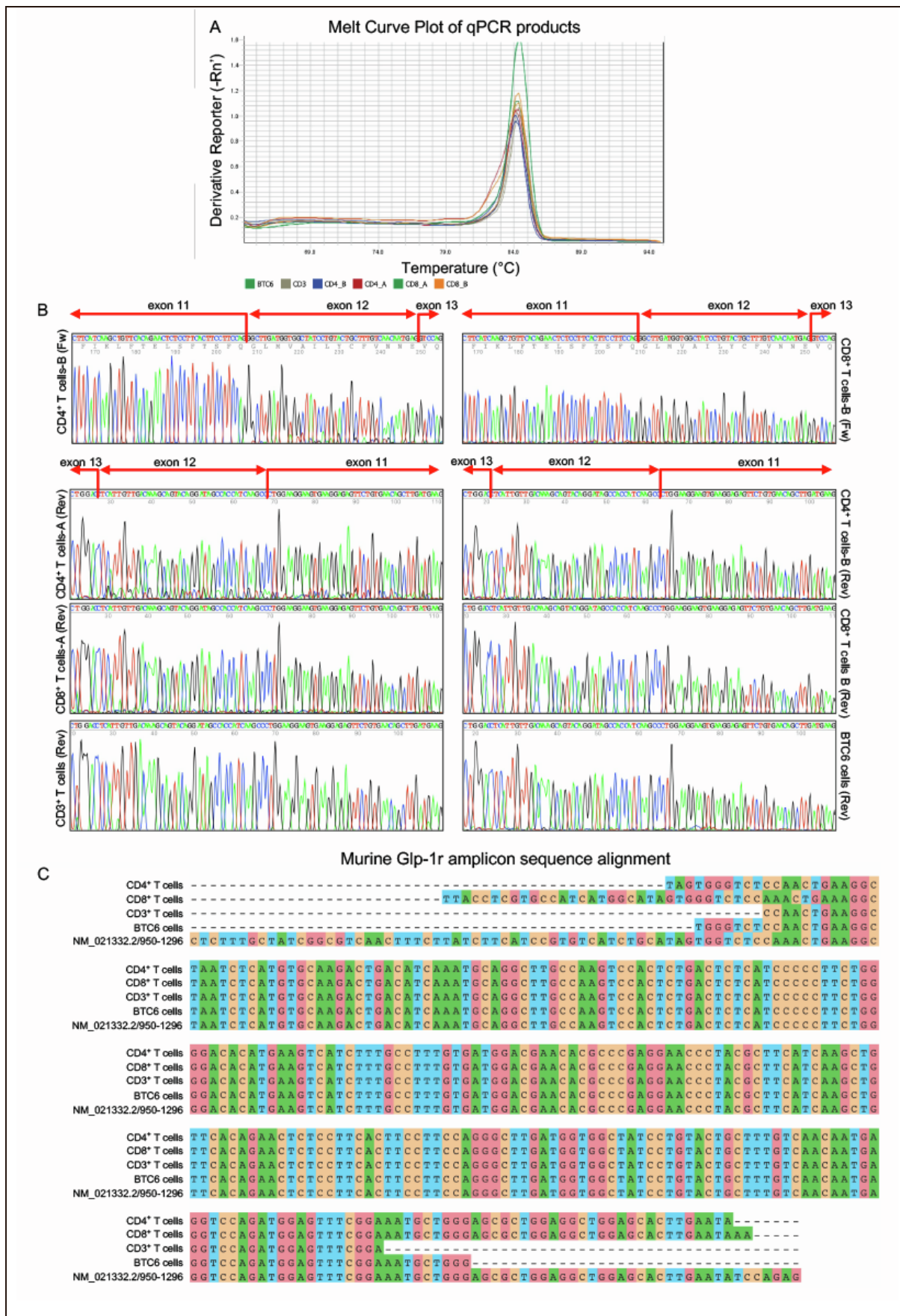
Supplemental Data_Figures

- Figure S1. Glp-1r mRNA expression in T cells was confirmed by Sanger sequencing, related to Figure 1.
- Figure S2. GLP-1R expression and murine immune cells, related to Figures 1 and 2.
- Figure S3. scRNAseq analysis reveals heterogeneity of GLP-1R^{pos} T cells, related to Figure 3.
- Figure S4. GLP-1R signaling modulates T cells function, related to Figure 4.
- Figure S5. GLP-1R signaling modulates the alloimmune response *in vivo*, related to Figure 5.
- Figure S6. GLP-1R is expressed by human T cells, related to Figure 7.
- Figure S7. Expansion of GLP-1R^{pos} T cells during human allograft rejection, related to Figure 7.

Supplemental Data_Tables

- Table S1. Relative quantification of the immunoprecipitated GLP-1R^{pos} CD3⁺ T cells, related to Figure 2.
- Table S2. Characteristics of kidney-transplanted patients, related to Figure S7 and to STAR Methods..
- Table S3. Characteristics of heart-transplanted patients, related to Figure S7 and to STAR Methods..

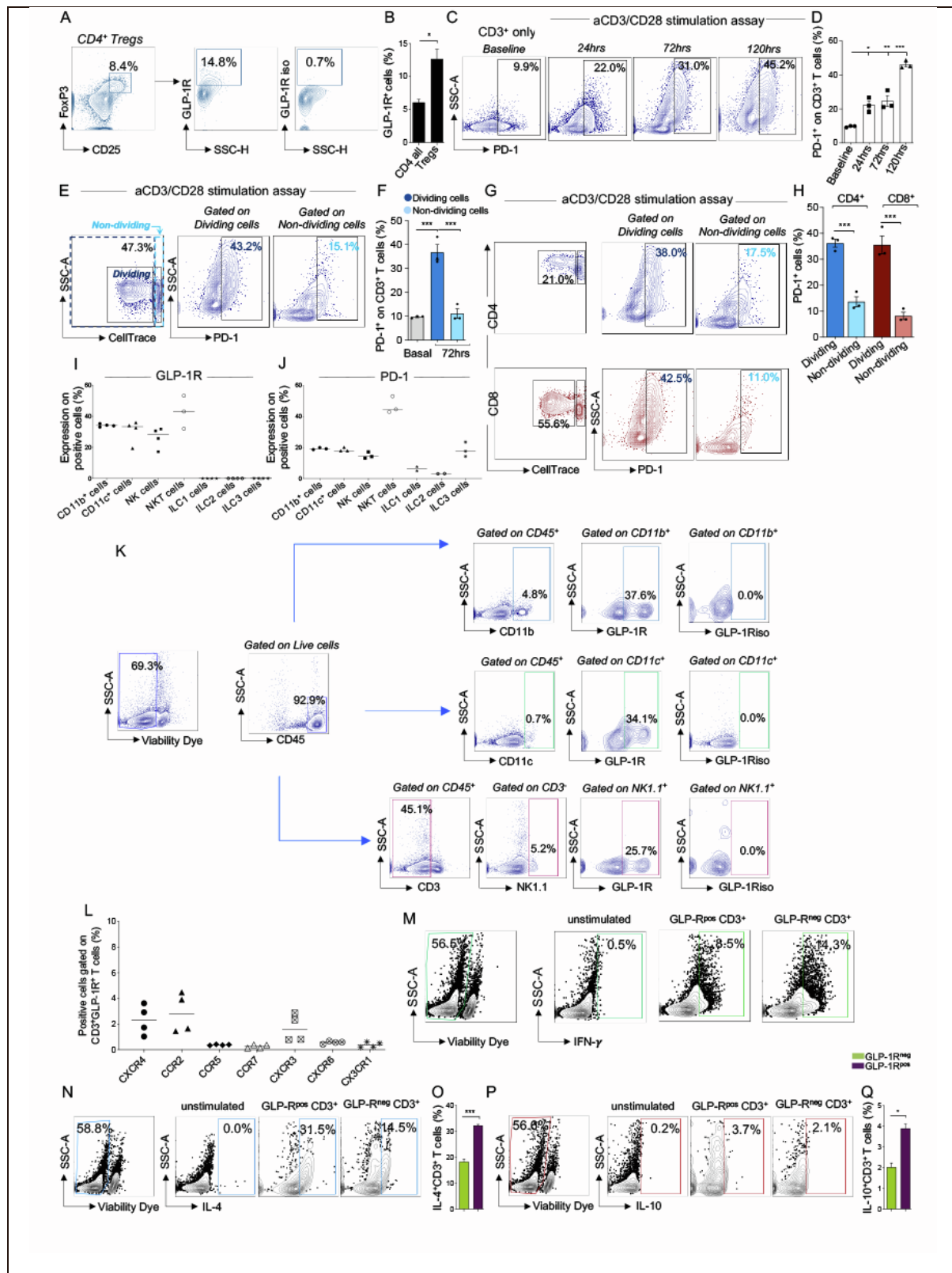
Figure S1. Glp-1r mRNA expression in T cells was confirmed by Sanger sequencing, related to Figure 1. **A:** Melting curve plots of qRT-PCR products showing a single peak at ~84°C confirming a unique amplification product obtained when the cDNA of BTC6, respectively 2 biological replicates of murine CD4⁺ and CD8⁺ T cells and CD3⁺ T cells was used. **B:** Representative electropherograms showing the 5'-to-3' sequence of the amplified *Glp-1r* region spanning exons 11 to 13 in murine CD4⁺, CD8⁺, CD3⁺ T cells and BTC6 cells obtained by Sanger sequencing. **C:** Sequence alignment of nucleotides 950-1296 of murine *Glp-1r* mRNA reference sequence NM_021332.2 to that of the qRT-PCR products obtained from RNA of CD4⁺, CD8⁺, CD3⁺ T cells and of BTC6 cells, further confirming the amplification of *Glp-1r* in these cells.



Abbreviations: BTC6, Beta-TC-6 cell line; qRT-PCR, Two-step quantitative reverse transcriptase-PCR; cDNA, complementary DNA.

Figure S2. GLP-1R expression and murine immune cells, related to Figures 1 and 2. **A**: Representative dot plots for gating strategy and GLP-1R expression by CD4⁺CD25⁺FoxP3⁺ regulatory cells. **B**: Quantification of flow cytometric analysis from A and comparison with whole CD4⁺ population. **C-D**: Cell trace violet-labelled CD3⁺ T cells were activated with anti-CD3/CD28 Abs. After 24 hours, 72 hours and 120 hours cells were harvested and stained for PD-1; representative dot plots for FACS analysis related to each time point (24, 72 and 120 hours) are shown in (C) and their corresponding bar graphs are shown in (D). **E-F**: PD-1 expression was depicted after 72 hours of stimulation with anti-CD3/CD28 Abs on dividing CD3⁺ T cells as compared to non-dividing CD3⁺ T cells; the quantification of PD-1 expression in both sub-populations is shown in (F). **G-H**: PD-1 expression was depicted after 72 hours of stimulation with anti-CD3/CD28 Abs on dividing CD4⁺ and CD8⁺ T cells as compared to non-dividing CD4⁺/CD8⁺ T cells, the quantification of PD-1 expression in both sub-populations is shown in (H). Data are representative of at least n=3 samples and are expressed as mean ± standard error of the mean (SEM). *P<0.05; **P<0.01; ***P<0.001. **I-K**: A head to-head comparison of GLP-1R and PD-1 expression on cells of innate immunity. **I**: GLP-1R expression was assessed by FACS analysis on respectively CD11b⁺ cells, CD11c⁺ cells, NK cells defined as CD3-/NK1.1⁺, NKT cells defined as CD4⁺/NK1.1⁺/CD44⁺/CD127⁺ and by ILCs (ILC1: NK1.1⁺/CD127⁺/CD49a⁺/CD335⁺; ILC2: CD117⁺/CD127⁺/IL33R⁺, ILC3: CD117⁺/CD127⁺/IL23R⁺); all derived from splenocytes isolated from C57BL/6 mice. **J**: PD-1 expression by the aforementioned cells of innate immunity are shown. **K**: Gating strategy delineating the expression of GLP-1R on CD11b⁺, CD11c⁺ and NK cells of innate immunity. **L**: The profile of several chemokine receptors (CXCR4, CCR2, CCR5, CCR7, CXCR3, CXCR6 and CX3CR1) was explored on GLP-1R^{pos} CD3⁺ T cells. **M**: FACS gating strategy of IFN-γ expression on GLP-1R^{pos}/ GLP-1R^{neg} CD3⁺ T cells. **N-Q**: FACS gating strategy and quantitative bar graph of IL-4/IL-10 expression on GLP-1R^{pos}/ GLP-1R^{neg} CD3⁺ T cells. Data

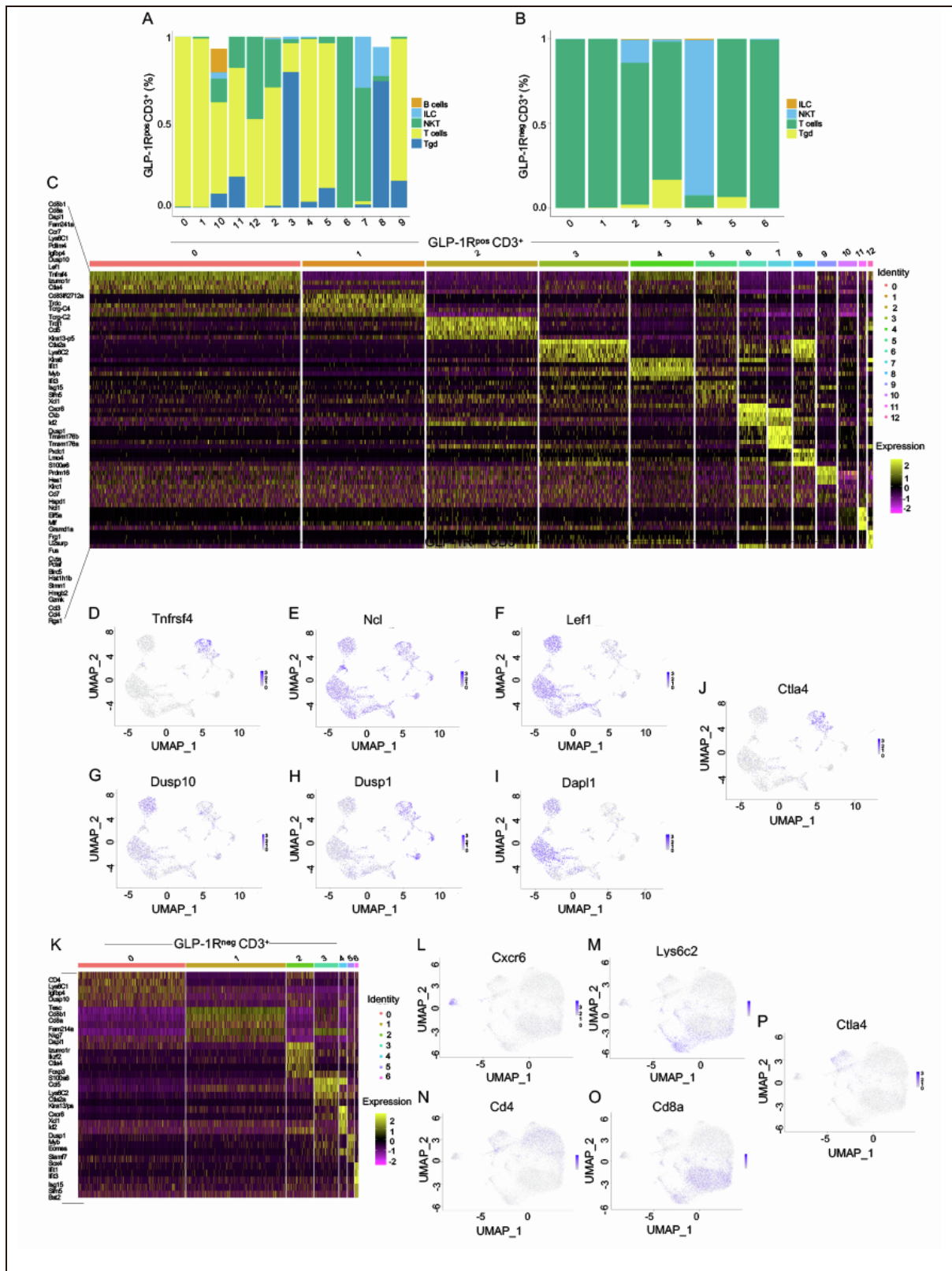
are representative of at least n=3 samples and are expressed as mean \pm standard error of the mean (SEM). *P<0.05; **P<0.01; ***P<0.001.



Abbreviations: GLP-1R, Glucagon-like peptide 1 receptor; FoxP3, forkhead box P3; Abs, antibodies; FACS, fluorescence-activated cell sorter scan; CT, cell trace; ILCs, Innate Lymphoid Cells.

Figure S3. scRNAseq analysis reveals heterogeneity of GLP-1R^{pos} T cells, related to

Figure 3. alloimmune response **A:** Barplot of the sorted GLP-1R^{pos} CD3⁺ T cells showing the SingleR annotation for the 13 identified clusters, using 30 nPCs and 0.5 resolution. **B:** Barplot of the sorted GLP-1R^{neg} CD3⁺ T cells showing the SingleR annotation for the 7 identified clusters, using 30 nPCs and 0.2 resolution. **C:** Heat-map showing the most relevant genes present within the GLP-1R^{pos} CD3⁺ subset. **D-J:** UMAPs delineating the main gene/markers identified in the GLP-1R^{pos} CD3⁺ T cell-scRNAseq dataset. **K:** Heat-map showing the most relevant genes present within the GLP-1R^{neg} CD3⁺ subset. **L-P:** UMAPs delineating the main gene/markers identified in the GLP-1R^{neg} CD3⁺ T cell-scRNAseq dataset.

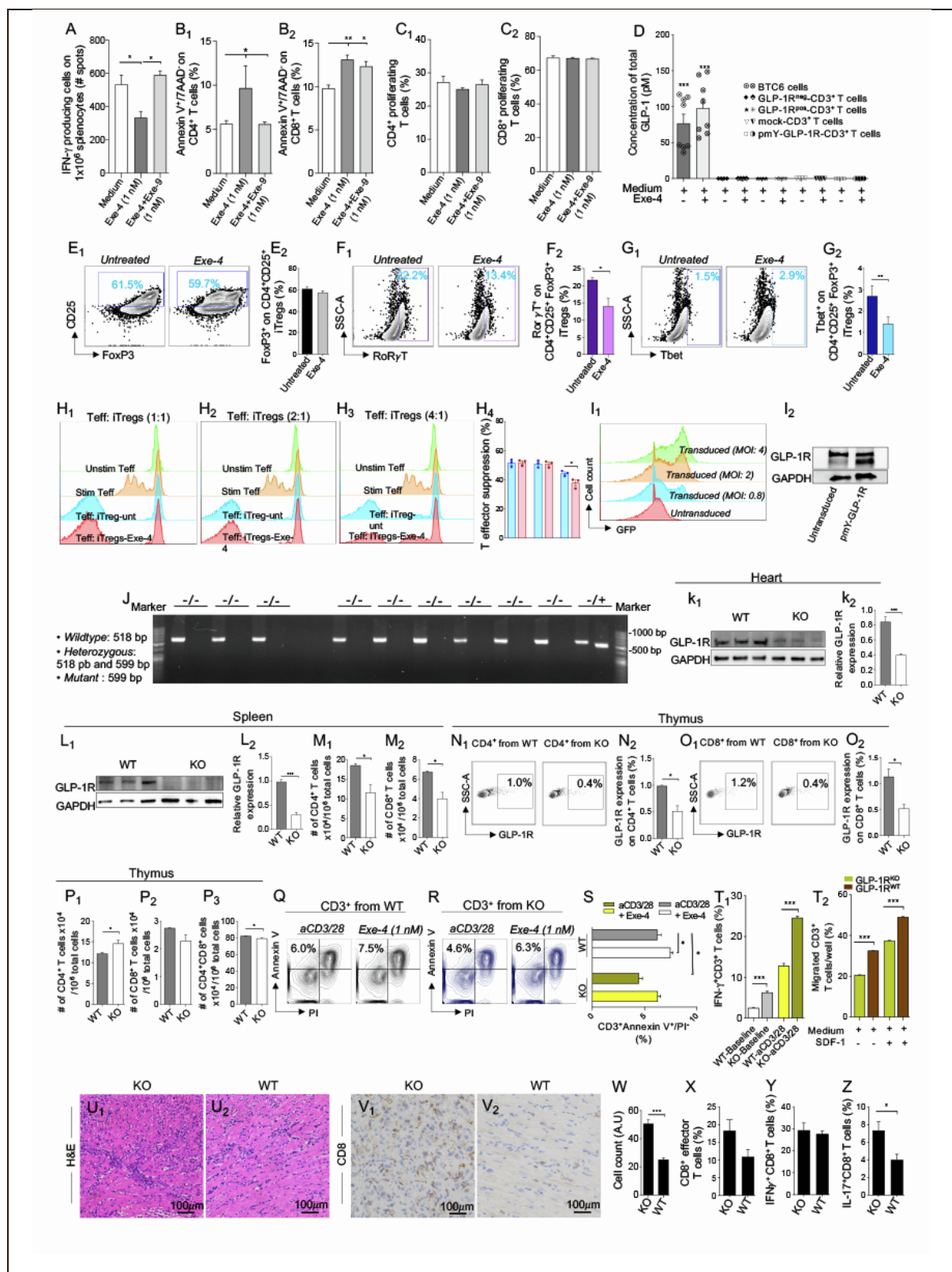


Abbreviations: GLP-1R, Glucagon-like peptide 1 receptor; ATP, adenosine triphosphate; UMAP, Uniform manifold approximation and projection; scRNAseq, single cell RNA sequencing.

Figure S4. GLP-1R signaling modulates T cells function, related to Figure 4. **A:** Exe-4 significantly reduced the number of IFN- γ producing cells by mitogen-stimulated splenocytes, which was dampened upon co-culture with GLP-1R antagonist Exendin-9-39 (Exe-9) (one way-ANOVA, $P<0.05$). **B₁-B₂:** Exe-4 treatment induced cell death on activated CD4 $^{+}$ and CD8 $^{+}$ T cells ($p<0.05$ in Exe-4 (1 nM) treated CD4 $^{+}$ T cells vs. medium, $p<0.01$ in medium vs. Exe-4 (1 nM) treated CD4 $^{+}$ T cells). **C₁-C₂:** No differences were observed comparing the percentages of proliferating (or cell trace positive) CD4 $^{+}$ and CD8 $^{+}$ T cells stimulated with anti-CD3/CD28 Abs upon their challenge with Exe-4 neither with the addition of the antagonist Exe-9. **D:** Total GLP-1 concentration measured in different assays with GLP-1R^{pos} or GLP-1R^{neg} CD3 $^{+}$ T cells, untransduced mock or pmY-GLP-1R CD3 $^{+}$ T cells with or without Exe-4 as compared to that measured when using BTC6 cell line, as a positive control. **E₁-E₂:** Representative FACS dot plots showing the percentage of FoxP3 $^{+}$ CD4 $^{+}$ CD25 $^{+}$ Tregs during Treg induction assay in response to Exe-4 treatment; the quantitative bargraph is shown in (E₂). **F₁-F₂:** Representative FACS dot plots showing the percentage of Ror- γ T on FoxP3 $^{+}$ CD4 $^{+}$ CD25 $^{+}$ Tregs during Treg induction assay in response to Exe-4 treatment; the quantitative bargraph is shown in (F₂). **G₁-G₂:** Representative FACS dot plots showing the percentage of Tbet on FoxP3 $^{+}$ CD4 $^{+}$ CD25 $^{+}$ Tregs during Treg induction assay in response to Exe-4 treatment; the quantitative bargraph is shown in (G₂). **H₁-H₄:** Representative FACS histograms reflecting effector T cell suppression shown as CTV dilution upon co-culture of untreated-iTregs or Exe-4-treated iTregs at respectively the following ratios: 1:1, 2:1 and 4:1; quantitative bargraph reflecting the percentage of effector T cell suppression is shown in (H₄). **I₁-I₂:** GLP-1R upregulation is verified by respectively FACS analysis (I₁) and western blot analysis (I₂), in pmY-GLP-1R-transduced CD3 $^{+}$ T cells as compared to their counterparts untransduced. **J:** The baseline phenotype of GLP-1R KO mice is shown on agarose gel, where Wildtype are identified by the presence of 518 bp band, Heterozygous by the presence of

respectively 518 pb and 599 bp bands and the Mutant allele is distinguished by the presence of 599 bp band. **K₁-K₂**: Knockdown of GLP-1R within heart was confirmed by western blot analysis. **L₁-L₂ and M₁-M₂**: Knockdown of GLP-1R within spleen of GLP-1R KO mice was confirmed by western blot analysis (L₁ and L₂); the absolute numbers of CD4⁺ and CD8⁺ T cells were assessed by FACS analysis within spleen of GLP-1R KO mice as compared to WT mice and shown in (M₁ and M₂). **N₁-N₂, O₁-O₂, and P₁-P₃**: The knockdown of GLP-1R was confirmed in CD4/CD8 T cells in the thymus of GLP-1R KO mice (N₁ and N₂ and O₁-O₂); the absolute numbers of respectively CD4⁺, CD8⁺ and CD4⁺CD8⁺ T cells were assessed by FACS analysis within the thymus of GLP-1R KO mice as compared to WT mice and shown in (P₁ P₃). **Q-S**: Apoptosis assay of CD3⁺ T cells from GLP-1R KO mice at baseline and after mitogenic stimulation as compared to their counterparts from WT mice, the quantification of apoptotic cells in both groups and at baseline and/or after mitogen stimulation is shown in (S). **T₁**: Quantitative bargraph depicting the percentage of splenic IFN- γ ⁺CD3⁺ T cells from GLP-1R KO mice as compared to WT mice at baseline and in response to mitogen stimulation. **T₂**: The percentage of CD3⁺ T cells from GLP-1R KO mice migrating to SDF-1 gradient was significantly lower as compared to their counterparts from WT mice. **U₁-U₂**: Hematoxylin and eosin staining in heart allografts obtained from C57BL/6 WT mice transplanted with BALB/c hearts and treated with low dose CTLA4-Ig and from C57BL/6 GLP-1R KO mice recipients of BALB/c hearts and treated with low dose CTLA4-Ig, (magnification 20X, and scale bar 100 μ m). **V₁-V₂ and W**: CD8 staining in heart allografts obtained from C57BL/6 WT mice transplanted with BALB/c hearts and treated with low dose CTLA4-Ig and from C57BL/6 GLP-1R KO mice recipients of BALB/c hearts and treated with low dose CTLA4-Ig, (magnification 20X, and scale bar 100 μ m); the relative quantification of CD8 infiltrating cells in both groups of transplanted mice is shown in (W). **X-Z**: Bargraphs depicting the quantification of respectively CD8 effector T cells as well as the significant increase in the

percentages of IL-17⁺ CD8⁺ T cells in splenocytes from both groups of transplanted mice as aforementioned. Data are representative of at least n=3 samples and are expressed as mean ± standard error of the mean (SEM). *P<0.05; **P<0.01; ***P<0.001. Data are representative of at least n=3 samples and are expressed as mean ± standard error of the mean (SEM). *P<0.05; **P<0.01; ***P<0.001.



Abbreviations: GLP-1R, Glucagon-like peptide 1 receptor; FACS, fluorescence-activated cell sorter scan; IFN- γ , interferon gamma; FoxP3, forkhead box P3; CTV; cell trace violet; iTregs; induced T regulatory cells; Exe-4, Exendin 4/Exenatide; WT; wildtype.

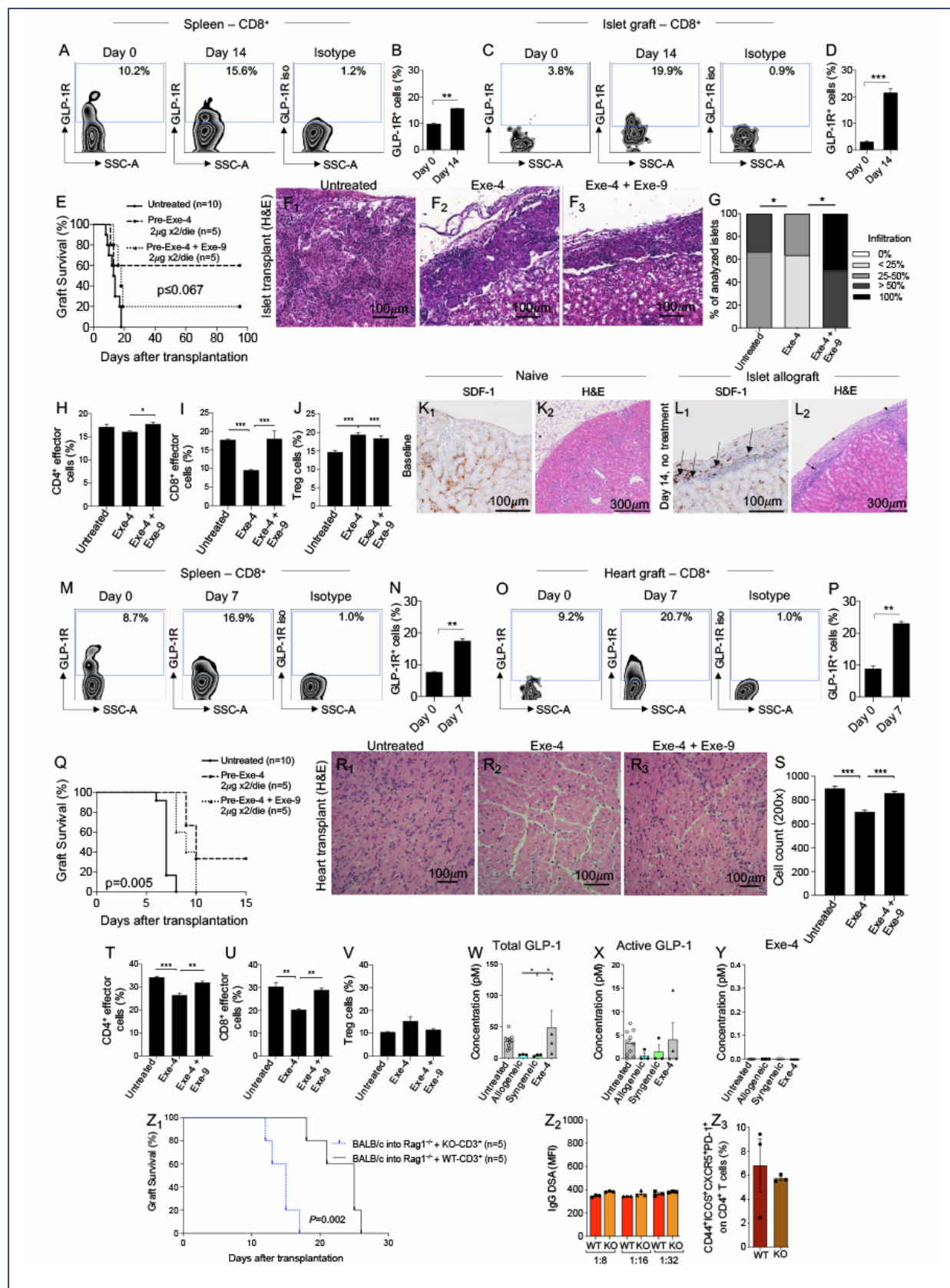
Figure S5. GLP-1R signaling modulates the alloimmune response *in vivo*, related to

Figure 5. **A:** Representative zebra plot of GLP-1R expression by splenic murine CD8⁺ T lymphocytes in basal condition and after islet allotransplantation; FACS plots are associated to related isotype control. **B:** Bargraph representing quantification of GLP-1R expression by spleen CD8⁺ lymphocytes in basal condition and after islet allotransplantation. **C:** Representative zebra plot of GLP-1R expression by murine CD8⁺ T lymphocytes in basal condition and after islet allotransplantation under kidney capsule; the plots are associated to related isotype control. **D:** Bargraph representing quantification of GLP-1R expression by CD8⁺ lymphocytes in normal kidneys and after islet allograft. **E:** Islet allograft survival curves from mice treated with GLP-1R agonist Exenatide (Exe-4, dashed line), a combination of Exe-4 and Exendin 9-39 (dotted line) or saline (dashed line); statistical analysis was performed using Student's t-test with Welch's correction. **F₁-F₃:** Representative hematoxylin and eosin histology staining of day-14 islet allografts from mice treated with saline, Exenatide 2 μ g twice/day, or both Exenatide and Exendin 9-39 2 μ g twice/day. **G:** Immune infiltrate quantification after hematoxylin and eosin histology staining in islet allografts from mice treated with saline, Exenatide 2 μ g twice/day, or both Exenatide and Exendin 9-39 2 μ g twice/day. **H-J:** Bargraph depicting the quantification of splenic CD4⁺ effector-memory, CD8⁺ effector-memory T cells or splenic CD4⁺ regulatory T cells in mice who underwent islet allograft and were treated with saline, Exenatide 2 μ g twice/day, or both Exenatide and Exendin 9-39 2 μ g twice/day. **K₁:** Representative immunohistochemistry staining for SDF-1 kidney at baseline, (magnification: 10X, scale bar: 300 μ m). **K₂:** Representative H&E histology staining on kidney at baseline (magnification: 10X, scale bar: 300 μ m). **L₁:** Representative immunohistochemistry staining for SDF-1 on islet allograft at day 14 post-transplant; the positive immunosignal (arrows) in the islet implant area is located in the inflammatory foci (black arrows), (magnification: 20X, scale bar: 300 μ m). **L₂:** Representative H&E histology

staining on islet allograft at baseline and at day 14 post-transplant, the islet implant site is thickened by a collagen fiber deposition encompassing both inflammatory foci and islet epithelial cells (magnification: 10X, scale bar: 300 μ m). **M:** Representative FACS zebra plot of GLP-1R expression by splenic murine CD8 $^{+}$ T lymphocytes in basal condition and after heart allotransplantation; the plots are associated to related isotype control. **N:** Bar graph representing quantification of GLP-1R expression by spleen CD8 $^{+}$ lymphocytes in basal condition and after heart allotransplantation. **O:** Representative zebra plot of GLP-1R expression by murine heart infiltrating CD8 $^{+}$ T lymphocytes in basal condition and in heart allograft; the plots are associated to related isotype control. **P:** Bar graph representing quantification of GLP-1R expression by heart infiltrating CD8 $^{+}$ lymphocytes in basal condition and in heart allograft. **Q:** Heart allograft survival curves from mice treated with GLP-1R agonist Exenatide/Exendin-4 (Exe-4, dashed line), a combination of Exe-4 and Exendin 9-39 (dotted line) or saline (dashed line); statistical analysis was performed using Student's t-test with Welch's correction. **R₁-R₃:** Representative hematoxylin and eosin (H&E) histology staining of day-7 heart allograft from mice treated with saline, Exenatide 2 μ g twice/day, or both Exenatide and Exendin 9-39 2 μ g twice/day. **S:** Immune infiltrate quantification after hematoxylin and eosin histology staining in heart allografts from mice treated with saline, Exenatide 2 μ g twice/day, or both Exenatide and Exendin 9-39 2 μ g twice/day. **T-V:** Bar graph depicting the quantification of splenic CD4 $^{+}$ effector-memory and CD8 $^{+}$ effector-memory T cells or splenic CD4 $^{+}$ regulatory T cells in mice who underwent heart allograft and were treated with saline, Exenatide 2 μ g twice/day, or both Exenatide and Exendin 9-39 2 μ g twice/day. **W-Y:** Total/active GLP-1 and Exe-4 peripheral levels are shown in respectively, untreated, heart transplanted (syngeneic and allogeneic) and Exe-4-treated mice, at least n=3 mice per group. **Z₁:** Heart allograft survival curves from Rag1 $^{-/-}$ mice that received heart allograft from BALB/c mice and were adoptively transferred with either CD3 $^{+}$ T cells from GLP-1R KO mice or from

WT mice; statistical analysis was performed using Student's t-test with Welch's correction.

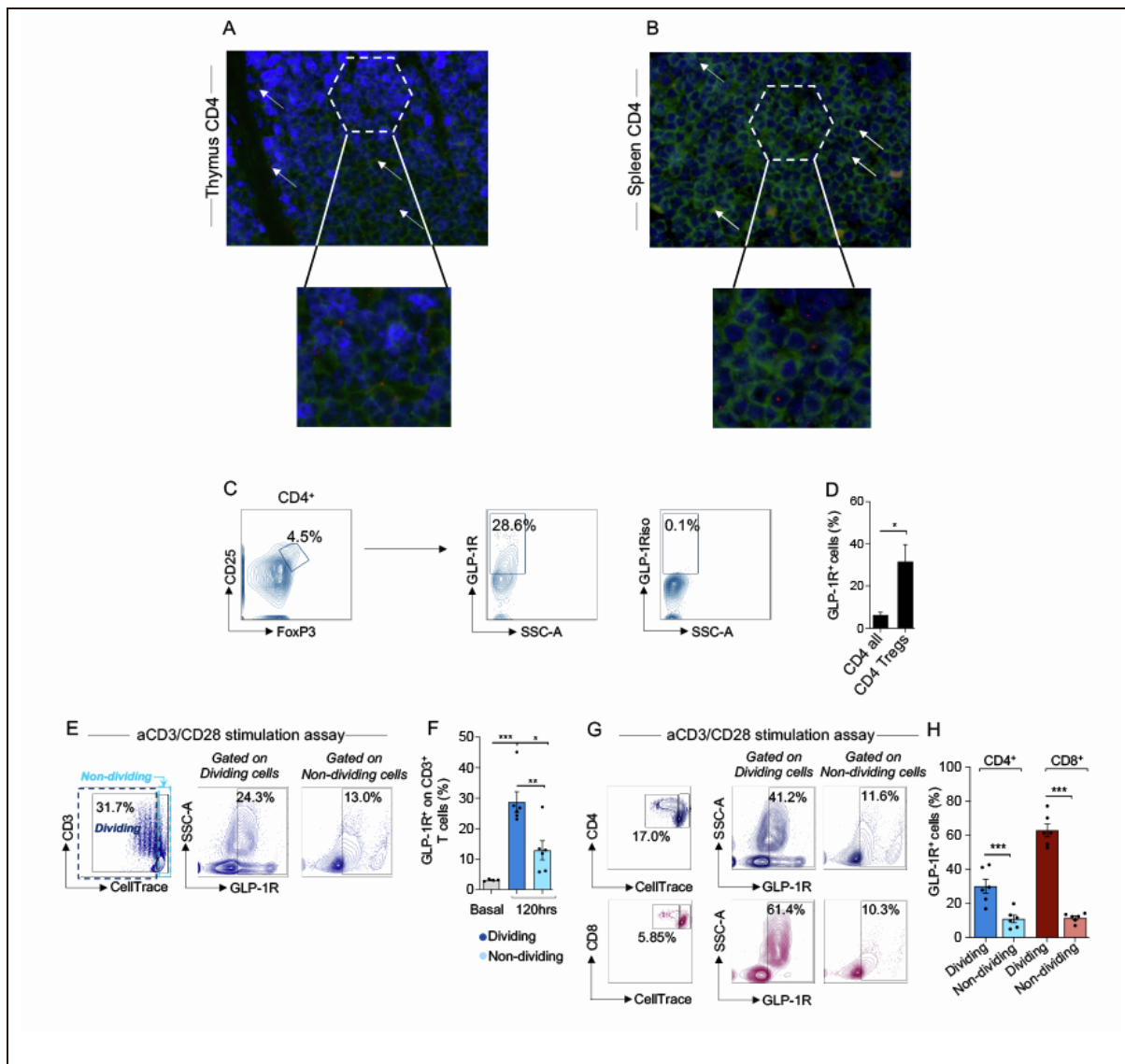
Z₂: Donor specific alloantibody levels (DSA) shown here as MFI in WT mice or from GLP-1R KO mice that received a heart allograft from BALB/c mice. **Z₃:** Quantitative bargraph showing the percentage of circulating T follicular helper cells were assessed on PBMCs from WT mice or from GLP-1R KO mice that received a heart allograft from BALB/c mice. Data are representative of at least n=3 samples and are expressed as mean ± standard error of the mean (SEM). *P<0.05; **P<0.01; ***P<0.001.



Abbreviations: GLP-1R, Glucagon-like peptide 1 receptor; FACS, fluorescence-activated cell sorter scan; Exe-4, Exenatide or exendin-4; FoxP3, forkhead box P3; WT, wild type; DSA;

donor specific alloantibody; MFI, mean fluorescence intensity; cTfh; circulating follicular helper T cells; PBMCs, peripheral blood mononuclear cells.

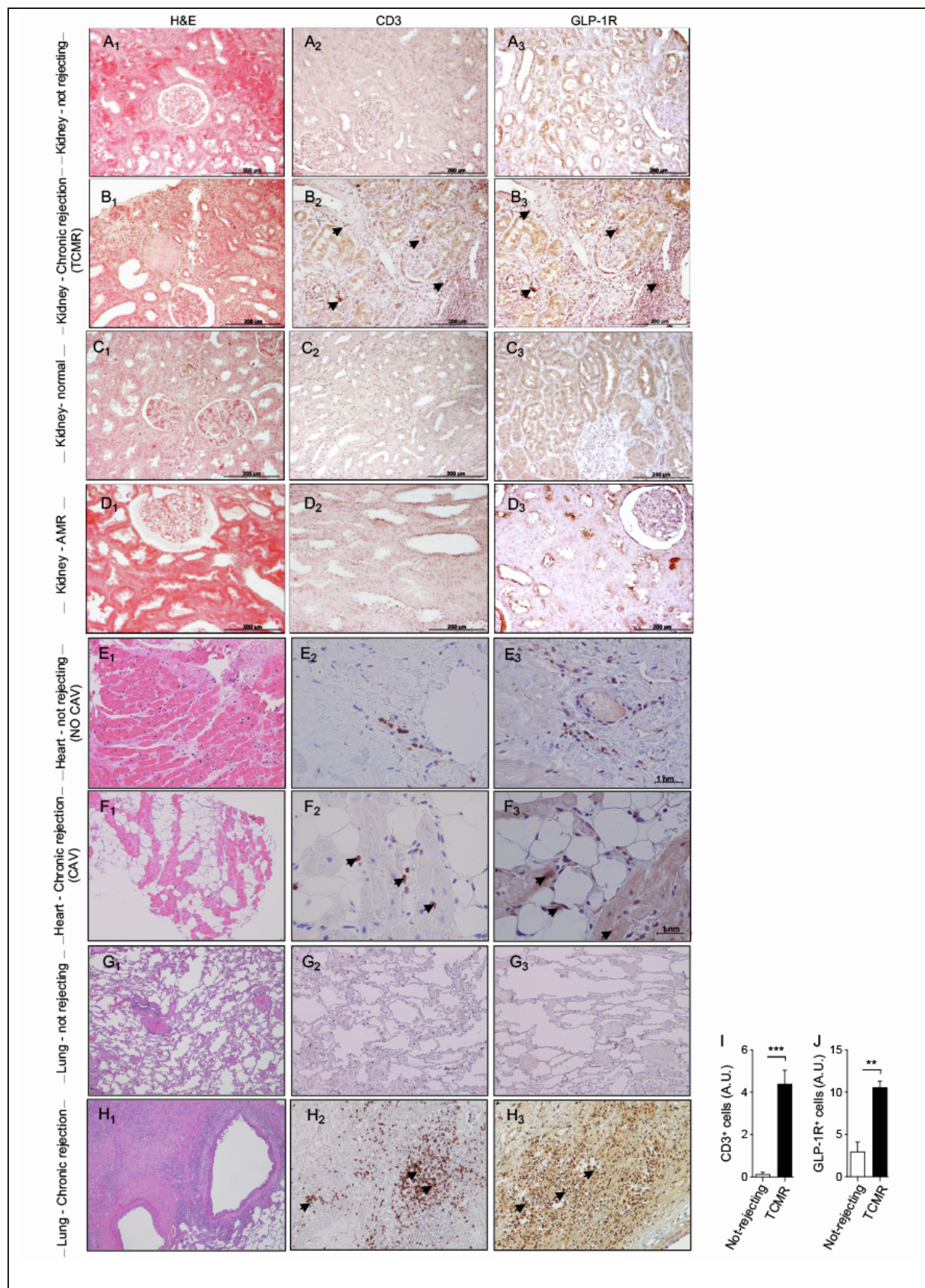
Figure S6. GLP-1R is expressed by human T cells, related to Figure 7. **A-B:** Images depicting Chromogenic *in situ* hybridization of GLP-1R on thymus, GLP-1R mRNA (red probe) in human thymus and spleen and co-localization with CD4 (green). **C:** Representative dot plots for gating strategy and GLP-1R expression by CD4⁺CD25⁺FoxP3⁺ regulatory cells. **D:** Quantification of flow cytometric analysis from (C) and comparison with whole CD4⁺ population. **E-F:** GLP-1R expression was depicted after 72 hours of stimulation with anti-CD3/CD28 Abs on dividing human CD3⁺ T cells or Cell trace Violet⁺ cells as compared to non-dividing CD3⁺ T cells; the quantification of GLP-1R expression in both sub-populations is shown in (F). **G-H:** GLP-1R expression was depicted after 72 hours of stimulation with anti-CD3/CD28 Abs on dividing non-dividing CD4⁺/CD8⁺ T cells, the quantification of GLP-1R expression in both sub-populations is shown in (H); experiments were performed in triplicates, and results are representative of one experiment.



Abbreviations: GLP-1R, Glucagon-like peptide 1 receptor;

Figure S7. Expansion of GLP-1R^{pos} T cells during human allograft rejection, related to

Figure 7. **A₁-A₃:** Hematoxylin and eosin, CD3 and GLP-1R staining on human renal biopsies from kidney-transplanted non-rejecting cases, (magnification: 20X, scale bar: 200 μ m). **B₁-B₃:** Hematoxylin and eosin, CD3 and GLP-1R staining on human renal biopsies from kidney-transplanted TCMR-rejecting cases, (magnification: 10X, scale bar: 200 μ m). **C₁-C₃:** Hematoxylin and eosin, CD3 and GLP-1R staining on human heart biopsies from heart-transplanted non-CAV cases, (magnification: 40X, scale bar: 1 nm). **D₁-D₃:** Hematoxylin and eosin, CD3 and GLP-1R staining on human heart biopsies from heart-transplanted CAV cases, (magnification: 40X, scale bar: 1nm). **E₁-E₃:** Hematoxylin and eosin, CD3 and GLP-1R staining on human lungs biopsies from non-transplanted cases, (magnification: 40X, scale bar: 1nm). **F₁-F₃:** Hematoxylin and eosin, CD3 and GLP-1R staining on human lungs biopsies from lung-transplanted chronic rejecting cases, (magnification: 40X, scale bar: 1nm). **G₁-G₃:** Hematoxylin and eosin, CD3 and GLP-1R staining on human renal biopsies from normal kidney cases, (magnification: 20X, scale bar: 200 μ m). **H₁-H₃:** Hematoxylin and eosin, CD3 and GLP-1R staining on human renal biopsies from antibody-mediated-rejecting cases (AMR), (magnification: 10X, scale bar: 200 μ m). **I-J:** The quantification of CD3⁺/GLP-1R⁺ in T cell-mediated-rejecting cases (TCMR) and no-rejecting cases is shown. Data are representative of at least n=3 samples and are expressed as mean \pm standard error of the mean (SEM). *P<0.05; **P<0.01; ***P<0.001.



Abbreviations: GLP-1R, Glucagon-like peptide 1 receptor; TCMR, T cell-mediated rejection; CAV, chronic allograft vasculopathy.

Table S1. Relative quantification of the immunoprecipitated GLP-1R^{pos} CD3⁺ T cells, related to Figure 2.

rank	Accession	Peptide
1	tr H2A2P9 H2A2P9_MUHV1 gpmDB psyt snap [1/0] protein peptide Small capsomere-interacting protein {ECO:0000256 HAMAP-Rule:MF_04021};	MSTNVSSAAS GGGSSGASSG GGGGGGGGGGS GG STNVSSAASG GGGGASSGGG GGGGGGGGGSG GSSK TNVSSAASGG GGGGASSGGG GGGGGGGGGGG SSKKEEE NVSSAASGGG SSGGASSGGGG GGGGGGGGGGG SGGK VSSAASGGGS SGASSGGGGG GGGGGGGGGGS KKE AASGGGGSGA SGGGGGGGGGG GGS SGGGGSSGASS GGGGGGGGGGGGG SGGS SGGGGSSGASS GGGGGGGGGGGGG SGSSKK GGGSSGASSG GGGGGGGGGGGGG SGSS SSGASSGGGG GGGGGGGGGGS S ASSGGGGGGGG GGGSGGS SGGGGGGGGGG GSGGSSKKEE
2	sp Q80U70 SUZ12_MOUSE gpmDB psyt snap [1/0] homo (1/1) protein peptide Polycomb protein Suz12; Suppressor of zeste 12 protein homolog;	APQKHGGGGG GGSGPSAGSG GGG PQKHHGGGGG GSGPSAGSGG GGFGGSAAAV HGGGGGGGSG PSAGSGGGGF GGSAA HGGGGGGGSG PSAGSGGGGF GGSAAVAAA ASGGK GGSGPSAGSG GGGFGGSAAA VAAAASGGKS GGG GPSAGSGGGG FGGSAAVAAA AASGGKSGGG GCG GGSAAVAAA ASGGKSGGGG CGGGGSYSAS S AAAASGGKSG GGGCAGGGSY AAAASGGKSG GGGCAGGGSY SA AAASGGKSGG GGCAGGGSYS ASSSSAAAAAA AAAGAA ASGGKSGGGG CGGGGSYS KSGGGGCGGG GSYSASSSSA AAAAAGAA V
3	sp E9Q3L2 PI4KA_MOUSE gpmDB psyt snap [1/0] homo (1/1) protein peptide Phosphatidylinositol 4-kinase alpha; PI4-kinase alpha; PI4K-alpha; PtdIns-4-kinase alpha; EC 2.7.1.67 {ECO:0000250 UniProtKB:P42356};	MAAAGARGGG GGGGGGGGGG SGSSSGSSTS RGF AAGARGGGGG GGGGGGGGGSG SSSG AGARGGGGGG GGGGGGGSGS SSGS AGARGGGGGGG GGGGGGGSGS SSGSSTSRSRGF Y GARGGGGGGG GGGGGGGSGS ARGGGGGGGG GGGGGSGS ARGGGGGGGG GGGGGSGSSS GSS GGGGGGGGGGG GSNSSSGS GGGGGGGGGGG GSNSSSGS GGGGGGGGGGG SGSSSGS
4	sp Q7TMA2 ZN503_MOUSE gpmDB psyt snap [1/0] protein peptide Zinc finger protein 503; Zinc finger protein Nolz-1;	SKHSGGGGGG GGGGGSGGGS ADPAWTSALS GNCSG KHSGGGGGGG GGGGSGG KHSGGGGGGG GGGGSGGGGS HSGGGGGGGG GGGSGGGSAD PAW SGGGGGGGGG GGGSGGGSADP AWTSALSGNC SGHGPG SALSGNCSGH G KPDPSPKSKL SSVASNGGGA GGAGNGAGGD K EPGGGGGGGG GGGGGGGVAA EKSGFR PEAGGGSSK GS GGASADGV PAGLGHG
5	sp Q8VD62 CK068_MOUSE gpmDB psyt snap [1/0] protein peptide UPF0696 protein C11orf68 homolog; Basophilic leukemia-expressed protein Bles03; Protein WF-3;	MAAAAAGAG AGRGGGGGGG GGGAAD AAAAAVAGAG RGGGGGGGGG GAADPGQERS RAR AAAAGAGAGR GGGGGGGGGG AADPGQER AAVAGAGRG GGGGGGGGGGA AD AVAGAGRGG GGGGGGGGAAD PGQERS GRGGGGGGGG GGAADPG GGGGGGGGGA ADP
6	sp Q8VDI9 ALG9_MOUSE gpmDB psyt snap [1/0] homo (2/2) protein peptide Alpha-1,2-mannosyltransferase ALG9 {ECO:0000305}; EC 2.4.1.259 {ECO:0000250 UniProtKB:Q9H6U8}; EC 2.4.1.261 {ECO:0000250 UniProtKB:Q9H6U8}; Dol-P-Man:Man(6)GlcNAc(2)-PP-Dol alpha-1,2-mannosyltransferase {ECO:0000305}; Dol-P-Man:Man(8)GlcNAc(2)-PP-Dol al ...	RQLKGGGGGG GGGGGDAGPA AEKLEQ QRLKGGGGGG GGGGDAGPAA EKLEQLGS LKGGGGGGGG GGDAGPAAEK LKGGGGGGGG GGDAGPAAEK LE KGGGGGGGGG GDAGPAA

7	sp P25444 RS2_MOUSE gpmDB psyt snap [1/0] homo (9/11) protein peptide no protein information available	DAGAAGGPGG PGGPGLGG AAGGPGGPGG PGLGGRGGFR AGGPGGP LIPAPRGTGI VSAPVPK
8	tr A0A2Z4EYB3 A0A2Z4EYB3_MUHV1 gpmDB psyt snap [1/0] protein peptide no protein information available	MSTNVSSAAS GGGSSGGSS G MSTNVSSAAS GGGSSGGSS GASSGGGSSS KK SGGGSSGGGS SGAS SGGGSSGGGS SGASSGGSS S
9	tr B1AVK5 B1AVK5_MOUSE gpmDB psyt snap [1/0] homo (1/1) protein peptide no protein information available	GDKGPIGVPG FVGISGIPG GLPLPGEKG HDGPI GDGGKVGITG DPGFPGPGL GTHGTPGASI TGVPGPAGLP GPKGER
10	sp D3YWQ0 DGKI_MOUSE gpmDB psyt snap [1/0] homo (2/2) protein peptide no protein information available	LSPTGLCSGT TSASFAA PTGLCSGTT ASFAAAGAVA MNPSSSAGEE RGA TTSASFAAAG AVAMNPSSA GEERGATGGS S CCLGAEGGAD PRGAGAAAAA ALEPAAAGQ KEK
11	sp O35295 PURB_MOUSE gpmDB psyt snap [1/0] protein peptide no protein information available	MADGDGSER GGGGGGGGGP GGFQPAP ADGDGSERG GGGGGGGGGP GFQPAPRGG DGDGSERGG GGGGGGGPGG FQPAPR SGSERGGGG GGGGPGGFQ
12	sp Q8BLX7 COGA1_MOUSE gpmDB psyt snap [1/0] homo (1/3) protein peptide no protein information available	ESNVTLGPSP LKGGKGERGL TGPSPK GAIGPMGPPG AGVSGPPGQK GLTGLTDKG EPGPPGQ PGPPGPQGPY GYGK
13	sp P09084 PAX1_MOUSE gpmDB psyt snap [1/0] homo (0/1) protein peptide no protein information available	VSWERAAGAAA AGPGAGGALG SGSLRVSSR AAAAAAAGPGA GGALGSGSLR GPRLLRALPL CLSGGGGARA LP
14	sp Q9Z2E1 MBD2_MOUSE gpmDB psyt snap [1/0] protein peptide no protein information available	PEQEEGESAA GGSGAGGDSA IEQGGQGSAL APSP GRGRGRPQSG GSGLGGDGGG GAGGCGGGS GRPQSGGSGL GGDGGGGAGG CGGGSGGGVA PRR
15	tr A0A1B0GRC0 A0A1B0GRC0_MOUSE gpmDB psyt snap [1/0] homo (1/2) protein peptide no protein information available	PGPYDVIKGE PGLPGPEGPP GLKGLQG EGPPGLKGLQ GQQGVTGSVG LPGPPGVPGF DGAPGQK
16	(H) sp P02463 CO4A1_MOUSE gpmDB psyt snap [1/0] homo (1/2) protein peptide no protein information available	GVPGIPG GQQGVTGSVG LPGPPGVPGF DGAPGQK HTSAGAEQSG QALASPQSC EEFR
17	sp Q8VHW2 CCG8_MOUSE gpmDB psyt snap [1/0] homo (2/2) protein peptide no protein information available	AGGGAGGSGG SGPSAILR GSVAAAGLASA GGGGSGAGVG AYG PAPPAPAPA PGTLSK
18	sp Q8C9W3 ATS2_MOUSE gpmDB psyt snap [1/0] homo (1/1) protein peptide no protein information available	PPASVRLVAA TEPPGGPPGQ GAERILAVPV
19	tr A0A140LI36 A0A140LI36_MOUSE gpmDB psyt snap [1/0] homo (0/3) protein peptide no protein information available	SEADINAEKW DAGKGGKEKD KTAKSPI DLISLTATL DKSQEELAIN EGVAK KGKLPAALR
20	sp Q91YE5 BAZ2A_MOUSE gpmDB psyt snap [1/0] homo (9/9) protein peptide no protein information available	LPPAPAASGL KPSPSSGEGL YTNGSPMN PLEGNPVIS ALDCPALSNA NAFSL EETTGGAVAV SGSGDVLK

Table S2. Characteristics of kidney-transplanted patients, related to Figure S7 and to STAR Methods.

	Normal			AMR			TCMR		
	1	2	3	1	2	3	1	2	3
General Characteristics									
Age (years)	29	52	31	48	69	60	53	35	70
Transplant Age (years)	1,3	0,1	2,2	13,9	10,3	9,2	1,2	0,2	0,4
Sex (M / F)	F	F	M	F	M	M	M	F	F
Hypertension (Yes / No)	Yes	No	No	Yes	No	Yes	No	Yes	No
Diabetes mellitus (Yes / No)	No	No	No	No	Yes	Yes	No	No	Yes
Biochemical Characteristics									
sCr (mg/dl)	2	1,54	2,36	1,91	1,24	1,29	1,7	2,97	1,4
eGFR (ml/min/1.73 m ²)	33	38,4	35,4	30,4	58,9	59,9	45	19,6	38
Urea (mmol/l)	95	57	51	90	67	39	56	109	54
Glucose (mg/dl)	81	86	82	118	161	187	83	77	128
HbA1C (mmol/mol, %)	40 (5,8)	35 (5,3)	38 (5,6)	31 (5)	47 (6,5)	64 (8)	45 (6,3)	42 (6%)	53 (7)
WBC (cells/ul)	4950	7300	8600	6700	3300	10000	6400	7900	5500
N% / L%	40 / 48	89 / 9	25 / 68	57 / 30	53 / 31	69 / 22	57 / 25	76 / 14	72 / 10
Hb, (g/dl)	9,8	10,6	11,7	11,6	12,8	15,3	11,8	9,9	11,7
CRP (mg/l)	0,06	0,11	0,42	0,05	0,38	0,21	0,16	0,08	0,63
Tacrolimus levels (ng/ml)	6,9	9	5,9	5,2	4,6	6,9	5,9	11,2	7,2
DSA (MFI)	/	/	/	DQ7 7235	DQ8 13600, DR53 4000 23'000	DQ4	Neg	Neg	Neg
Urinary Characteristics									
Proteinuria (g/24h)	0,05	0,1	0,1	0,8	0,27	1,9	0,06	0,39	0,9
Urinary Sediment	Neg	Low MH	Neg	Neg	Low MH	Neg	Neg	Low MH	Neg
Urine Culture	Neg	Neg	Neg	Neg	Neg	Neg	Neg	Neg	Neg
Immunosuppressive therapy									
Tacrolimus (mg/die)	2 + 1	4 + 4	4 + 5	2 + 2	1,5 + 1	2 + 1	5	7	2,5

Mycophenolate (mg/die)	360 x 2	1000 x 2	/	500 x 2	360 x 2	500 x 2	1000 + 500	500 x 2	720 +
Prednisone (mg/die)	5	5	5	5	5	5	5	10	360

Footsteps: AMR – Antibody Mediated Rejection, TCMR – T-Cell Mediated Rejection, sCr – Serum Creatinine, eGFR – estimated Glomerular Filtration Rate, HbA1C – Glycated Hemoglobin, WBC – White Blood Cells, N% - Percentage of Neutrophils, L% - Percentage of Leukocytes, Hb – Hemoglobin, CRP – C-Reactive Protein, DSA – Donor Specific Antibodies, MH – Microhematuria, MFI – Mean Fluorescent Intensity.

Table S3. Characteristics of heart-transplanted patients, related to Figure S7 and to STAR Methods.

<i>Diagnosis</i>	CAV		No-CAV	
<i>General Characteristics</i>				
Age (years)	58	47	50	42
Date of Transplantation	2010	2013	2013	2013
Sex (M / F)	M	M	M	F
Pre-transplant disease	non-ischemic	non-ischemic	ischemic	non-ischemic
<i>Post-transplant prognosis</i>				
End stage heart failure etiology	Dilated cardiomyopathy	Dilated cardiomyopathy	Ischemic cardiomyopathy	Dilated cardiomyopathy
Acute rejection graft episodes (Yes / No)	Yes	Yes	Yes	No
ATG induction (Yes / No)	Yes	Yes	Yes	Yes
<i>Immunosuppressive therapy</i>				
Methylprednisolone (Yes / No)	Yes	Yes	Yes	Yes
Mycophenolate (Yes / No)	No	Yes	Yes	Yes
Prednisone (Yes / No)	Yes	Yes	Yes	Yes
Cyclosporine (Yes / No)	Yes	Yes	Yes	Yes
Imuran (Yes / No)	Yes	No	No	No

Abbreviations. CAV, chronic allograft vasculopathy; M, male; F, Female; ATG, thymoglobulin.